"LIGAND EXCHANGE AND SUBSTITUTION ON FIVE-

COORDINATE COMPLEXES OF COPPER(II), NICKEL(II) AND COBALT(II)"

A thesis presented for the degree of

Doctor of Philosophy

in the University of Adelaide

by

Bruce Germein Doddridge

B.Sc.(Hons.), University of Adelaide, 1978

Department of Physical and Inorganic Chemistry,

University of Adelaide, Adelaide, S.A., 5001, Australia

February, 1986

CONTENTS

Summary

A variety of five-coordinate transition metal complexes containing the tripodal amine quadridentate ligand 2,2',2''-tri(N,N-dimethylamino)-triethylamine of the form $[M(Me_6tren)S](ClO_4)_2$; M = Co(II), Ni(II), Cu(II), Zn(II); S = dmf, def, dma, CH_3CN; have been prepared and characterized by elemental and metal analyses as well as by infrared spectroscopy.

These complexes were of interest as coordination of Me_6tren ligand to divalent transition metal ions in this study produces a five-coordinate species in which solvent in the fifth coordination site exhibits a large reduction in lability compared to that exhibited by $[M(solvent)_6]^{2+}$. This is unusual as it has been reported widely in the literature that the labilities of six-coordinate Co(II) and Ni(II) species commonly exhibit significant increases on coordination of amine groups. It was hoped that this study would give some mechanistic insight into these unusually slowly reacting systems.

Complexes of the form $[M(Me_6tren)X]^{n+}$ where M = Co(II), Ni(II), Cu(II); X = dmf, Br^-, N_3^-, NCS^- were characterized in dmf solution by ultraviolet/visible absorption spectroscopy and the stoichiometry of anated complexes was determined using the Job method of continuous variations.

Stopped-flow spectrophotometry at various temperatures has been used to examine the kinetics of anation reactions in dmf solution of $[M(Me_6tren)dmf]^{2+}$; M = Co(II), Ni(II), Cu(II) with monodentate ligands $X^- = Br^-$, N_3^-, NCS^- as shown below:

$$[M(Me_6tren)dmf]^{2+} + X^- \xrightarrow{k_{obs}} [M(Me_6tren)X]^+ + dmf$$
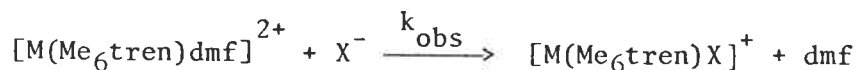
The variation of k_{obs} with excess $[X^-]$ for anation reactions on these complexes is consistent with the relationship.

$$k_{obs} = k_i K_o [X^-]/(1 + K_o[X^-]) + k_{-i}$$

which typifies an interchange (I) mechanism proceeding through two stages as shown below:

$$[M(Me_6tren)dmf]^{2+} + X^- \underset{fast}{\overset{K_o}{\rightleftharpoons}} [M(Me_6tren)dmf]^{2+}\ldots X^-$$

$$\underset{k_{-i}}{\overset{k_i}{\rightleftharpoons}} [M(Me_6tren)X]^+ + dmf$$
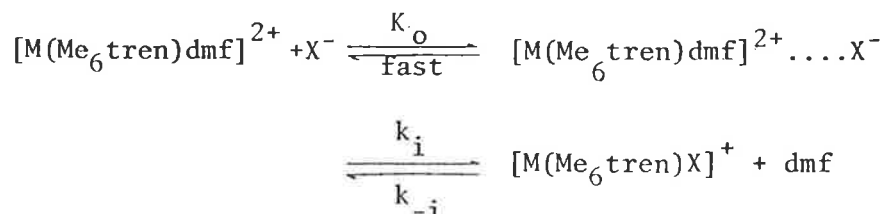
It has been found that there is little variation of k_i with the nature of X^- for both the Ni(II) and Cu(II) complexes which suggests that the activation mode for the substitution of dmf by X^- is probably dissociative. However, for Co(II), there are marked differences in derived k_i values as X^- is changed. This selectivity exhibited by $[Co(Me_6tren)dmf]^{2+}$ towards substitution of dmf by X^- suggests that the activation mode is probably associative in this case.

Considering the above observations along with the observed ligand substitution rate laws it can be proposed that an associative interchange (I_a) mechanism exists for anation on the Co(II) complex contrasting with the proposed dissociative interchange (I_d) mechanism characterizing anation on both Ni(II) and Cu(II) complexes.

Proton nuclear magnetic resonance spectroscopy has been used to determine exchange rate and activation parameters for solvent exchange processes on $[Cu(Me_6tren)S]^{2+}$; S = dmf, def, dma and $[M(Me_6tren)S]^{2+}$; M = Ni(II), Co(II); S = dmf, def in solution in the following manner.

The variation of the relaxation parameter, T_{2p} was studied over a large temperature range (governed by solvent physical properties) for a number of solutions of each complex at differing concentrations. The form of T_{2p} for one solvent molecule at a single site is given according to Swift and Connick by the equation:

$$\frac{1}{T_{2p}} = \frac{P_m}{\tau_m}\left[\frac{T_{2m}^{-2} + (T_{2m}\tau_m)^{-1} + \Delta\omega_m^2}{(T_{2m}^{-1} + \tau_m^{-1})^2 + \Delta\omega_m^2}\right] + \frac{P_m}{T_{2o}}$$

For each of the Cu(II) and Co(II) complexes studied the above equation

over the temperature range considered reduces to

$$(P_m T_{2p})^{-1} = \tau_m^{-1} = (k_B T/h)e^{-\Delta H^{\#}/RT}e^{\Delta S^{\#}/R} + A_o e^{-E_o/RT}$$

where τ_m is the mean lifetime of a coordinated solvent molecule and is

related to the rate constant for solvent exchange, k_{ex} by the following

relation

$$\tau_m^{-1} = k_{ex}$$

and the solvent, S, exchange rate = $k_{ex}[M(Me_6 tren)S^{2+}]$; (M = Cu,Co).

The derivation of kinetic parameters for solvent exchange in the case

of the Ni(II) complex was complicated by the presence of a minor species

believed to be $[Ni(Me_6 tren)(dmf)_2]^{2+}$, but with some appropriate

assumptions made, a similar approach to the Cu(II) systems was used to obtain

kinetic parameters.

Volume of activation data from other variable pressure nmr studies

have been obtained for each system and $\Delta V^{\#}$ for the Cu(II) systems was

found to be positive, indicating a dissociative activation mode for

solvent exchange on these complexes. $\Delta V^{\#}$ for solvent exchange on the

Co(II) systems was also obtained and found to be negative, indicating

an associatively activated mode for solvent exchange in these cases.

For the d^7 Co(II) complex $[Co(Me_6 tren)dmf]^{2+}$ in dmf solution the

significant dependence of k_i on the nature of incoming anion reacting

through a proposed I_a mechanism seems to be consistent with a proposed

associatively activated mechanism for dmf exchange already determined.

For the analogous d^8 Ni(II) and d^9 Cu(II) complexes in dmf solution

the following may be deduced in each case. The similarity of k_{ex} to k_i

and the small variation of k_i with differing entering anions suggest an I_d

mechanism for ligand substitution on these complexes, consistent with the

proposed dissociatively activated mechanism for solvent exchange.

These new observations support the argument that ligand substitution in these complexes tends towards an associative activation mode as the electronic occupancy of the d orbitals on the central metal ion decreases. By comparison with other systems of distinct structure possible effects of stereochemistry on this tendency have also been discussed. Possible reasons for the unusually low lability of these complexes have also been discussed.

Declaration

This thesis contains no material previously submitted for a degree or diploma in any University, and to the best of my knowledge and belief, contains no material previously published or written by another person, except where due reference is given in the text.

Upon being accepted for the award of the degree consent is given for this thesis being made available for photocopying and loan if applicable.

B.G. Doddridge

Acknowledgements

I wish to thank sincerely my supervisors, Dr. J.H. Coates and Dr. S.F. Lincoln for their keen interest, unfailing support and diligent guidance throughout the course of this research.

I am indebted to the jovial and efficient ancillary staff of the Department of Physical and Inorganic Chemistry at the University of Adelaide, particularly Messrs. A.L. Bowers, G.C. Duthie, J. Netting, R. Morris and K.R. Shepherdson for services rendered during this undertaking.

I am grateful to the members of academic staff and other research students for the stimulus provided in research discussion throughout this project.

I thank Mrs. A.M. Hounslow, Mr. J. Maeji and Dr. D.L. Pisaniello for the professional manner in which they ran the HX90E proton nmr spectra required.

I gratefully acknowledge financial assistance provided by a Commonwealth Postgraduate Scholarship.

Great thanks must go to Judith Doddridge for help with text corrections and to Sherri Nesbitt for the many headaches endured in typing this manuscript.

Finally, it is my great pleasure to honour sincerely my parents, Reg and Aileen, at this time, as it is their inestimable financial and moral support that has been a source of encouragement over the trying years of my postgraduate studies.

CHAPTER 1   -   INTRODUCTION

CHAPTER 1 - INTRODUCTION

1.1 Foreword

In the mid 1960's complexes of coordination number five for bivalent first-row transition metal ions were virtually unknown compared with those of coordination number four or six. No five-coordinate manganese-(II) and iron(II) complexes had been prepared, copper(II) and zinc(II) complexes were rare and those cobalt(II) and nickel(II) complexes that had been prepared were all low-spin. With the development of multidentate polyamine ligands that were sufficiently bulky to prevent a six-coordinate geometry by steric crowding about the central metal ion, the field expanded rapidly over the ensuing decade and has continued to hold the attention of many researchers since.

This study concerns itself with one such polyamine ligand, the quadridentate ligand 2,2',2''-tris(dimethylamino)-triethylamine, Me_6tren, which forms almost exclusively five-coordinate high-spin complexes with bivalent first-row transition metal ions. It is therefore pertinent to review previous work done in this field with discussion focusing on those complexes involving the Me_6tren ligand.

1.2 Historical review

The quadridentate polyamine ligand 2,2',2"-triaminotriethylamine, tren, a precursor of the Me_6tren ligand, was purified[1] and demonstrated to have the ability to form metal complexes with a variety of metal ions[2] in the late 1940's. More than fifteen years later Ciampolini and co-workers prepared[3] the hexamethyl derivative of tren, Me_6tren, and then undertook a systematic investigation of both the preparation[3,4] and some properties[3-5] of high-spin five-coordinate Me_6tren complexes of bivalent 3d transition metal ions. They proposed that Me_6tren might be a suitable ligand, as it was multidentate, sufficiently bulky that steric crowding would prevent the formation of a six-coordinate complex, and the ligand donor atoms were highly electronegative, thus promoting a high degree of ionic bonding character in the resultant metal complex. They found, using spectroscopic and X-ray techniques, as well as conductivity and molecular weight data, that the type of complex prepared had the structure [M(Me_6tren)X]X (where M=Fe(II), Co(II), Ni(II), Cu(II), Zn(II); X = a variety of inorganic anions), being of nearly trigonal-bipyramidal geometry in both the solid state and in chloroform solution. Magnetic susceptibility data (with the obvious exception of the diamagnetic d^{10} zinc(II) complex) were consistent with the complexes being of high-spin type. The spectra of the Me_6tren complexes of cobalt(II) and nickel(II) were further treated by simplified crystal field theory and the spectral transitions identified. The similarity of these spectra to those of analagous complexes known to have five-coordinate geometry, further supported the stereochemical assignment made for this class of complex.

Soon after this pioneering work there was much activity concerned with the preparation and understanding of the properties of this class of complex. A five-coordinate complex of chromium(II) was prepared[6], [Cr(Me_6tren)Br]Br, the first such chromium(II) complex exhibiting

trigonal-bipyramidal stereochemistry. Paoletti and Ciampolini undertook a calorimetric study[7] of a series of complexes [M(Me$_6$tren)Br]Br where M ranged across the first-row transition metals from manganese(II) to zinc(II). These authors, after applying crystal field stabilization energy corrections to measured values, calculated enthalpies of formation having a monotonic dependence on the atomic number. Calculated relative bond dissociation energies allowed a rationalization of trends for the heats of conversion between coordination numbers of five and six for these complexes.

Some detailed X-ray diffraction studies followed for the complexes [M(Me$_6$tren)Br]Br (where M= Co(II), Ni(II), Cu(II)). DiVaira and Orioli[8] examined the complex [Co(Me$_6$tren)Br]Br by X-ray methods to investigate the important role the geometry of the multidentate ligand molecule plays in the resultant stereochemistry of the complex. The crystalline complex was found to consist of [Co(Me$_6$tren)Br]$^+$ and Br$^-$ ions with the geometry about the cobalt being trigonal-bipyramidal, this C$_{3V}$ symmetry being quite novel at the time for cobalt(II). The same researchers also studied the analogous copper(II) and nickel(II) complexes[9] and found distinct similarities between results for the copper complex and a previously reported[10] complex [Cu(tren)(NCS)].SCN known to have a distorted trigonal-bipyramidal stereochemistry. Results for the two crystalline complexes studied indicated essentially an identical structure to the analogous cobalt(II) complex. DiVaira and Orioli then extended on their own work, undertaking another detailed X-ray crystallographic study[11] of [M(Me$_6$tren)Br]Br (where M= Mn(II), Fe(II), Zn(II)) finding that these complexes were of similar structure and stereochemistry to other complexes in the series already reported[9]. Similarities in metal-to-ligand bond distances and bond angles were found to exist between the zinc complex and a previously reported[12] pentacoordinate complex, Zn(tren)(SCN)$_2$. The

manganese complex was the first pentacoordinate structure for manganese(II) to be elucidated by a complete X-ray analysis and the iron complex was the first known case of pentacoordinate iron(II) exhibiting trigonal-bypyramidal geometry.

The use of ligand field theory and related molecular orbital energy level splitting diagrams to make transitional assignments and interpret absorption spectra of five-coordinate complexes, including complexes containing the Me_6tren ligand, in both the solid state and in solution, was the subject of a detailed review by Furlani[13]. Following this review there appeared a number of papers[14-16] concerned, at least in part, with five-coordinate 3d metal complexes containing the Me_6tren ligand, specifically detailing energy level diagrams and spectral transitions between them.

In a general review by Orioli[17], X-ray diffraction data on five-coordinate nickel(II) and cobalt(II) complexes containing the Me_6tren ligand were examined and conclusions drawn concerning stereochemical properties of these complexes, the electronic structures of the metal atoms and the nature of the metal-to-ligand bond. Bertini and coworkers[18] obtained single-crystal polarized electronic spectra of the [Ni(NCS)(Me_6tren)].SCN monohydrated complex and used information from X-ray structural analysis, to determine the exact geometry of the chromophore and the molecular orientation in the crystals which enabled them to assign spectral transitions. Bertini et al[19] also obtained single-crystal polarized electronic spectra of the analogous cobalt(II) trigonal-bipyramidal complex [Co(NCS)(Me_6tren)].SCN.H_2O with a view to substantiating assignments of observed spectral transitions. These results have been used in obtaining a significant ligand field interpretation[20] of the electronic spectra of high-spin trigonal-bipyramidal cobalt(II) complexes.

O^{17} nuclear magnetic resonance (nmr) techniques have been used to

study water exchange processes[21] in tren substituted aquo ions of copper(II) and nickel(II)[22]. In the case of the Ni(II)-tren species two distinct exchange rates for bound water were observed, suggesting that the nickel is six-coordinate in the complex, $[Ni(tren)(H_2O)_2]^{2+}$. For the Cu(II)-tren complex however, only a single, slower than expected rate of exchange was observed suggesting a five-coordinate $[Cu(tren)(H_2O)]^{2+}$ arrangement. West and Lincoln[23] used visible absorption spectrophotometry and ^{14}N nuclear magnetic resonance to study acetonitrile exchange on complexes of nickel(II) and cobalt(II) formed with tren and Me_6tren. They too observed two distinct exchange rates for bound acetonitrile on the Ni(II)-tren species, presumably $[Ni(tren)(CH_3CN)_2]^{2+}$. However, the analogous Me_6tren complex was found to have only one exchange rate consistent with the structure $[Ni(Me_6tren)(CH_3CN)]^{2+}$, this difference possibly being due to steric crowding of the available coordination sites on the central metal ion by the more bulky Me_6tren ligand. Cobalt(II) complexes of either tren or Me_6tren showed only one exchange rate indicating a five-coordinate structure. A significant reduction in lability was noted for complexes containing the Me_6tren ligand, possibly due to the relatively inflexible nature of the Me_6tren ligand preventing the close approach of solvent to the metal atoms thus reducing solvent assistance in the mechanism of exchange. West and Lincoln[24] also used ^{14}N nuclear magnetic resonance to study acetonitrile exchange on the analogous copper(II) complexes of tren and Me_6tren. They observed only one exchange rate in each case consistent with a five-coordinate structure in solution. Contrasting with previous results[23], where coordination to nickel(II) and cobalt(II) of the tren ligand increased lability of coordinated solvent, coordination of tren to copper(II) resulted in an order of magnitude reduction in lability of coordinated solvent. It appears that the electron donating characteristics of the coordinated tren ligand towards

the central metal ion, considered responsible for this labilization in the Ni(II)- and Co(II)-tren complexes, is outweighed by the reduction in solvent lability induced by the removal of the dynamic Jahn-Teller effect[25,26] operative in $[Cu(CH_3CN)_6]^{2+}$ but not in d^9 complexes of C_{3V} symmetry such as $[Cu(tren)(CH_3CN)]^{2+}$. The even greater reduction in lability observed for acetonitrile exchange in $[Cu(Me_6tren)(CH_3CN)]^{2+}$ is also consistent with the absence of Jahn-Teller distortion effects coupled with a reduction in transition-state flexibility of Me_6tren complexes as previously reported for nickel(II) and copper(II) analogues, which also show greatly reduced lability.

The recent advances in the understanding of the spectroscopy and magnetism of five-coordinate iron(II), cobalt(II) and nickel(II) Me_6tren complexes are discussed in a comprehensive review by Morassi et al.[27]. In another review by Zipp et al.[28] concerning tripodal amines in general, some thermodynamic and kinetic data involving tren, and to a lesser extent, Me_6tren complexes, are discussed.

Using acid-base titrations Coates et al.[29] were able to study the influence of a local hydrophobic environment on acid dissociation constants of metal coordinated water molecules. This study involved the complexes $[M(Me_6tren)(H_2O)]^{2+}$ (where M = Co(II), Ni(II), Cu(II), Zn(II)) contrasting with the complexes $[M(tren)(H_2O)]^{2+}$ (where M = Co(II), Cu(II), Zn(II)). The results were used in an attempt to rationalize the low pKa values for the coordinated water molecule in carbonic anhydrase[30].

^{129}I Mössbauer spectroscopy, considered useful for differentiating between different ligand coordinations, has been used by Potasek et al.[31] to study the compounds $[M(Me_6tren)I_2]$ (where M = Ni(II), Zn(II)). It was concluded that the two iodine atoms were equivalent and therefore bound in the same way in both complexes, ruling out the previously suggested formula $[M(Me_6tren)I]I$. However, preliminary measurements on $Co(Me_6tren)I_2$

showed the presence of both free and bound iodide compatible with the suggested structure for the analogous bromide compound[8]. However, before any further elucidation in this direction was published Orioli and Nardi[32] found by X-ray diffraction analysis that the complex [Ni(Me$_6$tren)I]I was in fact five-coordinate and of trigonal-bipyramidal geometry, thus casting some doubt on the reliability of conclusions derived from Mössbauer studies.

So far only first-row transition elements had been used in the preparation of five-coordinate Me$_6$tren complexes. Senoff[33] however, prepared Me$_6$tren complexes of the second-row transition element palladium. It was found that the molecular structure of the resultant palladium complex isolated from aqueous solution was pH dependent with the Me$_6$tren ligand functioning as a tridentate ligand in [Pd(Me$_6$tren H)Cl]Cl$_2$ and as a potentially tetradentate ligand in [Pd(Me$_6$tren)Cl]Cl. A crystal structure of [Pd(Me$_6$tren)(NCS)].NCS by Ferguson and Parvez[34] established that the palladium atom in this complex is four-coordinate and bound by an isothiocyanato nitrogen and three Me$_6$tren ligand nitrogens in a square planar geometry. The fourth Me$_6$tren ligand nitrogen is not coordinated. The potential for Me$_6$tren to function as either a tri- or tetradentate ligand was further explored for a series of palladium (II) complexes by Bhattacharya and Senoff[35], who found the coordination to depend upon the physical state (solid or solution phase) of the complex. In the solution phase, in protic and aprotic solvents, rapid intramolecular rearrangement between a five- and six-coordinate palladium centre was found to occur for all of the complexes studied.

Following on from previous work[29] Coates et al. made a study of the influence of hydrophilic versus hydrophobic environment upon ligand substitution processes[36]. They undertook kinetic and equilibrium studies in aqueous solution of the hydrophilic [Cu(tren)(H$_2$O)]$^{2+}$ and hydrophobic [Cu(Me$_6$tren)(H$_2$O)]$^{2+}$ complexes and their lability of the aqua ligand towards

anionic substitution by azide and thiocyanate. This substitution was thought to occur via a dissociative interchange, I_d, mechanism[37,38] and the lability of the aqua ligand in $[Cu(Me_6tren)H_2O]^{2+}$ towards ligand substitution was found to be several orders of magnitude less than for the aqua ligand in $[Cu(tren)(H_2O)]^{2+}$. This disparity in lability is thought to be a reflection of the difference in local environment at the site of substitution. This work was later extended[39] to include other nucleophiles such as cyanate, chloride and bromide substituting onto $[Cu(Me_6tren)(H_2O)]^{2+}$ in aqueous solution. Substitution was again thought to proceed through an interchange mechanism and the low rate of anionic substitution observed is consistent with bond breaking contributing significantly in the mechanism, bearing in mind the inferred[24,36] low lability of the aqua ligand in $[Cu(Me_6tren)(H_2O)]$[24].

Benelli and Gatteschi[40] have recently used electronic spin resonance spectroscopy to study a series of five-coordinate trigonal-bipyramidal high-spin cobalt(II) complexes including some containing the Me_6tren ligand. Lincoln and co-workers[41] have used nmr methods to study solvent exchange of N,N-dimethylformamide, dmf, on $[Zn(Me_6tren)dmf]^{2+}$. They found that coordinated dmf in $[Zn(Me_6tren)dmf]^{2+}$, is considerably less labile than in $[Zn(dmf)_6]^{2+}$ [42] and $[Zn(tren)dmf]^{2+}$, consistent with similar observations made on the similar cobalt(II), nickel(II) and copper(II) complexes with acetonitrile as the coordinating solvent[23,24]. The steric effect induced by coordination of Me_6tren in this complex was again deemed predominantly responsible for the observed decreased lability.

Banci and co-workers[43] have recently used the angular-overlap model to interpret magnetic moment and susceptibility data in a study of the paramagnetism of $[Ni(Me_6tren)Br]Br$ and make some judgement as to the effect responsible for the unusually low magnetic moments of high-spin trigonal-bipyramidal nickel(II) complexes. Their results appeared to contrast with the predictions of a previous theoretical treatment[44] using

empirical ligand field theory. This work was extended upon by Deeth and Gerloch[45] to involve angular-overlap model analyses of the complexes

[M(Me$_6$tren)Br]Br (where M = Cr, Fe, Co, Ni, Cu) facilitating the investigation of changes in ligand-field parameters and bond length variations throughout a series where only d^n, the number of d electrons varies.

1.3 Objectives of this project

It has already been noted that the tetradentate ligand Me_6tren coordinates to bivalent first-row transition metal ions in solution to form five-coordinate complexes of approximate trigonal-bipyramidal geometry in which the fifth coordination site is occupied by an anionic ligand or solvent molecule.

It has been demonstrated previously[46] for the copper(II) complex of Me_6tren that solvent occupying the fifth coordination site exhibits a significantly large reduction in lability compared to that exhibited by the purely solvated ion, $[Cu(solvent)_6]^{2+}$. The lability of $[Cu(solvent)_6]^{2+}$ is greater than that usually expected for bivalent first-row transition metal ions, which may be attributed to the Jahn-Teller effect,[25,26] a tetragonal distortion that alternates rapidly over all three axes and produces a pairwise labilization of all six solvent molecules[24,47]. This source of labilization is not available to $[Cu(Me_6tren)(solvent)]^{2+}$ as the Jahn-Teller effect is not operative in d^9 systems of C_{3V} symmetry. It is improbable however, that this alone accounts for the reduction in lability of this species below that anticipated for other bivalent first-row transition metal ions and other effects must be responsible. It has also been shown[23] that acetonitrile exchange on $[Ni(Me_6tren)(CH_3CN)]^{2+}$ is characterized by an exchange rate constant which is several orders of magnitude less than that characterizing acetonitrile exchange on $[Ni(CH_3CN)_6]^{2+}$.

These results are in marked contrast to the substantial increases in coordinated solvent lability induced in six-coordinate cobalt(II) and nickel(II) species by the coordination of multidentate amines[21] where electron donation from the coordinated amine nitrogen atoms is thought to lower the charge of the central metal ion thereby labilizing the solvent molecule[48]. It would therefore be of interest to carry out a detailed
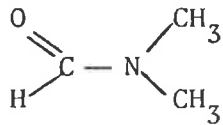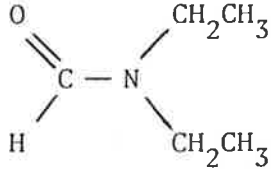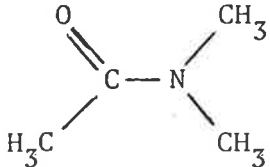
study of solvent exchange and anionic ligand substitution on the complexes $[M(Me_6tren)(solvent)]^{2+}$ (where M = cobalt(II), nickel(II), copper(II)) to seek some mechanistic insight into these unusually slowly reacting systems.

The choice of solvent in such a study is subject to several important considerations. Some excellent reviews[49,50] discuss the influence of the properties of solvents on ligand substitution processes of labile metal complexes. The use of a non-aqueous solvent was considered desirable for the following reasons. Studies on complexes $[M(Me_6tren)(H_2O)]^{2+}$ (where M = Co(II), Ni(II), Cu(II), Zn(II)) have determined that the form of the solvent ligand at the fifth coordination site is pH dependent[29,46,51] and consequently a dependence of complex molar extinction coefficient on pH has also been observed[46,52]. Conducting kinetic experiments that rely on spectrophotometric methods in non-aqueous media eliminates this problem. An interchange mechanism involving an ion-paired encounter complex (see section 2.1.3) has already been demonstrated[36,39] to be operative in aqueous solution for anionic substitution in $[Cu(Me_6tren)(H_2O)]^{2+}$. Studying this reaction in a non-aqueous solvent with a significantly lower dielectric constant would be expected to facilitate ion pairing as solvent effects separating charges in solution are reduced compared to those in aqueous solution.

A series of substituted amides, N,N-dimethylformamide (dmf), N,N-diethylformamide (def) and N,N-dimethylacetamide (dma) have been chosen. Table 1.1 shows the structure and some properties[50,53,54] of these solvents. This series of solvents affords the opportunity to investigate the influence of solvent structure, particularly steric considerations, on solvent exchange at the somewhat sterically hindered site of exchange on $[M(Me_6tren)(solvent)]^{2+}$. These solvents have been chosen for nmr studies also as a consequence of their wide liquid

Table 1.1

Structure and some physical properties[50,53,54] of the non-aqueous
solvents used in this study.

N,N-dimethylformamide

    dmf

C_3H_7NO

N,N-diethylformamide

    def

$C_5H_{11}NO$

N,N-dimethylacetamide

    dma

C_4H_9NO

Solvent	dmf	def	dma
Molecular weight $(gmol^{-1})$	73.09	101.15	87.12
Freezing temp. at 1 atm.(K)	213	-	253
Boiling temp. at 1 atm.(K)	426	451	439
Dielectric constant at 298K	36.71	-	37.8
Dipole moment (D)	3.86	-	3.72
Donor number	26.6	30.9	27.8

temperature ranges and ability to dissolve the metal complexes studied at the required concentrations.

It is intended to compare solvent exchange rates for these complexes with rates of anionic substitution by various anions. The chosen solvent for this comparison is dmf for several reasons. As suggested by Coetzee[49] dmf is favoured for such studies as a consequence of its low volatility, strong solvating properties and relative ease of purification, storage and handling. Preliminary experiments indicated dmf to be most effective in solvating both metal complex and anionic salts in addition to giving striking colour changes due to anionic substitution (see chapter 4).

It is possible to employ high pressure nmr methods in the elucidation of solvent exchange mechanisms[55,56] with persuasive evidence existing that positive and negative volumes of activation, $\Delta V^{\#}$, are diagnostic of dissociative (d) and associative (a) modes respectively[57-59]. Such data obtained for the complexes of interest here, together with anionic substitution kinetic data, would be useful in determining if these complexes have an increasing tendency to undergo solvent exchange and substitution through an associative (a) activation mode as the electronic occupancy of the d orbitals on the central metal ion decreases. This trend has been observed in solvent exchange for the first-row transition metal series $[M(solvent)_6]^{2+}$ for which $\Delta V^{\#}$ data indicate that for M = V(II), Mn(II) an associatively activated mechanism operates and when M = Fe(II), Co(II), Ni(II) a dissociatively activated mechanism operates[56,60].

1.4 References to chapter 1

1. H. Ackermann, G. Schwarzenbach, Helv.Chim.Acta, 1949, 32, 1543.

2. J.E. Prue, G. Schwarzenbach, Helv.Chim.Acta, 1950, 33, 963.

3. M. Ciampolini, N. Nardi, Inorg.Chem., 1966, 5, 41.

4. M. Ciampolini, N. Nardi, Inorg.Chem., 1966, 5, 1150.

5. M. Ciampolini, N. Nardi, G.P. Speroni, Coord.Chem.Rev., 1966, 1, 222.

6. M. Ciampolini, Chem.Comm., 1966, 47.

7. P. Paoletti, M. Ciampolini, Inorg.Chem., 1967, 6, 64.

8. M. DiVaira, P.L. Orioli, Inorg.Chem., 1967, 6, 955.

9. M. DiVaira, P.L. Orioli, Acta Cryst., 1968, B24, 595.

10. P.C. Jain, E.C. Lingafelter, J.Amer.Chem.Soc., 1967, 89, 724.

11. M. DiVaira, P.L. Orioli, Acta Cryst., 1968, B24, 1260.

12. P.C. Jain, E.C. Lingafelter, J.Amer.Chem.Soc., 1968, 90, 519.

13. C. Furlani, Coord.Chem.Rev., 1968, 3, 141.

14. M. Ciampolini, I. Bertini, J.Chem.Soc. (A), 1968, 2241.

15. L. Sacconi, in "Coordination Chemistry X, Plenary lectures of X ICCC, Tokyo.", 1967; Pure Appl.Chem., 1968, 17, 95.

16. M. Ciampolini, Struct.Bond., 1969, 6, 52.

17. P.L. Orioli, Coord.Chem.Rev., 1971, 6, 285.

18. I. Bertini, M. Ciampolini, P. Dapporto, D. Gatteschi, Inorg.Chem., 1972, 11, 2254.

19. I. Bertini, M. Ciampolini, D. Gatteschi, Inorg.Chem., 1973, 12, 693.

20. I. Bertini, D. Gatteschi, A. Slozzafava, Inorg.Chem., 1975, 14, 812.

21. J.P. Hunt, Coord.Chem.Rev., 1971, 7, 1.

22. D.P. Rablen, H.W. Dodgen, J.P. Hunt, J.Amer.Chem.Soc., 1972, 94, 1771.

23. R.J. West, S.F. Lincoln, Inorg.Chem., 1973, 12, 494.

24. R.J. West, S.F. Lincoln, J.Chem.Soc., Dalton Trans., 1974, 281.

25. H.A. Jahn, E. Teller, Proc.Roy.Soc., 1937, A161, 220.

26. H.A. Jahn, Proc.Roy.Soc., 1938, A164, 117.

27. R. Morassi, I. Bertini, L. Sacconi, Coord.Chem.Rev., 1973, 11, 343.

28. S.G. Zipp, A.P. Zipp, S.K. Madan, Coord.Chem.Rev., 1974, 14, 29.

29. J.H. Coates, G.J. Gentle, S.F. Lincoln, Nature, 1974, 249, 773.

30. R.H. Prince, P.R. Woolley, Angew.Chem., Int.Ed., 1972, 11, 408.

31. M.J. Potasek, P.J. Debrunner, W.H. Morrison Jr., D.H. Hendrickson, J.Chem.Soc. Chem.Comm., 1974, 170.

32. P.L. Orioli, N. Nardi, J.Chem.Soc. Chem.Comm., 1975, 229.

33. C.V. Senoff, Inorg.Chem., 1978, 17, 2320.

34. G. Ferguson, M. Parvez, Acta Cryst., 1979, B35, 2207.

35. S.N. Bhattacharya, C.V. Senoff, Inorg.Chem., 1983, 22, 1607.

36. J.H. Coates, P.R. Collins, S.F. Lincoln, J.Chem.Soc., Faraday Trans. I, 1975, 75, 1236.

37. M. Eigen, R.G. Wilkins, Adv.Chem.Ser., 1965, 49, 55.

38. C.H. Langford, H.B. Gray, in "Ligand Substitution Processes", W.A. Benjamin, N.Y., 1965.

39. J.H. Coates, P.R. Collins, S.F. Lincoln, Aust.J.Chem., 1980, 33, 1381.

40. C. Benelli, D. Gatteschi, Inorg.Chem., 1982, 21, 1788.

41. S.F. Lincoln, A.M. Hounslow, J.H. Coates, Inorg.Chim.Acta, 1983, 77, L7.

42. M.N. Tkaczuk, S.F. Lincoln, Aust.J.Chem., 1979, 32, 1915.

43. L. Banci, C. Benelli, D. Gatteschi, Inorg.Chem., 1984, 23, 3262.

44. J.C. Hempel, M.E. Miller, J.Chem.Phys., 1981, 75, 2959.

45. R.J. Deeth, M. Gerloch, Inorg.Chem., 1985, 24, 4490.

46. P.R. Collins, Ph.D. Thesis, University of Adelaide, 1979.

47. R. Poupko, Z.Luz, J. Chem.Phys., 1972, 57, 3311.

48. D.J. Hewkins, R.H. Prince, Coord.Chem.Rev., 1970, 5, 64.

49. J.F. Coetzee, Pure Appl. Chem., 1977, 49, 27.

50. V. Gutmann, R. Schmid, Coord.Chem.Rev., 1974, 12, 263.

51. B.G. Doddridge, Honours Thesis, University of Adelaide, 1978.

52. B.G. Doddridge, University of Adelaide, unpublished results.

53. J.A. Riddick, W.B. Bunger, in "Techniques of Chemistry", Vol. II,
     "Organic solvents - Physical properties and methods of purification",
     A. Weissberger, ed., third ed., Interscience, N.Y., 1970.

54. R.C. Weast, ed., "CRC Handbook of Chemistry and Physics", 63rd edition.,
     CRC Press, 1983.

55. D.A. Palmer, H. Kelm, Coord.Chem.Rev., 1981, 36, 89.

56. A.E. Merbach, Pure Appl.Chem., 1982, 54, 1479.

57. D.R. Stranks, Pure Appl.Chem., 1974, 38, 303.

58. T.W. Swaddle, Rev.Phys.Chem. Jpn, 1980, 50, 230.

59. Y. Ducommun, K.E. Newmann, A.E. Merbach, Inorg.Chem., 1980, 19, 3696.

60. F.K. Meyer, K.E. Newmann, A.E. Merbach, J.Amer.Chem.Soc., 1979, 101,
     5588.

CHAPTER 2 - THE KINETIC AND EQUILIBRIUM METHODS EMPLOYED

CHAPTER 2 — THE KINETIC AND EQUILIBRIUM METHODS EMPLOYED

2.1. General kinetic principles

2.1.1. Introduction

Before starting any discussion concerning reactions at metal centres it is advantageous to review the environmental features of the solvated metal ion as this is often the precursor of a metal complex. A model of the hydrated metal ion due to Frank and Wen[1,2] may be used to adequately demonstrate these features. In this model the metal ion is at the centre of a series of four concentric regions of water as shown in figure 2.1. The innermost region, A, is the first or primary coordination sphere where the water molecules are bonded through oxygen to the metal ion by electrostatic attraction and are hence highly ordered. Because of the intimate proximity to the metal centre, this region is of major importance in any study of reaction mechanisms at that centre. Region B is the second hydration sphere, where the water molecules are orientated by both electrostatic interaction with the charged metal centre and enhanced hydrogen bonding with polarized water molecules in the primary coordination sphere. The first monolayer of water molecules outside the primary coordination sphere is termed the secondary coordination sphere. The boundary between these coordination spheres is well defined for most ions and any ligand exchange between regions A and B must proceed over this boundary. Region C is the third hydration sphere where water molecules are disordered in orientation due to competitive influences from regions C and D (the bulk water) where orientation of water molecules is influenced only by neighbouring water molecules. Boundaries between regions B, C and D are indistinct and will vary in distance from the metal centre with the charge density of the metal ion.
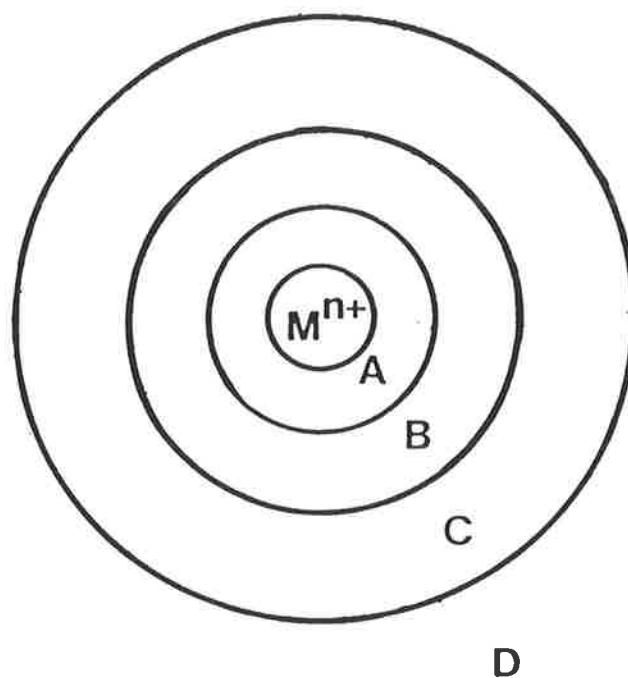
Figure 2.1

A model for the hydrated metal ion.

Region A: first coordination sphere - water molecules highly
   ordered.

Region B: second hydration sphere - water molecules ordered.

Region C: third hydration sphere - water molecules disordered.

Region D: bulk water.

2.1.2. Definition of ligand exchange and substitution processes

The classes of reactions of interest in this study may be defined as follows and these definitions will apply throughout the text. For simplicity, consider a metal ion, M^{n+} which exists in solution of a solvent, S as MS_6^{n+}. In solution the labile solvent molecules in the primary coordination sphere may be replaced by identical solvent molecules from the bulk solvent, S^* (where the asterisk is merely a typographical distinction) in the following manner:

$$MS_6^{n+} + S^* \rightleftharpoons MS_5S^{*n+} + S$$
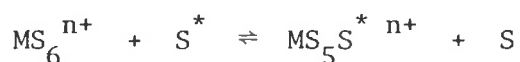
This is ligand exchange or more specifically, and as will be termed in this text, solvent exchange. In solvent exchange no net chemical change occurs as a result of that exchange.

However, if one considers the same species MS_6^{n+} in a solution of solvent, S with a quantity of another chemically distinct solvated species L^{m-} which may act as a unidentate ligand (i.e. occupying one coordination site on the metal) the following reaction may occur:

$$MS_6^{n+} + L^{m-} \rightleftharpoons MS_5L^{(n-m)+} + S$$

Note that for simplicity a solvation sphere around L^{m-} has been omitted although it exists. This is a realistic simplification as most inorganic reaction mechanisms and certainly those considered in this study rely on the assumption that the solvation shell of the substituting ligand is very much more labile than that of the metal ion.

This reaction is termed ligand substitution and differs from solvent exchange as a net chemical change does in this case occur. In addition, if $m > o$ then the ligand L^{m-} is a negatively charged anion and the reaction may be conveniently termed anation.

This is, of course, a very simplistic overview of exchange and substitution reactions and the possible mechanisms of these processes need
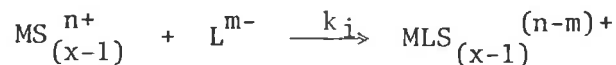
now to be reviewed.

2.1.3. General mechanisms of inorganic exchange and substitution processes

Langford and Gray[3] have postulated four general mechanisms common to inorganic substitution processes. These are the dissociative (D), associative (A) and the interchange mechanisms, dissociative interchange (I_d) and associative interchange (I_a). A mechanism may be characterized by the nature of the transition state, or the reactive intermediate, involved and each mechanism will now be reviewed in turn.

For the purposes of illustration the examples of reacting species will be; solvated metal ion, MS_x^{n+} and solvated ligand, L^{m-},

a) Dissociative (D) mechanism

This mechanism involves an intermediate of reduced coordination and may be viewed as paralleling the classical S_n1 mechanism[4,5].

$$MS_x^{n+} \rightleftharpoons S + MS_{(x-1)}^{n+} \qquad \text{(dissociated intermediate)}$$

$$MS_{(x-1)}^{n+} + L^{m-} \xrightarrow{k_i} MLS_{(x-1)}^{(n-m)+}$$

It may be seen that the entering group is not involved in the generation of the reactive intermediate.

The rate at which this reaction proceeds is dependent only upon the rate at which the leaving group dissociates, which may be equated to the rate of solvent exchange. The reaction rate, k_i would be expected to be independent of the nature of the entering group, L.

(b) Associative (A) mechanism

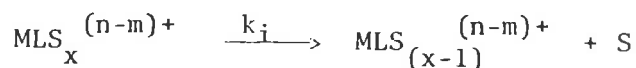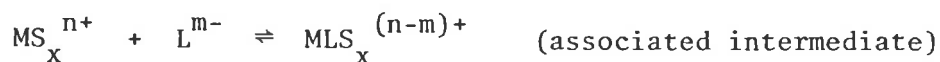This mechanism involves an intermediate of increased coordination, paralleling the classical S_N2 mechanism[4,5],

$$MS_x^{n+} + L^{m-} \rightleftharpoons MLS_x^{(n-m)+} \qquad \text{(associated intermediate)}$$

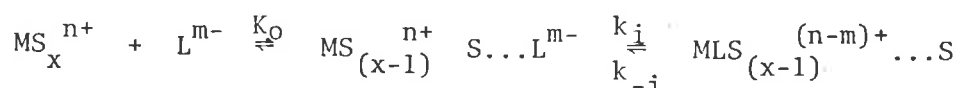$$MLS_x^{(n-m)+} \xrightarrow{k_i} MLS_{(x-1)}^{(n-m)+} + S$$

Here the entering group is actively involved in the formation of the reactive intermediate.

As a result of this involvement the rate of an associative reaction will be dependent on the rate at which the entering group enters the primary coordination sphere of the solvated metal ion and hence dependent on the nature of the entering group and obeying a first-order dependence on the concentration of that group if the latter is present in great excess.

(c) Interchange mechanisms I_d, I_a

The concept of an interchange mechanism is more sophisticated than the simpler dissociative and associative mechanisms outlined above as the reactive intermediate involves both leaving and entering groups.

$$MS_x^{n+} + L^{m-} \overset{K_o}{\rightleftharpoons} MS_{(x-1)}^{n+} S...L^{m-} \overset{k_i}{\underset{k_{-i}}{\rightleftharpoons}} MLS_{(x-1)}^{(n-m)+} ...S$$

<div align="center">encounter complex or
ion-pair</div>

The intermediate formed in this process may be alternatively termed an encounter complex, or more popularly, an ion-pair. Outgoing and incoming ligands move synchronously into and out of the first coordination sphere of the central metal ion throughout the process, so the intermediate formed is not capable of an independent existence and therefore not directly detectable. But it is the degree of bond making and breaking in the formation of this intermediate that will determine the classification of the process which may, in principle, continuously span the conceptual "gap" that exists between that observed for the D mechanism and that observed for the A mechanism.

The dissociative interchange (I_d) mechanism for ligand substitution involves the elongation of a M-S bond followed by interchange with L^{m-} in the encounter complex. One should note that competition exists for the vacancy generated by the bond extension between S (the incipiently

leaving solvent molecule), L^{m-} and solvent molecules in the second coordination sphere.

With $[L^{m-}]$ in large excess over $[MS_x^{n+}]$ the first-order observed rate constant, k_{obs}, for the formation of $MLS_{(x-1)}^{(n-m)+}...S$ is [6]:

$$k_{obs} = \frac{k_i K_0 [L^{m-}]}{1 + K_0 [L^{m-}]} + k_{-i} \qquad (2.1)$$

with k_i = rate constant for the forward interchange step

k_{-i} = rate constant for the backward interchange step

K_0 = equilibrium constant for encounter complex formation

Two limiting conditions exist for this equation. If $K_0 [L^{m-}] << 1$ the equation reduces to $k_{obs} \sim k_i K_0 [L^{m-}] + k_{-i}$ which has a linear dependence on $[L^{m-}]$ with a slope of $k_i K_0$ and an intercept at k_{-i}. Alternatively, at large $[L^{m-}]$ and/or K_0 the pre-equilibrium step forming the encounter pair lies completely to the right and the equation reduces to $k_{obs} \sim k_i + k_{-i}$ with the rate being independent of $[L^{m-}]$. Hence, the form of the curve representing the variation of k_{obs} (ordinate) versus excess anion concentration (abscissa) for a process occuring through an I_d mechanism should be as shown in figure 2.2.

The magnitude of k_i is intimately connected with the ability for L^{m-} to compete with other (solvent) species for the vacancy in the first coordination sphere generated in this mechanism. As the rate determining step for an I_d mechanism may be viewed to be nearly complete dissociation of S, it is to be expected that k_i should be similar in magnitude to the rate constant characterizing solvent exchange on the complex (bond breaking is kinetically important in both mechanisms) and show insignificant variation with the nature of L^{m-}. As the reverse process involves effectively dissociation of L^{m-} from the first coordination sphere of the central metal ion then k_{-i} characterizing that process should by analogy be strongly dependent on the nature of L^{m-}.
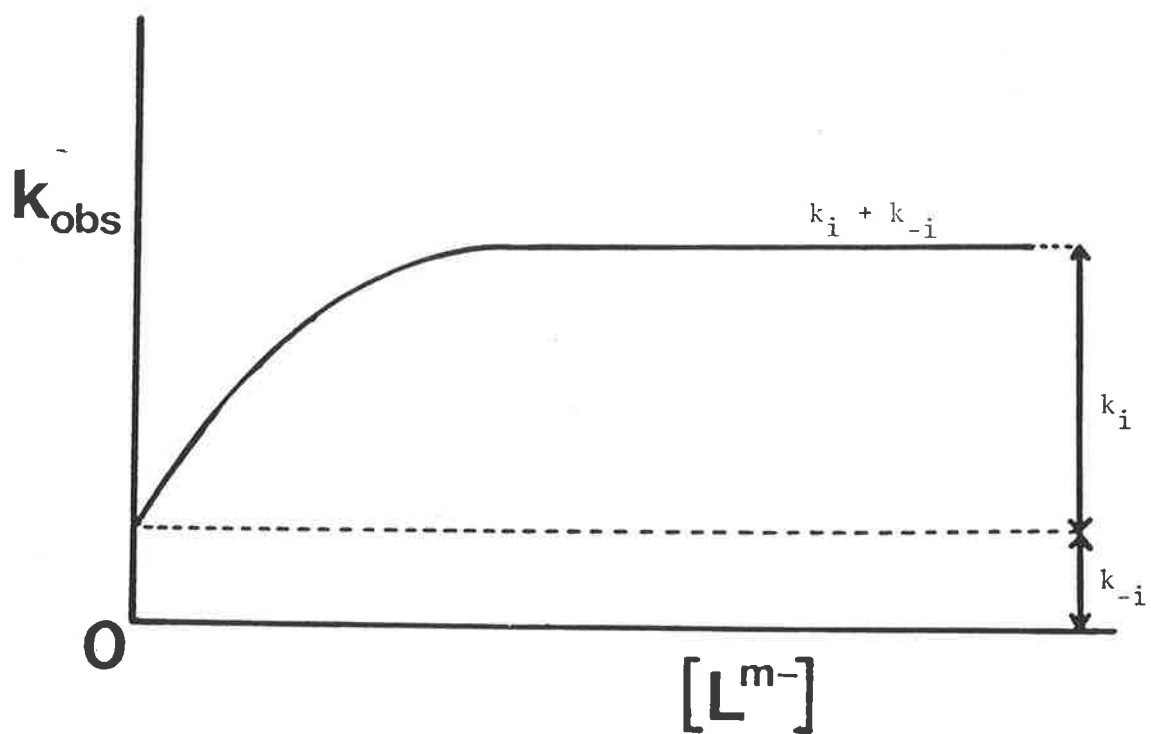
Figure 2.2

Theoretical curve typifying an interchange (I) mechanism.

The associative interchange (I_a) mechanism for ligand substitution involves the formation of a bond between the central metal ion and L^{m-} in the second coordination sphere. The variation of k_{obs} with excess $[L^{m-}]$ characterizing an I_a mechanism is identical to that already expressed for the I_d mechanism (equation 2.1). As bond formation to L^{m-} is the kinetically important step and therefore rate limiting, the magnitude of k_i should be strongly dependent on the nature of L^{m-} and consequently the rate constant characterizing solvent exchange on the complex is not necessarily a constraint upon k_i.

Determination of K_O for labile systems is difficult but K_O may be estimated from the Fuoss equation[7,8] equation 2.2.

$$K_O = \frac{4\pi Na^3}{3000} \frac{z_+ z_- e^2}{\epsilon k_B T} \tag{2.2}$$

where: N $\quad=\quad$ Avagadro's number

$\quad$ a $\quad=\quad$ centre to centre distance between M^{n+} and L^{m-}

$\quad$ $z_+ z_-$ $\quad=\quad$ valency n,m of M^{n+} and L^{m-} respectively

$\quad$ e $\quad=\quad$ charge on an electron

$\quad$ ϵ $\quad=\quad$ dielectric constant of solvent

$\quad$ k_B $\quad=\quad$ Boltzmann constant

$\quad$ T $\quad=\quad$ temperature

The applicability of this equation to metal complexes is questionable as it makes no allowances for stereochemistry and (complicated) effects of species in solution upon the dielectric constant of the medium. However, the Fuoss equation may be useful in some cases as a first approximation for K_O (see section 5.3).

It may be pertinent to point out at this stage that the distinction between I_d and I_a mechanisms, as deduced experimentally, is difficult as such a "grey" area exists between the limiting D and A mechanisms and additional information such as measured volumes of activation (see

section 2.4.3) may be required in any elucidations of this type.

2.2 The Job method of continuous variations

2.2.1. Introduction

It is important in the elucidation of any reaction mechanism to be aware of the nature of the reaction product. For the anation reactions of interest in this study the stoichiometry in solution of the product complexes of type $[M(Me_6tren)X_n]^{(2-n)+}$ (where M = Co(II), Ni(II), Cu(II); $X^- = Br^-$, N_3^-, NCS^-) are required to be determined. A convenient and well understood method of such determinations is the Job method of continuous variations[9] which has been used elsewhere[10-13] successfully in the past.

Consider the following simplified substitution reaction where a ligand, L substitutes for a solvent molecule on a metal centre, M according to the following equation.

$$M + nL \overset{K}{\rightleftharpoons} ML_n$$
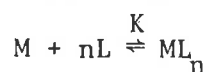
The numerical value of n and the implied stoichiometry of the complex ML_n may be conveniently determined by an adaptation[14-16] of the Job method as follows.

Consider two solutions:

Metal complex M at concentration [M]

Ligand L at concentration [L]

with [M] = r[L]

if one mixes (1-V) volumes of M with V volumes of L with V varying from 0-1 the concentration of ML_n is at a maximum at a value $V = V_{max}$ where

$$K[M]^n \, r^{n-1} \, [(n+r) \, V_{max} - n]^{n+1} = (r-1)^n [n - (n+1)V_{max}]$$

where K is the overall stability constant for complex formation.

For V_{max} to be independent of [M]

$$(n+r) \, V_{max} - n = n - (n+1) \, V_{max}$$

if [M] = [L] then r = 1 and

$$(n+1) V_{max} - n = n - (n+1) V_{max}$$

$$(n+1) V_{max} = n$$

$$n = V_{max}/(1-V_{max})$$

2.2.2 The Job method and its experimental limitations

If one prepares equimolar stock solutions of the solvated metal complex perchlorate salt and of solvated anion salt, by volumetric mixing of these stocks, a series of solution mixtures differing in metal complex to anion concentration ratio can be prepared. The absorbance of each solution is measured spectrophotometrically at a wavelength at which substantial differences in molar absorptivity between the product anated complex, $[M(Me_6tren)X_n]^{(2-n)+}$ and reactant solvated complex, $[M(Me_6tren)dmf]^{2+}$ occur so as to maximize sensitivity. Ideally, the reactant solutions should not absorb at the wavelength selected but it is not always possible to meet this condition. This limitation may be overcome by assuming that a high overall stability constant exists and subtracting, when the absorbing reactant species is in excess, from the experimentally determined solution mixture absorbance a contribution calculated from the known molar absorptivity of the particular reactant species and its assumed excess concentration, using Beer's law. The corrected absorbance is then used in the analysis. The questionable validity of this treatment may be justified by considering the high stability constants found to characterize anation for all systems examined in this study (see chapter 4).

As it is experimentally difficult to prepare precisely equimolar solutions, particularly at a small concentration under anhydrous conditions, it is advantageous to treat solutions not in terms of V, a mixing parameter, but define each solution in terms of mol fraction of metal complex, χ, in that solution mixture

$$\chi_i = \frac{[M]_i}{[M]_i + [L]_i}$$

where $[M]_i$ and $[L]_i$ are the initial concentrations of metal complex and anion respectively in the i_{th} reactant solution mixture.

The Job plot is generated by plotting solution absorbance (corrected if necessary) as the ordinate versus mol fraction of metal complex as the abscissa.

2.2.3 Interpretation of results

If the predominant product of the substitution reaction is a single complex of high overall stability constant, K, then the corresponding Job plot should give a sharp maximum. If the complex is of form ML (n=1) then this maximum is at $\chi = 0.5$ and the complex may be defined as 1:1. If the maximum is somewhat broadened[13] this is indicative of a less stable product complex[16] (with a lower K value), this broadening being qualitatively related to the extent of dissociation of the complex and is a reflection on the magnitude of K. The typical shape of Job plots characterizing a 1:1 species with very high and low overall stability constants are given in figure 2.3. Although one must be cautious not to place too much emphasis on Job plot data[15] the method is nonetheless a useful tool for determining the stoichiometry of complexes in solution and a guide to the magnitude of the overall formation stability constant.
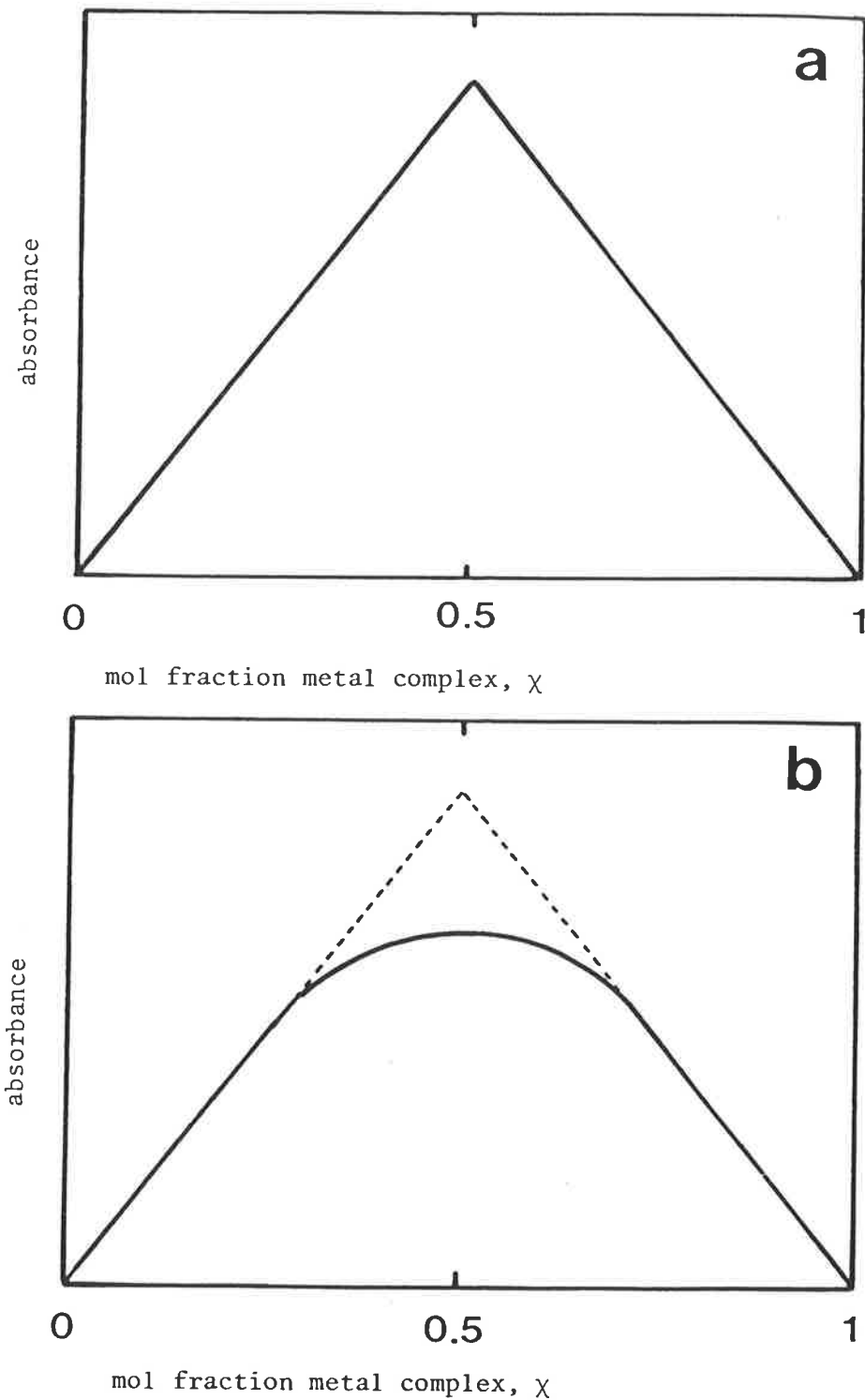
Figure 2.3

Typical Job plots characterizing a 1:1 species with very high (a) and low (b) overall stability constants.

2.3 Stopped-flow spectrophotometry

2.3.1. Introduction

Experimental methods for studying rates of chemical reactions may
be divided into three main classes with respect to the time scale of
reaction which may be satisfactorily followed.

i)   conventional rate studies with reaction half-lives, $t_{\frac{1}{2}} > 10s$
(reaction rate constant, $k \leq 0.069 \ s^{-1}$)

ii)   flow methods where $10^{-3}s \leq t_{\frac{1}{2}} \leq 10s$ ($690s^{-1} \geq k \geq 0.069s^{-1}$)

iii)   relaxation techniques where $t_{\frac{1}{2}} \leq 10^{-2}s$ ($k \geq 690s^{-1}$)

As noted in the introduction (see chapter 1) the reduction in
lability of coordinated dmf in $[M(Me_6tren)dmf]^{2+}$ with respect to that
for the purely solvated metal ion, brings the anion substitution rate
of $[M(Me_6tren)dmf]^{2+}$ in dmf solution broadly into class (ii) above. An
existing stopped-flow apparatus was upgraded (see section 3.4.3) for use
with non-aqueous solutions and data acquisition facilities improved
(see section 3.4.4). The stopped-flow method is convenient as it
combines reagent economy with simplicity of apparatus operation.

2.3.2 General principles and pseudo first-order kinetic trace analysis

The use of flow methods to study rapid reactions is commonplace
and has been discussed in several[17-19] texts. The stopped-flow method
evolved from early work by Hartridge and Roughton who pioneered the
continuous-flow technique[20]. Experimental limitations of this method led
Roughton to develop the stopped-flow method[21] but the method emerged into
prominence with modifications to the stopping device by Gibson[22].

The stopped-flow method involves two reactant solutions flowing
through a mixing chamber which causes rapid and complete mixing before
entry into the observation cell. When the flow is rapidly stopped, a
trigger switch activates spectrophotometric observation of the contents
of the observation cell while the reaction proceeds to completion. A

detailed description of the stopped-flow apparatus used in this study appears in section 3.4.3.

The theory of the method and manner of pseudo first-order reaction trace analysis is as follows[23].

At any time the photomultiplier voltage, V_t, is related to the intensity of light transmitted from the observation cell, I_t, thus,

$$V_t = \text{constant} \times I_t$$

With only reference solution (solvent) in the cell

$$V_o = \text{constant} \times I_o$$

where voltage, V_o, arises from 100% transmission of light of intensity, I_o. Using Beer's law the absorbance may be defined

$$A_t = \log_{10} (I_o/I_t) = \log_{10} (V_o/V_t)$$

Thus an increase in absorbance results in a fall in the signal voltage. Likewise, an increase in optical density results in a rise in the signal voltage. Under appropriate conditions the variation of the voltage as a function of time takes the exponential form as shown in figure 2.4. Symbols appearing in this figure correspond to and define those in this discussion.

Consider the case of a reaction in which the absorbance increases with extent of reaction. The voltage at any time during the reaction, V_t, may be defined with respect to the voltage at reaction completion (infinite time voltage), V_∞, by measuring the voltage difference, y_t (see figure 2.4).

$$V_t = V_\infty + y_t$$

With V_t and V_o known the absorbance can be calculated as shown previously. If, as in all reactions followed by stopped-flow in this study, conditions are made to be those which satisfy first-order kinetics, the estimation
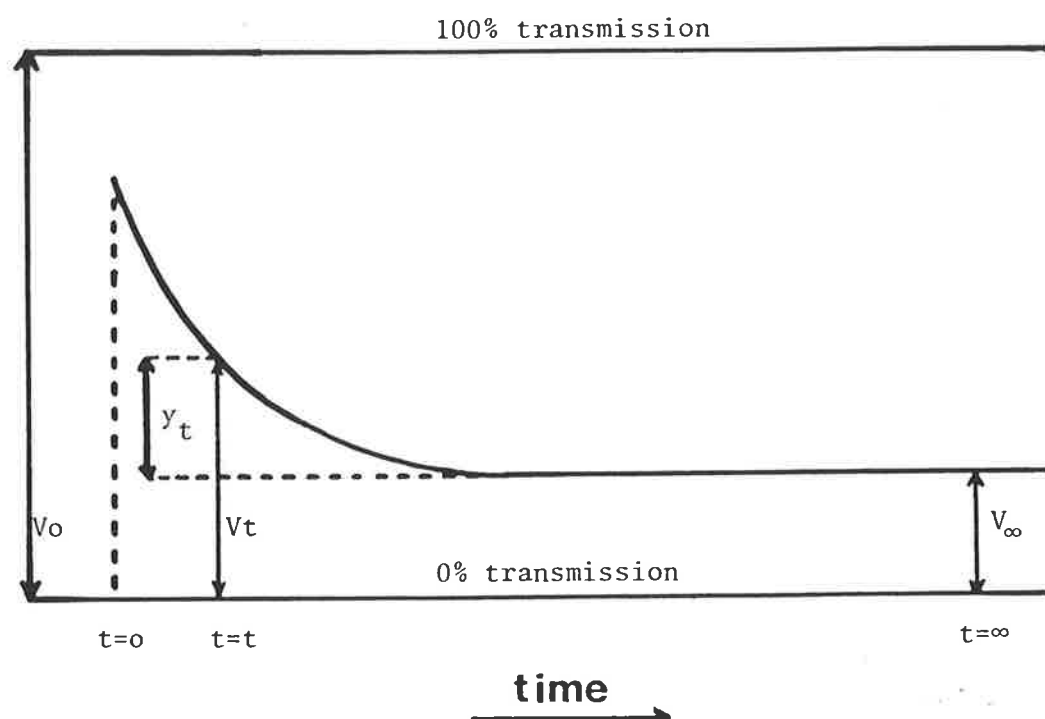
Figure 2.4

Idealized stopped-flow reaction trace for a reaction involving an increase in absorbance with extent of reaction (ie $A_\infty > A_t$, $V_\infty < V_t$).

of the pseudo first-order rate constant characterizing the reaction trace may be made as follows[24].

If the absorbances A_o, A_t and A_∞ at times zero, during the reaction and at reaction completion respectively, are known, then the rate constant, k, may be estimated using the well known first-order rate equation.

$$\ln\left[(A_\infty - A_t)/(A_\infty - A_o)\right] = -kt$$

but

$$A_t = \log_{10}(V_o/V_t)$$

thus

$$A_\infty - A_t = \log_{10}(V_t/V_\infty)$$

similarly

$$A_\infty - A_o = \log_{10}(V_o/V_\infty)$$

substituting for $(A_\infty - A_t)$ and $(A_\infty - A_o)$ in the rate expression above

$$\ln\left\{[\log_{10}(V_t/V_\infty)]/[\log_{10}(V_o/V_\infty)]\right\} = -kt$$

as values of V_o and V_∞ are constant

$$\ln[\log_{10}(V_t/V_\infty)] = constant - kt$$

Similarly, for a reaction involving a decrease in absorbance with extent of reaction

$$\ln[\log_{10}(V_\infty/V_t)] = constant - kt$$

Note that this treatment does not require the value of V_o to be known to obtain k.

It may be easily seen that if one plots a series of $\ln[\log_{10}(V_t/V_\infty)]$ data points as ordinate against the corresponding values of t as abscissa the slope of the resulting straight line will give rise to an estimate of the first-order rate constant.

2.3.3 Determination of activation parameters

The preceeding section has dealt with the method for obtaining the pseudo first-order rate constant, k, from the stopped-flow experiment. However, useful insight into reaction mechanism can be attained by

consideration of the activation parameters $\Delta H^{\#}$, the enthalpy of activation and $\Delta S^{\#}$, the entropy of activation.

Transition state theory[25] gives the following expression for the temperature dependence of rate constants,

$$k = \frac{k_b T}{h} \ e^{-\Delta H^{\#}/RT} \ e^{\Delta S^{\#}/R}$$

where: k_b = Boltzmann constant

T = Absolute temperature

h = Plank constant

R = Gas constant

Fitting of experimentally determined values of k measured at a variety of temperatures by a non-linear least-squares procedure will result in optimized values for $\Delta H^{\#}$ and $\Delta S^{\#}$.

2.3.4 Limitations of the stopped-flow technique

Although the application of the method is limited by inherent broad time scale restrictions (see section 2.3.1.), certain design features can significantly improve performance[18]. Of these design features, mixing efficiency and observation cell path length particularly influence the "dead-time" of a specific instrument. The dead-time may be defined as the time period elapsing between when the reaction is initiated (upon mixing) and when monitoring of the reaction in the observation cell commences. This factor is of some importance in determining whether the method is suitable to follow a specific reaction particularly when the reaction half-life is small, say, several milliseconds. The dead-time of the instrument used in this study was determined by the method of Gutfreund[26] and found to be of the order of 2 milliseconds.

2.4 Nuclear magnetic resonance (nmr) spectroscopy

2.4.1 Introduction and the paramagnetic effect

This study concerns itself in part with the examination of solvent exchange processes on paramagnetic metal centres utilizing nuclear magnetic resonance (nmr) spectroscopy. Other researchers have done this before for both paramagnetic[27-29] and diamagnetic[30-32] systems. Some excellent reviews[33-35] have appeared in the literature on this subject which encompass most aspects of the technique. As a consequence of this only a brief review of the theory pertinent to this particular study follows.

Copper(II), cobalt(II) and high-spin nickel(II) are paramagnetic metal ions with electron spin, S of 1/2, 3/2 and 1 respectively. During the solvent exchange process, the interchange of solvent coordinated to a paramagnetic metal ion of a metal complex and bulk solvent means molecules from the bulk solvent continually come into contact with the paramagnetic centre and then return back to their original environment. The dramatic change in magnetic environment from that of coordinated to free solvent molecule is reflected in changes in chemical shift, ω and transverse relaxation time, T_2. The modulation of the bulk solvent nmr signal caused by exchange produces a variation in both the observed chemical shift, ω_{obs} and signal line width at half maximum amplitude $\nu_{\frac{1}{2}}$ of the solvent with respect to that for the solvent in the absence of a paramagnetic species.

In studies concerning diamagnetic systems one may use complete line-shape analysis of coordinated and free solvent resonances under both slow and fast exchange conditions. However, in studies concerning paramagnetic systems the coordinated solvent resonance is too broad to allow complete lineshape analysis[36] as for diamagnetics. This problem has been overcome by Swift and Connick in their celebrated treatment which will now be described.

2.4.2 Nmr kinetic theory

The wide use of nmr spectroscopy in the study of ligand exchange processes has stemmed from the development of a set of equations describing the nmr kinetic experiment by Swift and Connick[37,38] derived through the phenomenological Block equations[39,40] modified to account for chemical exchange[41]. The type of exchanging system applicable to the systems examined in this study is one in which a diamagnetic species is exchanging with one that is paramagnetic as described in the preceeding section 2.4.1. The following treatment applies to this class of system in dilute[35] solution where the mol fraction of solvent coordinated to the paramagnetic site is less than 0.05[42].

The experimentally determined transverse relaxation time of the observed nucleus in a solvent molecule in, say, bulk solvent, T_{2ref} is related to the nmr resonance line width by the following

$$T_{2ref} = \frac{1}{\Pi \nu_{\frac{1}{2}}} \ sec^{-1}$$

where $\nu_{\frac{1}{2}}$ is the full line width (in Hertz) at half maximum intensity. As detailed earlier in section 2.4.1 the introduction of a paramagnetic metal complex into the system will cause a broadening of the bulk solvent resonance linewidth. This is reflected in the relaxation parameter characteristic of exchange at the paramagnetic site, T_{2p} which may be defined in terms of the experimentally determined transverse relaxation time for the solution, T_2 and that similarly determined for a reference solution, T_{2ref} thus

$$T_{2p}^{-1} = T_2^{-1} - T_{2ref}^{-1}$$

To correct for any viscosity effects a reference solution of pure solvent with an added diamagnetic entity of similar structure and in identical concentration to the paramagnetic species under study is used rather than a simple solvent reference. This procedure will allow for any minor difference in magnetic susceptibility between solvent coordinated to the

diamagnetic reference compound and pure solvent.

Swift and Connick[37,38] derived expressions for the effect of solvent exchange on T_2 and $\Delta\omega$, the chemical shift for the nmr resonance line of bulk solvent molecules in the presence of a paramagnetic species relative to that of pure solvent. However, subsequent results[43] have shown that these expressions require modification to account for contributions arising from effects outside of the first coordination sphere of the exchanging species. The modified expressions are given by equations 2.3 and 2.4.

$$T_{2p}^{-1} = \frac{P_m}{\tau_m} \left[\frac{T_{2m}^{-2} + (T_{2m}\tau_m)^{-1} + \Delta\omega_m^{2}}{(T_{2m}^{-1} + \tau_m^{-1})^2 + \Delta\omega_m^{2}} \right] + \frac{P_m}{T_{2o}} \tag{2.3}$$

$$\Delta\omega = \frac{P_m \Delta\omega_m}{(\tau_m/T_{2m} + 1)^2 + \tau_m^{2} \Delta\omega_m^{2}} + P_m\Delta\omega_o \tag{2.4}$$

where: P_m = mol fraction of coordinated solvent

τ_m = mean residence time of solvent in the first coordination sphere

T_{2m} = transverse relaxation time of coordinated solvent

$\Delta\omega_m$ = chemical shift between coordinated and bulk solvent

T_{2o} = contribution to T_{2p} arising from outside the first coordination sphere

$\Delta\omega_o$ = contribution to $\Delta\omega$ arising from outside the first coordination sphere

The introduction of these outer-sphere terms T_{2o} and $\Delta\omega_o$ allow for long-range dipolar magnetic interactions[44].

One can identify four different exchange regions by simplifying equation 2.3 under a series of limiting conditions

(i) very slow exchange limit

At low temperatures when the exchange rate is very slow with respect

to the nmr time scale, $\tau_m^{-1} \ll T_{2m}^{-1}$, $\Delta\omega_m$ and equation 2.3 reduces to

$$1/T_{2p} = 1/T_{2o}$$

This region contains no chemical exchange parameters but characterizes outer-sphere effects.

(ii) slow exchange limit

At higher temperatures, $\tau_m^{-1} \sim T_{2m}^{-1} \ll \Delta\omega_m$ and equation 2.3 reduces to

$$1/T_{2p} = 1/\tau_m$$

This region contains the wealth of kinetic information required to determine chemical exchange parameters.

(iii) fast exchange limit

At still higher temperatures, $\tau_m^{-1} > \Delta\omega_m$ and equation 2.3 reduces to

$$1/T_{2p} = \tau_m \, \Delta\omega_m^2$$

Kinetic information is attainable in this region provided $\Delta\omega_m$ can be measured.

(iv) very fast exchange limit

At high temperatures $\tau_m^{-1} \gg T_{2m}^{-1}$, $\Delta\omega_m$ and equation 2.3 reduces to

$$1/T_{2p} = 1/T_{2m}$$

No chemical exchange information is contained in this region.

These different exchange regions (i)-(iv) may be combined to produce a temperature dependence of $\ln(T_{2p})$ on reciprocal temperature as shown in figure 2.5.

The residence time, τ_m is intimately related to the pseudo first-order solvent exchange rate constant, k_{ex}, the temperature dependent form of which comes from transition state theory[45] and is given by the Eyring expression

$$\tau_m^{-1} = k_{ex} = \frac{k_b T}{h} \, e^{-\Delta H^{\#}/RT} \, e^{\Delta S^{\#}/R}$$
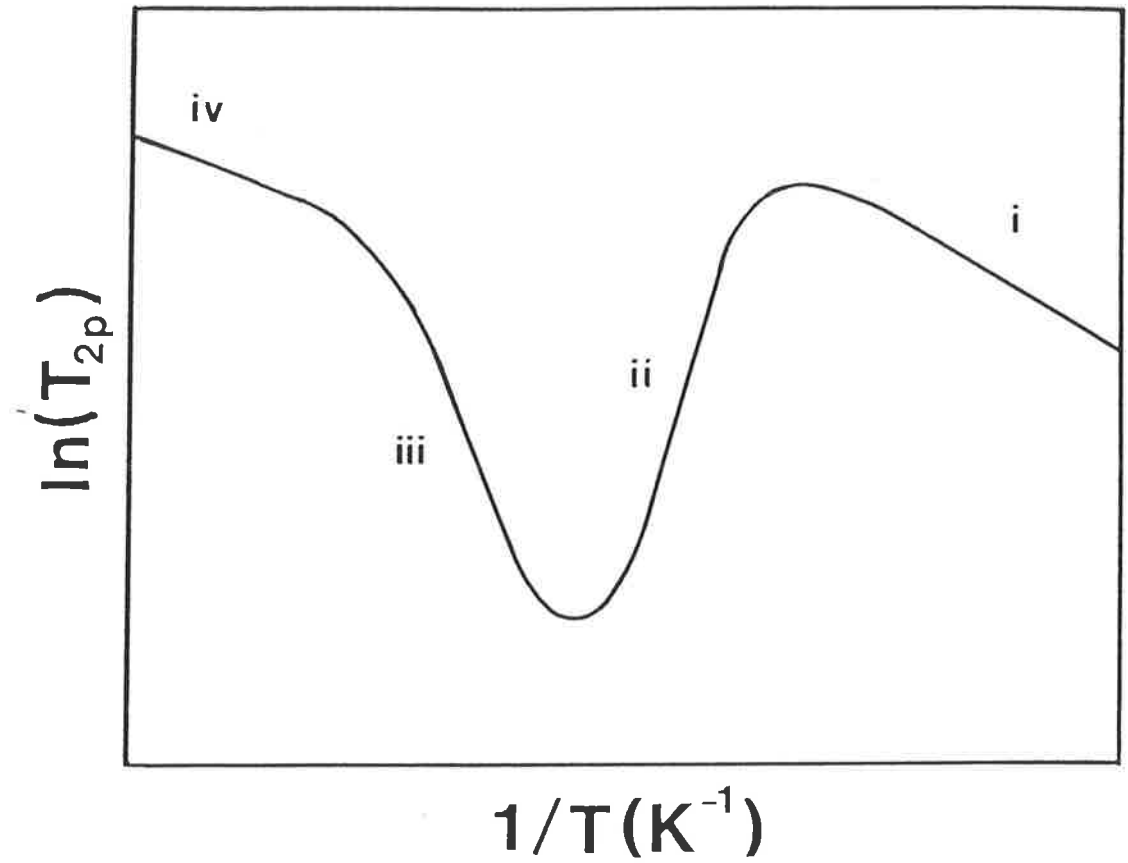
Figure 2.5

Temperature dependence of $\ln(T_{2p})$. Regions (i)-(iv) represent the series of limiting conditions to equation 2.3 referred to in the text.

where the symbols have their usual significance. Fitting of experimental data characterizing the very slow and slow exchange regions (regions (i) and (ii) above respectively) by a non-linear least-squares fit computer program can yield[44] optimized values for k_{ex}, activation parameters $\Delta H^{\#}$, $\Delta S^{\#}$ and outer-sphere activation terms A_o, E_o subject to the following function

$$(P_m T_{2p})^{-1} = \tau_m^{-1} + T_{2o}^{-1} = \frac{k_b T}{h} \ e^{-\Delta H^{\#}/RT} \ e^{\Delta S^{\#}/R} + A_o \ e^{-E_o/RT}$$

where: A_o = pre-exponential activation term characterizing outer-sphere relaxation

E_o = activation energy characterizing outer-sphere relaxation

This relation demonstrates the applicability of variable temperature nmr in the determination of exchange parameters useful in giving some mechanistic insight into the detailed nature of the exchange process.

2.4.3 Variable pressure nmr kinetic theory

As all variable pressure work was performed by Prof. A.E. Merbach and co-workers outside of this laboratory only a brief overview of the theory of variable pressure nmr kinetics appears here.

According to transition state theory[46,47] the volume of activation, $\Delta V^{\#}$ is related to the exchange rate constant, k as follows

$$\Delta V^{\#} = -RT \ (\partial \ln k/\partial P)_T \tag{2.5}$$

It is conventional to express $\Delta V^{\#}$ in terms of the zero pressure volume of activation, $\Delta V_o^{\#}$ and the (pressure independent) compressibility coefficient of activation, $\Delta \beta^{\#}$ thus

$$\Delta V^{\#} = \Delta V_o^{\#} - \Delta \beta^{\#} P \tag{2.6}$$

Combining the integrated form of equation 2.5 with equation 2.6 one obtains an expression for the pressure dependence of the exchange rate constant as follows

$$\ln k = \ln k_o - \Delta V_o^{\#} P/RT + \Delta\beta^{\#}/2RT$$

where k_o is the zero pressure rate constant. Thus if one obtains experimentally a data set of k and P values at a single temperature a non-linear least-squares fitting procedure may be used to optimize k_o, $\Delta V^{\#}$ and $\Delta\beta^{\#}$ parameters. The significance of volume of activation data with respect to the elucidation of solvent exchange and anation mechanisms has been treated in the literature[48,49].

2.5 References to chapter 2

1. H.S. Frank, W.Y. Wen, Discuss. Faraday. Soc., 1957, 24, 133.

2. B.G. Cox, G.R. Hedwig, A.J. Parker, D.W. Watts, Aust.J.Chem., 1974, 27, 477.

3. C.H. Langford, H.B. Gray, in "Ligand Substitution Processes", W.A. Benjamin, N.Y., 1965.

4. C.K. Ingold, in "Structure and Mechanism in Organic Chemistry", Chapter 7, Cornell University Press, N.Y., 1953.

5. J. Burgess, in "Metal Ions in Solution", Chapter 11, Ellis Horwood, Chichester, 1978.

6. M. Eigen, R.G. Wilkins, Adv.Chem.Ser., 1965, 49, 55.

7. R.M. Fuoss, J.Amer.Chem.Soc., 1957, 79, 3301.

8. R.M. Fuoss, J.Amer.Chem.Soc., 1958, 80, 5059.

9. P. Job, Ann.Chim.Paris, 1928, 9, 113.

10. W.C. Vosburgh, G.R. Cooper, J.Amer.Chem.Soc., 1941, 63, 437.

11. R.L. Moore, R.C. Anderson, J.Amer.Chem.Soc., 1945, 67, 167.

12. R.T. Foley, R.C. Anderson, J.Amer.Chem.Soc., 1948, 70, 1195.

13. G. Schwarzenbach, Helv.Chim.Acta, 1949, 32, 839.

14. D.M.M.A. Hadi, Ph.D. Thesis, University of Adelaide, 1981.

15. F.J.C. Rossotti, H. Rossotti, in "The Determination of Stability Constants", Chapter 3, McGraw-Hill, N.Y., 1961.

16. G. Pass, H. Sutcliffe, in "Practical Inorganic Chemistry", second ed., Chapter 17, Chapman and Hall, London, 1974.

17. E.F. Caldin, in "Fast Reactions in Solution", Blackwell Scientific, London, 1964.

18. B. Chance, in "Techniques of Chemistry", Vol. VI, "Investigation of Rates and Mechanisms of Reactions", part 2, G.G. Hammes, ed., third ed., Chapter II, Wiley, N.Y., 1974.

19. C.F. Bernasconi, in "Relaxation Kinetics", Academic Press, N.Y., 1976.

20. H. Hartridge, F.J.W. Roughton, Proc.Roy.Soc.A, 1923, 104, 376.

21. F.J.W. Roughton, Proc.Roy.Soc.B, 1934, 115, 473.

22. see ref. [51], Chapter 3 of Caldin, "Fast Reactions in Solution", (17).

23. P. Moore, in "Stopped-Flow. An experimental Manual", University of Warwick, 1972.

24. A.A. Frost, R.G. Pearson, in "Kinetics and Mechanism", second ed., Wiley, N.Y., 1961.

25. G.G. Hammes, in "Principles of Chemical Kinetics", Academic Press, N.Y., 1978.

26. H. Gutfreund, in "Enzymes: Physical Principles", page 179, Wiley, London, 1975.

27. R.J. West, S.F. Lincoln, Aust.J.Chem., 1971, 24, 1169.

28. R.J. West, S.F. Lincoln, Inorg.Chem., 1972, 11, 1688.

29. R.J. West, S.F. Lincoln, Inorg.Chem., 1973, 12, 494.

30. R.P. Bowen, S.F. Lincoln, E.H. Williams, Inorg.Chem., 1976, 15, 2126.

31. J. Crea, R. Digiusto, S.F. Lincoln, E.H. Williams, Inorg.Chem., 1977, 16, 2825.

32. G.J. Honan, S.F. Lincoln, E.H. Williams, J. Solution Chem., 1978, 7, 443.

33. G.N. LaMar, W. DeW. Horrocks, R.H. Holm, eds, in "Nmr of Paramagnetic Molecules", Academic Press, N.Y., 1980.

34. E.D. Becker, in "High Resolution Nmr", second ed., Academic Press, N.Y., 1980.

35. T.R. Stengle, C.H. Langford, Coord.Chem.Rev., 1967, 2, 349.

36. S.F. Lincoln, Prog.React.Kinet., 1977, 9, 1.

37. T.J. Swift, R.E. Connick, J. Chem.Phys., 1962, 37, 307.

38. T.J. Swift, R.E. Connick, J.Chem.Phys., 1964, 41, 2553.

39. F. Block, Phys.Rev., 1946, 70, 460.

40. T.J. Swift, in "Techniques of Chemistry", Vol. VI, "Investigation of Rates and Mechanisms of Reactions", G.G. Hammes, ed., third ed., Chapter XII, Wiley, N.Y., 1974.

41. H.M. McConnell, J.Chem.Phys., 1950, 28, 430.

42. R.J. West, Ph.D. Thesis, University of Adelaide, 1973.

43. Z. Luz, S. Meiboom, J.Chem.Phys., 1964, 40, 2686.

44. K.E. Newman, F.K. Meyer, A.E. Merbach, J.Amer.Chem.Soc., 1979, 101, 1470.

45. S. Glasstone, K.J. Laidler, H. Eyring, in "Theory of Rate Processes", McGraw-Hill, N.Y., 1941.

46. H. Eyring, J.Chem.Phys., 1935, 3, 107.

47. M.G. Evans, M. Polanyi, Trans. Faraday Soc., 1935, 31, 875.

48. A.E. Merbach, Pure Appl. Chem., 1982, 54, 1479.

49. D.A. Palmer, H. Kelm, Coord. Chem. Rev., 1981, 36, 89.

CHAPTER 3 - EXPERIMENTAL DETAILS AND APPARATUS EMPLOYED

CHAPTER 3 - EXPERIMENTAL DETAILS AND APPARATUS EMPLOYED

3.1. Source, purification and analysis of chemicals

3.1.1. Solvents

All water used in this study was deionised then distilled. Dmf (BDH) was purified by the following method[1]. The LR commercial solvent was shaken with anhydrous AR copper sulphate (BDH) (ca 4.0g per litre of solvent) and kept stoppered for ca 3 days prior to fractional distillation under reduced pressure with a dry nitrogen bleed. The initial and final 10% fractions of distillate were discarded. The pure solvent was stored sealed over 4A molecular sieves and under dry nitrogen at 238 K until required. This method has been found[2] to produce solvent of very high purity, being relatively free of amine hydrolysis products and also highly anhydrous.

Def (Fluka) was purified in the same manner. Anhydrous, redistilled dma and CH_3CN were obtained from Dr. S.F. Lincoln and were used without further purification.

Purified dmf and def were analysed for contaminants by ^{13}C and ^{1}H nmr and in the case of dmf, for water content by solution infrared spectroscopy. The results of these analyses showed the products to be pure and anhydrous.

3.1.2. Deuterated solvents

CD_3NO_2 and $(CD_3)_2SO$ (Stohler) were purified by fractional distillation and dried over 4A molecular sieves prior to analysis by ^{13}C nmr for purity. Solvents thus obtained were stored sealed over active sieves and under dry nitrogen at room temperature until required.

3.1.3. Anion Salts

NaSCN (Ajax), NaN_3 (BDH) and NaBr (Univar) were obtained as AR salts and recrystallized from water. The recrystallized products were oven dried at 355K for several days prior to drying under vacuum at 325K until removal of water was complete as determined by infrared spectroscopy. One day of vacuum drying was usually sufficient for this purpose. The infrared spectra of

NaSCN and NaN$_3$ were compared with literature standards[3,4] and found to be anhydrous. NaBr does not absorb appreciably[4] in the infrared wavenumber region 4000-500cm^{-1} (the working range of the spectrophotometer available) and thus even the observed absence of any water bands in the spectrum is of questionable significance. However, metal analysis (see section 3.2.2) on duplicate samples of the dried NaBr salt indirectly indicated the anhydrous nature of the product. Analysis calculated for NaBr: Na, 22.3% Found: Na, 22.3%.

A sample of NaSCN was dried by the more rigorous but also more laborious method used to dry water impregnated [Cu(Me$_6$tren)ClO$_4$]ClO$_4$ (see section 3.2.2) but the resulting product was found to be identical to that obtained by the preferred vacuum drying method just described.

All anion salts were stored sealed in a dry box continuously.

3.1.4. Perchlorate salts

NaClO$_4$ (BDH) was obtained as the AR salt, recrystallized from water and dried in the same manner as for anion salts. The purified dry salt was stored sealed in the dry box until required. Nujol mull and solution infrared spectra were periodically used to determine any water content in NaClO$_4$ crystals and dmf solutions respectively and no evidence of bound or unbound water was found.

Hydrated perchlorates of divalent cobalt (BDH), nickel (BDH), and copper (Fluka) were obtained as AR salts. These were used without further purification and stored in sealed containers until required.

3.1.5. Dehydrating agents[5]

Phosphorous pentoxide LR (May & Baker) for use in the dry box was used as obtained. Molecular sieves (4A) (BDH) were washed in AR ethanol followed by copious amounts of double distilled water and regenerated by heating at 620K for ca 12 hours being continually flushed with dry nitrogen. Sieves were stored tightly sealed in the dry box until required.

Only sieves regenerated in this manner were used as troublesome micro-fine sieve dust normally associated with newly acquired commercial sieves is eliminated by this process. Triethylorthoformate (Fluka) was AR and used without further purification.

3.2 Preparation, purification and analysis of the metal complexes

3.2.1. Me$_6$tren ligand

The ligand 2,2',2"-tris(dimethylamino)triethylamine, Me$_6$tren, was prepared from commercially available solid tren.3HCl (Strem) or liquid tren free base (Strem) by an adaptation[6] of the method employed by Ciampolini and Nardi[7], shown schematically in figure 3.1. It has been noted previously[8] that commercially available liquid tren is contaminated with ca 5% N,N'-di(2-aminoethyl)-ethylene diamine, trien impurity thus necessitating acidification/recrystallization steps[9-11] to obtain pure tren.3HCl before the ligand preparation process can proceed. No such trien impurity has been found[8] to exist in the commercial tren.3HCl.

Pure tren.3HCl was refluxed at 393K with 38% formaldehyde solution (Ajax) and 98% formic acid (Searle) (3 and 1.5 molar excess over the ligand hydrochloride respectively) for 9 hours. The solvent was then removed by rotary evaporation leaving a pale yellow oily residue of crude Me$_6$tren.3HCl which solidified on cooling to room temperature. An ion exchange column[12] was prepared containing sufficient Amberlite IRA-400 resin (BDH) in the chloride bound form to completely react, when activated, with the ligand hydrochloride. This column was activated to the hydroxide bound form with 1 Molar sodium hydroxide until the effluent was basic as determined by wide range pH indicator strips (Merck) then washed with water until the effluent was likewise tested to be neutral. The crude Me$_6$tren.3HCl was dissolved in water and slowly passed through the column twice with water as elutant and with the column being reactivated between passes in the same manner as for the initial activation. The collected effluent thus treated contained crude Me$_6$tren free base in water. The water was removed by azeotropic distillation with sodium dried benzene (May & Baker) using a Dean-Stark apparatus[13]. After extraction of water was completely effected by this process benzene was removed by rotary evaporation leaving a dark
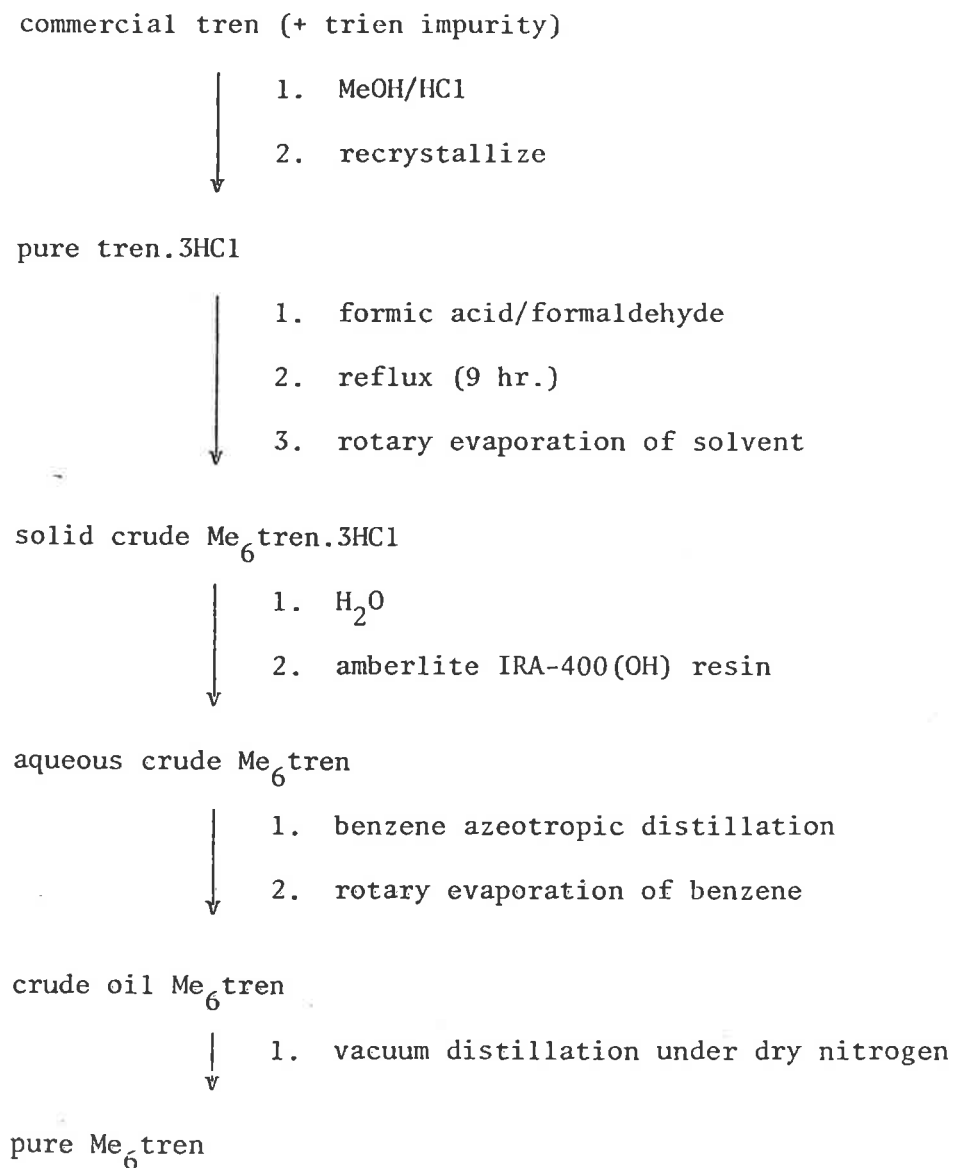
commercial tren (+ trien impurity)

      1.   MeOH/HCl

      2.   recrystallize

pure tren.3HCl

      1.   formic acid/formaldehyde

      2.   reflux (9 hr.)

      3.   rotary evaporation of solvent

solid crude Me_6tren.3HCl

      1. H_2O

      2.   amberlite IRA-400(OH) resin

aqueous crude Me_6tren

      1.   benzene azeotropic distillation

      2.   rotary evaporation of benzene

crude oil Me_6tren

      1.   vacuum distillation under dry nitrogen

pure Me_6tren

Figure 3.1

Schematic representation of the method for preparation of Me_6tren ligand.

yellow oil. Pure colourless Me_6tren liquid was obtained by vacuum distillation[13] under nitrogen. For each Me_6tren preparation effected in this manner the yield of pure ligand exceeded 90%.

The product was analyzed for purity by ^{13}C nmr spectroscopy on a Brüker WP80 spectrometer. Me_6tren ligand has three magnetically non-equivalent carbon environments (see figure 3.2.(i)) and thus the ^{13}C nmr spectrum of this product should show three resonances. This was found to indeed be the case (see figure 3.2.(ii)). As a consequence of the Nuclear Overhauser effect[14] relative peak areas may be considered accurate only to within ca 10%[15]. However, relative resonance peak integrals (see figure 3.2.(ii)) seem to be in accordance with expectation.

3.2.2. Metal complexes

The complex perchlorate salts of copper(II) and zinc(II) containing Me_6tren ligand of type $[M(Me_6tren)ClO_4]ClO_4$ were the first preparations attempted in this study. These complexes were prepared in an improved[6] manner to that previously described by Ciampolini and Nardi[7]. However, infrared analysis of the crystalline product showed a broad band above $3000cm^{-1}$ characteristic of the presence of water of crystallization. This water of crystallization was found difficult to remove in vacuum so removal of this water from the product was effected by the following method as illustrated for the copper (II) complex.

The complex (3.7g) was dissolved in dry dmf ($10cm^3$) at 340K, triethylorthoformate (BDH)(13.4g) added and the mixture stirred at this temperature for one hour. This dehydration step involves an acid catalyzed dehydration resulting in the conversion of aquo species to ethanol by triethylorthoformate[16]. Upon cooling the crystalline product $[Cu(Me_6tren)dmf](ClO_4)_2$ precipitated and a further crop was obtained with the addition of sodium dried ether (BDH). The combined products were filtered off, washed with ether under dry nitrogen and dried under vacuum
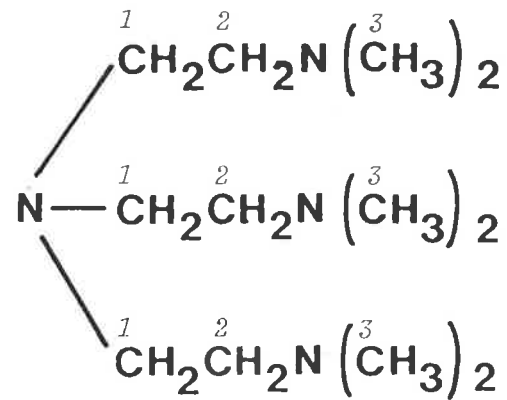
$$\begin{array}{c} \overset{1}{C}H_2\overset{2}{C}H_2N\left(\overset{3}{C}H_3\right)_2 \\ \diagup \\ N-\overset{1}{C}H_2\overset{2}{C}H_2N\left(\overset{3}{C}H_3\right)_2 \\ \diagdown \\ \overset{1}{C}H_2\overset{2}{C}H_2N\left(\overset{3}{C}H_3\right)_2 \end{array}$$

Figure 3.2.(i)

Structural formula for Me_6tren ligand showing three distinct carbon environments denoted by *1,2,3* typographical distinctions.
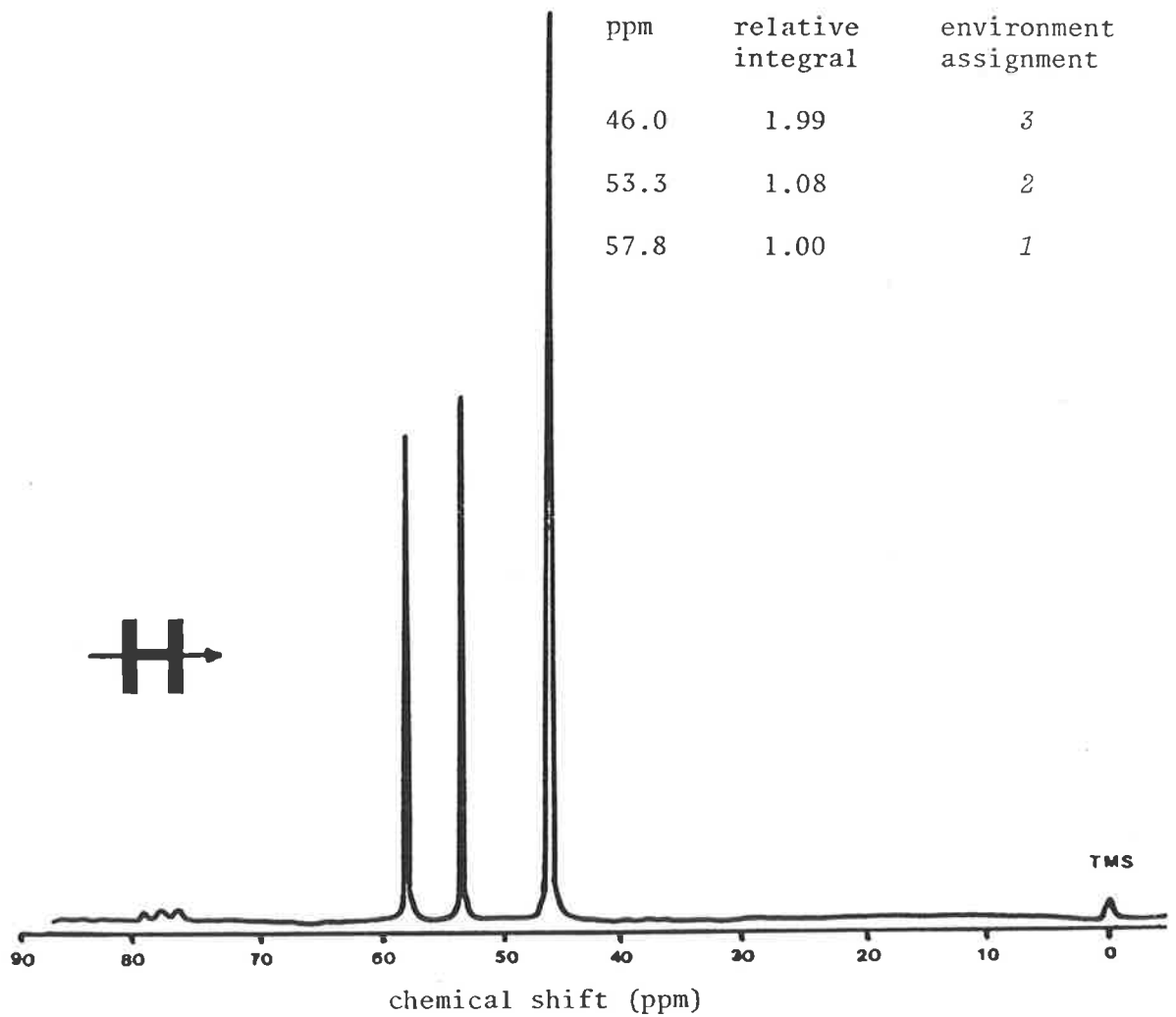

ppm	relative integral	environment assignment
46.0	1.99	*3*
53.3	1.08	*2*
57.8	1.00	*1*

chemical shift (ppm)

Figure 3.2.(ii)

[13]C nmr broad band decoupled spectrum of pure Me_6tren in $CDCl_3$ solution with 2% tetramethylsilane as reference.

at ambient temperature for 6 hours. $[Zn(Me_6tren)dmf](ClO_4)_2$ was similarly

prepared. Excellent elemental analysis were obtained (see table 3.1) for

both complexes and the infrared spectra of both salts exhibited no water

bands.

A simpler, one step procedure[17] similar to that of van Leeuwen and

Groeneveld[18] was employed in subsequent complex preparations. The

appropriate hydrated metal perchlorate (x mol) was dissolved in

triethylorthoformate (10x mol) and stirred at 330K for one hour. A silica

gel guard tube was employed to exclude atmospheric water vapour. A

mixture of Me_6tren ligand (1.1x mol) and the appropriate ligand (either

dmf, def, dma or CH_3CN to occupy the fifth coordination site on the central

metal ion in the complex)(10x mol) was prepared and added dropwise to the

metal solution with stirring. Crystals of the complex salt precipitated

immediately but stirring was continued at 330 K for another hour. The

mixture was then allowed to cool and crystals filtered by gravity, washed

with ether under dry nitrogen and dried under vacuum at ambient temperature

for 6 hours. All preparations in this manner proceeded in ca 90% yield.

The infrared spectra in Nujol mull of all salts prepared in this

manner showed no O-H stretch due to water of crystallization. Infrared

spectroscopic analysis of each of the complexes prepared also allows

characterization of the bonding nature of perchlorate by the number of

bands present at around 626 cm^{-1} as being[19]:

(i)   free (ionic), T_d symmetry - one band

(ii)   coordinated (unidentate), C_{3v} symmetry - two bands

(iii) coordinated (bidentate), C_{2v} symmetry - three bands

This type of analysis has its limitations[20] in some cases but can be,

albeit with reservation, informative[19,21] as a single band in this region

indicates the presence of ionic perchlorate and two or more bands indicate

coordinated perchlorate of particular symmetry. Each of the metal complexes

Table 3.1 Analytical results for metal complexes

Compound		% Metal	% C	% H	% N
$[Cu(Me_6tren)dmf](ClO_4)_2$	calc.	11.2	31.8	6.6	12.4
	fnd.	11.2	31.8	6.5	12.2
$[Cu(Me_6tren)def](ClO_4)_2$	calc.	10.7	34.4	6.9	11.8
	fnd.	10.9	34.3	6.9	11.7
$[Cu(Me_6tren)dma](ClO_4)_2$	calc.	11.0	33.1	6.8	12.1
	fnd.	11.3	32.4	6.5	11.8
$[Cu(Me_6tren)CH_3CN](ClO_4)_2$	calc.	11.9	31.5	6.2	13.1
	fnd.	12.0	31.2	6.3	13.0
$[Ni(Me_6tren)dmf](ClO_4)_2$	calc.	10.5	32.1	6.7	12.5
	fnd	10.5	32.1	6.7	12.5
$[Ni(Me_6tren)def](ClO_4)_2$	calc.	10.0	34.7	7.0	11.9
	fnd.	10.0	34.6	7.0	12.0
$[Co(Me_6tren)dmf](ClO_4)_2$	calc.	10.5	32.1	6.6	12.5
	fnd.	10.5	32.0	6.6	12.4
$[Co(Me_6tren)def](ClO_4)_2$	calc.	10.0	34.7	7.0	11.9
	fnd.	10.0	34.6	7.0	12.0
$[Zn(Me_6tren)dmf](ClO_4)_2$	calc.	11.5	31.7	6.6	12.3
	fnd.	11.6	31.7	6.5	12.2
$[Zn(Me_6tren)def](ClO_4)_2$	calc.	11.0	34.3	6.9	11.8
	fnd.	11.0	34.3	6.9	11.9
$[Zn(Me_6tren)dma](ClO_4)_2$	calc.	11.2	33.0	6.8	12.0
	fnd.	11.3	32.8	6.8	12.1

prepared in this study exhibited only one band at ca 620 cm^{-1} indicative of perchlorate being present in purely ionic form.

Each prepared complex was analyzed for percentage metal content by an ion exchange (Dowex 50W ion exchange resin)/titration method as described by Vogel[12]. Samples of each complex were sent to the Canadian Microanalytical Service; Vancouver, Canada for elemental analysis. Analytical results appear in table 3.1.

All complexes prepared in this study are hygroscopic but are quite stable when stored under dry conditions.

3.2.3. Hazards in the use of perchlorates

The preparation, handling and use of some perchlorate salts is potentially dangerous[22-24]. Perchlorate salts of metal complexes in particular are shock sensitive and may explode under certain circumstances, especially in the combined presence of acid and organic material as in the dehydration step discussed in section 3.2.2. Care should always be exercised in the handling of perchlorate salts of metal complexes. No explosion hazard was encountered under the conditions of this study.

3.3 Preparation of experimental solutions

3.3.1. Laboratory glassware and other apparatus

All volumetric glassware used was A grade borosilicate and prepared for use in the following manner. Both flask and stopper were soaked in a 5% v/v Decon 90 solution for 24 hours prior to an acid rinse with 20% v/v HCl (Adelaide and Wallaroo) followed by thorough and repeated rinsing with doubly distilled water and draining in a dust free environment until dry. Flasks required for non-aqueous solution preparation were further dried in an oven at ca 390K for at least one hour before rapid transfer to the dry box to cool. Under these conditions of temperature the volume of borosilicate flasks is not expected to alter within experimental error[25]. Accompanying stoppers were further dried in vaccuo (ca 18mmHg) at ambient temperature over phosphorous pentoxide overnight before transfer to the dry box.

Teflon magnetic stirrers, spatulas, metal syringe stoppers, glass sinter filter funnels and other non-volumetric glassware were rinsed repeatedly with doubly distilled water, drained and also dried in an oven at 390K for at least one hour prior to cooling in the dry box.

Quartz spectrophotometer cells and plastic storage syringes for stopped-flow work were cleaned in the same manner as for volumetric glassware but dried in vaccuo over phosphorous pentoxide overnight before transfer to the dry box.

All nmr tubes, 10 mm, 5 mm and 2 mm inserts (Wilmad Glass Co.) were rinsed with distilled acetone and repeatedly with doubly distilled water, drained and dried at 390K overnight before transfer to the dry box.

3.3.2. Notes on maintaining anhydrous conditions

In order to maintain the strictly anhydrous conditions required for some work in this study a dry box of conventional design was prepared. This dry box was made large enough to house a magnetic stirrer and retort

stand as well as shelves where reagents and specialist anhydrous laboratory apparatus could be stored. The dry box assembly was continually flushed with dry nitrogen (CIG industrial dry) which had already been further dehydrated as a result of passing through a series of traps containing potassium hydroxide pellets (BDH) and pure sulphuric acid (Adelaide & Wallaroo). The working area and smaller annex each contained an evaporating dish containing active phosphorous pentoxide.

All transfers to and from the dry box were done in a manner to minimize any water vapour contamination and appropriate time allowances were made after any transfer before work commenced so as to ensure a dry atmosphere.

3.3.3 Preparation of solutions for nmr spectroscopy

All solutions for use in nmr experiments other than routine analyses were prepared, by weight, in the dry nitrogen atmosphere of the dry box, as were any transfers. These solutions were prepared in the following manner.

The complex to be studied was weighed into a dry volumetric flask. Then an inert additive, either cyclohexane or benzene as desired, was weighed in so as to make a 2% (w/v) solution when finished. This inert additive acted as both a chemical shift reference and an aid to monitor magnetic field homogeneity during experiments. Finally, the solvent required was weighed in, thus a measure of both molarity and molality is known and accurate mol fractions of coordinated and uncoordinated solvent required for data analysis may be easily determined.

A small amount (ca 0.03 cm^3) of the solution was then sealed under vacuum in a 2mm diameter nmr tube insert which was in turn positioned concentrically in a 5mm diameter nmr tube containing either CD_3NO_2 or $(CD_3)_2SO$, depending on the temperature range studied, which provided the deuterium lock signal required in the nmr experiments.

All nmr tubes and inserts were stored sealed at 238K until required.

3.3.4 Preparation of solutions for uv/visible spectroscopy

All dmf solutions studied by ultraviolet/visible spectroscopy were prepared at an ionic strength, μ, of 0.5 mol dm^{-3}, adjusted with sodium perchlorate.

Solutions required in the study of the spectral variations associated with the reaction of $[M(Me_6tren)dmf]^{2+}$ with X^- (M = Co(II), Ni(II), Cu(II); $X^- = Br^-$, N_3^-, NCS^-) were prepared in the dry box by dissolving a known weight of $NaClO_4$ in dry dmf. Care must be exercised during this procedure as heat is evolved with dissolution. Appropriate quantities of $[M(Me_6tren)dmf](ClO_4)_2$, NaBr, NaN_3 and NaNCS were weighed into individual volumetric flasks in the dry box. Appropriate volumes of pure dmf solvent (calculated to compensate for the ionic strength contribution of the salt to the total ionic strength) were added by pipette to the salt in each flask and solutions made to the mark with the $\mu = 0.5$ mol dm^{-3} sodium perchlorate solvent already prepared.

Stock solutions of complex and anion salts having thus been prepared, simple volumetric mixing of complex stock solution with an anion stock solution gave the reaction mixture required in each case. In all such preparations the initial concentration of $[M(Me_6tren)dmf]^{2+}$ in a reaction mixture never exceeded 10% of the excess anion concentration in that mixture. This condition was believed to ensure almost complete anation as the overall stability constant for the formation of $[M(Me_6tren)X]^+$ was intuitively expected to be high and was infact, from later experimental results (see sections 4.1.2, 4.2.2, 4.3.2) deduced to be so.

Equimolar stock solutions of complex and anion salts for Job's law plots (see section 2.2.1) were prepared at $\mu = 0.5$ mol dm^{-3} in the same manner as already described for stock solutions. For each separate anion experimental solutions at a variety of mol fractions of (each) complex

were then prepared in the dry box by appropriate volumetric mixing of stock solutions.

In all cases experimental solutions once prepared were quickly transferred in the dry box to tightly stoppered quartz spectrophotometric cells for immediate analysis.

3.3.5 Preparation of solutions for stopped-flow spectrophotometry

All dmf solutions studied by stopped-flow spectrophotometry were also prepared at an ionic strength of 0.5 mol dm^{-3}, adjusted with sodium perchlorate.

Complex and anion salt stock solutions were prepared in an identical manner to that described for stock solutions in section 3.3.4. Kinetic solutions required for stopped-flow spectrophotometric experiments were prepared from these stocks by volumetric dilution in 50 dm^3 flasks. Each solution was then quickly transferred to (usually) four 10 cm^3 capacity plastic storage syringes. Plastic syringes were preferred over glass types as they are effectively gas tight. These syringes were then stoppered with sealed off metal syringe needles.

All solution preparations and transfers were conducted in the dry box and filled syringes were stored in the dry box annex until required. The need for experimentally tedious degassing of dmf solutions was circumvented by the observation that undegassed dmf solutions used in the stopped-flow apparatus did not give rise to any troublesome bubbles, which can adversely affect spectrophotometric monitoring of reactions, during the course of experiments. This is probably a result of the low solubility of nitrogen in dmf under the experimental conditions.

In order to maintain pseudo first-order conditions for all stopped-flow kinetic experiments the initial concentrations of $[M(Me_6tren)dmf]^{2+}$ in all cases never exceeded 10% of the excess anion concentrations.

3.4 Description of apparatus

3.4.1. Nmr spectrometers

Routine ^{1}H and ^{13}C nmr measurements such as to determine structure and purity of organic solvents and reagents were made at ambient temperature utilizing a Brüker WP80 80MHz spectrometer. An internal [2]H (D) lock was provided by the use of deuterated diluents either $CDCl_3$ (Stohler) or D_2O (AAEC) depending on choice, these diluents containing 2% tetramethylsilane as an internal chemical shift reference.

Kinetic ^{1}H nmr studies were carried out on a Brüker HX90E spectrometer at 90MHz in Pulsed Fourier Transform (PFT) mode using quadrature detection and locked on the deuterium signal frequency. Typically, a delay time of 2s between each 3μs pulse with a sweep width of 2kHz was used. The number of transients collected was dependent on the width of the bulk solvent formyl proton (for dmf and def studies) or α-methyl protons (dma studies) resonance at half-of-maximum amplitude, $\nu_{\frac{1}{2}}$ (see section 2.4), usually falling in the range between 50 and 500 and were collected as 4K (4096) real data points prior to Fourier transformation. A line broadening effect of 0.5Hz introduced by the spectrometer computer was allowed for in all resonance line width determinations from outputed chart paper spectra. Stability in controlled sample temperature was ±0.3K, the thermostat being calibrated against a copper constantan thermocouple which was routinely checked with standard methanol and ethylene glycol samples[26].

3.4.2. Uv/visible and infrared spectrophotometers

Spectrophotometric measurements between 280 and 900 nm were made with a Zeiss DMR10 double beam spectrophotometer equipped with a thermostatted cell block and constant temperature water bath controlled with a MGW Lauda Thermoboy temperature controller. Reference and sample cell temperature stability was ±0.05K monitored at all times with a calibrated STC F53 directly heated bead-type thermistor connected to a digital

voltmeter. Spectral measurements between 900 and 1050 nm were made with a Unicam SP800 spectrophotometer. Both instruments were chart recording, necessitating hand digitization of all spectra reported in this study.

Infrared spectra routinely run on reagents and preparative products throughout this study were of Nujol mulls (using sodium chloride plates) or of solutions (using sodium chloride IR solution cells) prepared under anhydrous conditions immediately prior to being recorded on a chart recording Perkin-Elmer 402 infrared spectrophotometer.

3.4.3. The stopped-flow apparatus

All stopped-flow spectrophotometric studies were carried out on existing apparatus[8] modified for variable temperature work involving toxic non-aqueous solutions. Although dmf was the only solvent involved in stopped-flow work during this study the applicability of this apparatus for use with other non-aqueous solvents is appreciable. The system design is based on a concept due to Faeder[27], a modification of the Durrum-Gibson apparatus[28]. An excellent article by Chance[29] reviews in detail the important considerations one must be aware of in the design and use of apparatus to follow rapid reactions. The instrument as used is described below and also schematically in figure 3.3.

Reactant solutions are entered via two plastic (Pharma-Plast) gas-tight reservoir syringes and introduced into two glass Hamilton gas-tight drive syringes. The drive syringes have teflon plungers and luer tip inserts and are filled by means of two three-way Hamilton luer lock valves. Triggering a valve switch initiates a nitrogen gas pressure push of ca 5.5 psi, supplied from a commercially available cyclinder (CIG industrial dry) via a pressure reservoir, pushing forward a piston which moves a preset (effected by winding back a threaded mechanical stop seven revolutions) amount, introducing approximately 0.2 ml of each solution into the observation cell via an eight jet tangential mixer[8,30] designed to
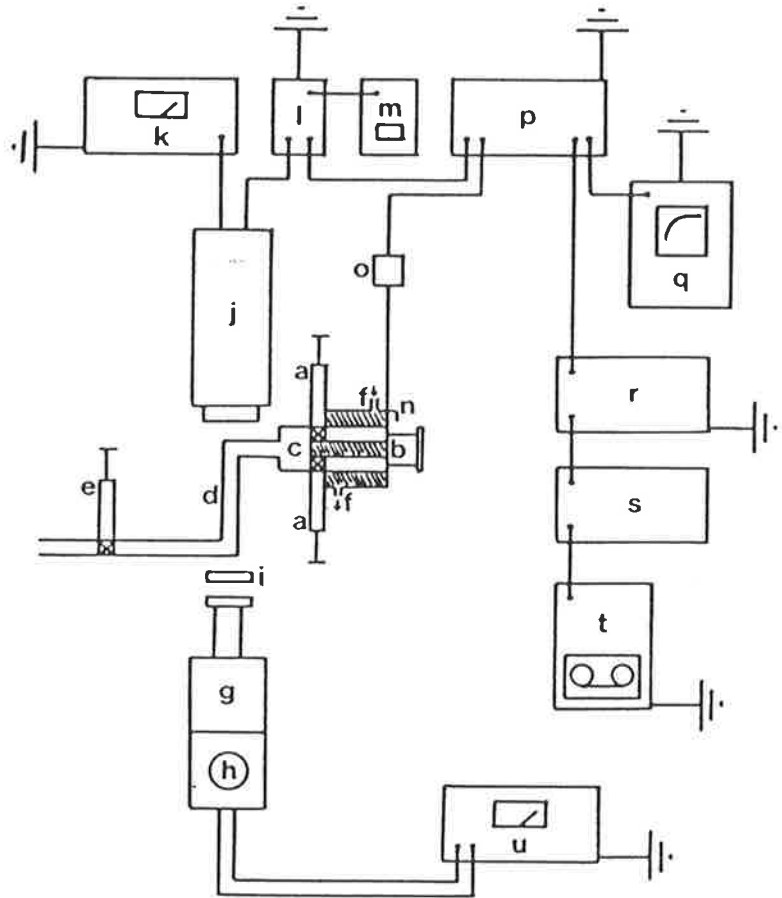
a.	Storage syringes	l.	Back-off device/amplifier
b.	Drive syringes	m.	Digital voltmeter
c.	Mixer	n.	Microswitch
d.	Observation cell	o.	Microswitch DC supply
e.	Waste reservoir syringe	p.	DL905 datalogger
f.	Thermostating jacket	q.	Oscilloscope
g.	Monochromator	r.	SDK-8085 microprocessor
h.	Xenon lamp	s.	CDB-150 cassette interface
i.	Optical filter	t.	C-202LP cassette tape recorder
j.	Photomultiplier	u.	Xenon lamp power supply
k.	High tension supply		

Figure 3.3

Schematic diagram of the stopped-flow apparatus used in this study including digital data acquisition facilities.

minimize mixing time. The observation cell path length is 2cm bounded by two well sealed conical quartz windows; the light beam passing along the cell rather than across it to eliminate errors[31,32]. The observation cell is located as close as practicable to the mixer so as to minimize dead-time. The spent solution flows into a glass waste reservoir syringe upon successive pushes through another three-way valve. This waste syringe may be bled through the same valve to a toxic residue container via a glass tube arrangement.

The block containing the mixer, observation cell, cell windows and waste valve is entirely composed of Kel-F. The apparatus is designed to ensure that dmf solutions passing through it during the course of an experiment come into contact only with inert materials such as plastic, glass, quartz, teflon and Kel-F. Solutions in the drive syringes were thermostated by circulating water through machined channels in a surrounding brass jacket. Water temperature was maintained at ±0.05K by apparatus identical to that for uv/visible spectrophotometric work. To prevent fogging of quartz observation cell windows at low temperatures an attachment was developed, fitting to the top of the observation cell block, to play dry nitrogen at a flow rate of 7 dm^3s^{-1} onto the windows. The entire mechanical component of the apparatus is constructed on a vibrationally insulated stainless steel template and housed in a fume hood which remained operative during experimental work to minimize any inhalation of toxic dmf fumes.

Light is supplied from a constant voltage Xenon lamp (Illumination Industries) useful in both the ultraviolet and visible regions of the electromagnetic spectrum. Light from this lamp passes through a Bausch and Lomb high intensity grating monochromator (with adjustable slits and iris) and through an appropriate optical filter (COREX for 280-380 nm and 0Y10 for 380-700nm) before passing through the observation cell. Light

passing through the cell enters a seven dynode photomultiplier powered
by a high tension power supply. Stray light can be effectively excluded
from the optical system by surrounding the monochromator, observation
cell and photomultiplier by a matt-finished metal guard housing.

Before a push is initiated (with spent solution in the observation
cell) the signal voltage from the photomultiplier is backed-off against
a variable (usually -1.90V) voltage. When a push is initiated the
piston actuates reactant solution into the observation cell until the
mechanical stop terminates the flow and simultaneously contacts a micro-
switch triggering the DL905 data acquisition facilities. A two-way switch
on the variable back-off voltage device allows a digital voltage readout
by way of a Beckman Tech 300 digital multimeter (in DC Volts mode) of
photomultiplier output directly or amplified signal output being recorded,
this comprising the reaction trace. This signal output is fed into the
voltage input port of a Datalab DL905 transient recorder for reaction
trace data biomation. Reaction traces may be viewed after a push on a
Tektronix oscilloscope connected to the DL905 in order to assess whether
the trace is suitable for storage and analysis.

3.4.4. Stopped-flow data storage and analysis

Two methods were utilized as a manner of stopped-flow experimental
data storage in this study.

Initially, each acceptable exponential reaction trace was recorded
from the DL905 transient recorder onto calibrated chart paper using a
Hewlett-Packard 7101BM strip chart recorder and hand digitized. A minimum
of twenty data points over at least four reaction half-lives were fitted
by a linear least-squares routine (see section 2.3.2) using a Computer
Data Products LSI-II minicomputer to give the first-order rate constant.
Individual rate constants characterizing at least five reaction traces
were averaged for each solution studied and this average value used in the

generation of kinetic plots.

During the course of this study an alternative method which improved both accuracy and ease of data management was developed[33]. Like the first method above a Datalab DL905 transient recorder collected photomultiplier voltages as a function of calibrated time for each transient as 1K (1024) 8-bit data points. Acceptable traces were transferred in the laboratory from transient recorder memory to high resolution TDK SA-C60 magnetic cassette tape via an Intel SDK-8085 microprocessor connected to a Pennywise Peripherals CDB-150 cassette interface system and superscope C-202LP cassette tape recorder. The same transferral system was used to transfer data on cassette tape to an IBM double density floppy diskette loaded into a Computer Data Products LSI-II minicomputer. Five to ten reproducible transients for each solution were computer averaged and analyzed in the following manner. The computer averaged reaction trace was computer fitted to the exponential form of the first order rate equation

$$V_t = B(1) \exp(B(2).t)$$

where $B(1)$ = reaction trace voltage pre-exponential term

$B(2)$ = the first order rate constant

V_t = reaction trace voltage at time, t

by a non-linear least-squares fitting subroutine[34] to give an average first-order rate constant.

The advantages of this method over the first include an increased speed and reliability in data analysis, a permanent computer record of data aiding more efficient data management and improved signal-to-noise ratio inherently characteristic of the computer averaging method.

3.5   References to chapter 3

1.   J.N. Butler, in "Advances in Electrochemistry and Electrochemical Engineering," P. Delahay and C.W. Tobias, eds, volume 7, Interscience, N.Y., 1970.

2.   C.J. James, Ph.D. Thesis, University of Adelaide, 1972.

3.   S.D. Ross, in "Inorganic Infrared and Raman Spectra", McGraw-Hill, London, 1972.

4.   R.A. Nyquist, R.O. Kagel, in "Infrared Spectra of Inorganic Compounds", Academic Press, N.Y., 1971.

5.   E. Merck, in "Drying in the Laboratory", Merck, Darmstadt, 1983.

6.   D.M.M.A. Hadi, University of Adelaide, Private communication.

7.   M. Ciampolini, N. Nardi, Inorg.Chem., 1966, $\underline{5}$, 41.

8.   P.R. Collins, Ph.D. Thesis, University of Adelaide, 1979.

9.   G. Searle, University of Adelaide, Private communication.

10.   L.J. Wilson, N.J. Rose, J.Amer.Chem.Soc., 1968, $\underline{90}$, 6041.

11.   J. Glerup, J. Josephsen, K. Michelsen, E. Pedersen, C.E. Schäffer, Acta Chem.Scand.,1970, $\underline{24}$, 247.

12.   A.I. Vogel, in "Quantitative Inorganic Analysis", third ed., Longmans, London, 1962.

13.   A.I. Vogel, in "Practical Organic Chemistry", third ed., Longmans, London, 1962.

14.   E.D. Becker, in "High Resolution nmr", second ed., Academic Press, N.Y., 1980.

15.   S.F. Lincoln, University of Adelaide, Private communication.

16.   N.M. Karayannis, C. Owens, L.L. Pytlewski, M.M. Labes, J.Inorg.Nucl. Chem., 1969, $\underline{81}$, 2059.

17.   M.N. Tkaczuk, S.F. Lincoln, Aust.J.Chem., 1979, $\underline{32}$, 1915.

18.   P.W.N.M. van Leeuwen, W.L. Groeneveld, Inorg.Nucl.Chem.Lett., 1967, $\underline{3}$, 145.

19. B.J. Hathaway, A.E. Underhill, J.Chem.Soc., 1961, 3091.

20. M.R. Rosenthal, J.Chem.Ed., 1973, 50, 331.

21. B.J. Hathaway, D.G. Holah, M. Hudson, J.Chem.Soc., 1963, 4586.

22. W.C. Wolsey, J.Chem.Ed., 1973, 50, A335.

23. K. Everett, F.A. Graf, in "Handbook of Laboratory Safety", N.V. Steere, ed., CRC, Cleveland, Ohio, 1971.

24. J.C. Schumacher, in "Perchlorates, Their Properties, Manufacture and Uses", Amer.Chem.Soc.Monograph Series no. 146, Reinhold, N.Y., 1960.

25. Labware and Scientific Catalogue, Corning Limited, Laboratory Division, England.

26. A.L. van Geet, Anal.Chem., 1968, 40, 2227.

27. E.J. Faeder, Ph.D. Thesis, Cornell University, Ithaca, N.Y., 1970.

28. Durrum Instrument Corporation, Bulletin no. 131.

29. B. Chance, in "Techniques of Chemistry", Vol. VI, "Investigation of Rates and Mechanisms of Reactions", part 2, G.G. Hammes, ed., third ed., Chapter II, Wiley, N.Y., 1974.

30. B. Chance, in "Technique of Organic Chemistry", Vol. VIII, "Rates and Mechanisms of Reactions", part 2, A. Weissberger, ed., second ed., Chapter XIV, Interscience, N.Y., 1963.

31. Q.H. Gibson, E. Antonini, Biochem.J., 1960, 77, 328.

32. R.H. Prince, Z. Elecktrochem., 1960, 64, 13.

33. R.L. Schiller, Honours Thesis, University of Adelaide, 1981.

34. J.H. Coates, B.G. Plush, University of Adelaide, 1982.

CHAPTER 4 - RESULTS

CHAPTER 4 - RESULTS

4.1 Cu(II) complexes in solution

4.1.1 Spectral variation on formation of $[Cu(Me_6tren)X]^+$ in dmf

The ultraviolet/visible absorption spectra in dmf solution (ionic strength adjusted to 0.5 mol dm^{-3} with sodium perchlorate) of the solvated complex $[Cu(Me_6tren)dmf]^{2+}$ and anated species $[Cu(Me_6tren)X]^+$, where $X^- = Br^-$, N_3^-, NCS^-, were recorded at 298.2K and the resulting molar absorbance versus wavelength plot is shown in figure 4.1.

As will be discussed in more detail in chapter 5, the two absorption bands in the wavelength range 600-1100nm are indicative of approximately trigonal-bipyramidal geometry and may be assigned to the $^2E'' \leftarrow {}^2A'$, and $^2E' \leftarrow {}^2A'$, transitions[1].

From inspection of the spectral plot (figure 4.1), and contrasting the spectrum of each anated complex in turn with that of the solvated complex, one can establish likely wavelengths at which kinetic studies may be effected for each anion system subject to the following criteria:

(i) Optimum sensitivity and signal-to-noise ratio can be expected at a wavelength where the difference in absorbance between the two spectra has a maximum value.

(ii) Absorption peaks were selected wherever possible, as incident light bandwidth associated errors are consequently minimized. In the absence of any peak, shoulders were selected for the same reason.

Bearing these considerations in mind, the primary and secondary kinetic observation wavelengths were determined and the result are given in table 4.1.

4.1.2 Job plots for $[Cu(Me_6tren)X]^+$ formation in dmf

A series of solutions at differing ratios of initial $[Cu(Me_6tren)dmf]^{2+}$ concentration to initial anion concentration were prepared as described in
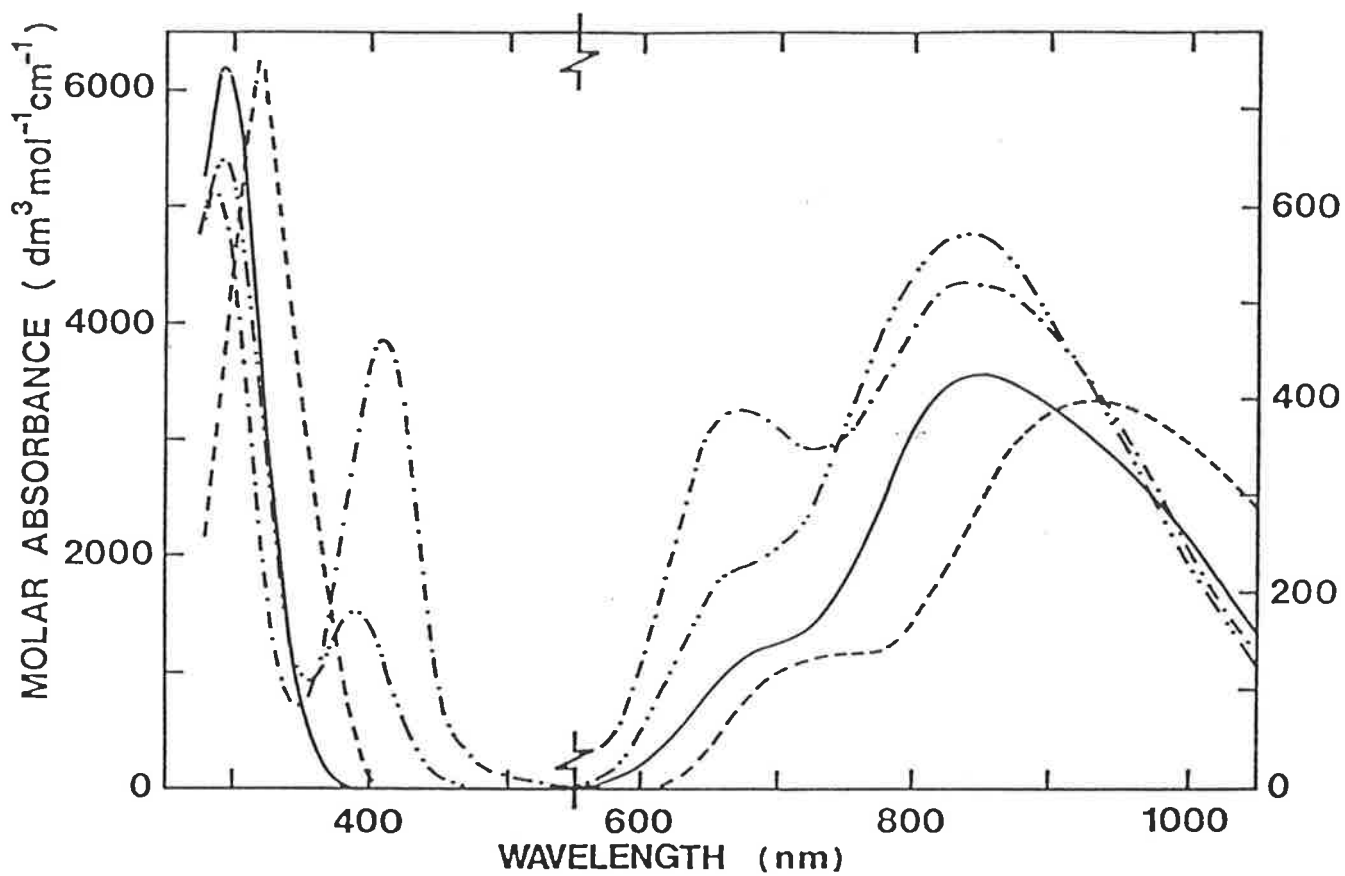
Figure 4.1

Ultraviolet/visible absorption spectra of $[Cu(Me_6tren)dmf]^{2+}$

(——) and $[Cu(Me_6tren)X]^+$ (X$^-$ = Br$^-$ (---), N$_3^-$ (—·—),

NCS$^-$ (—··—)) in dmf solution.

Table 4.1

Kinetic observation wavelengths for the formation of $[Cu(Me_6tren)X]^+$ in dmf solution (ionic strength adjusted to 0.5 mol dm^{-3} with sodium perchlorate) at 298.2K.

anion X^-	wavelength λ (nm)	change in molar absorbance $\Delta\varepsilon^a$ $(dm^3\ mol^{-1}\ cm^{-1})$
Br^-	315	1380
	330	2910
N_3^-	300	-1580
	410	3880
NCS^-	390	1540
	700	100

(a $\Delta\varepsilon = \varepsilon_{[Cu(Me_6tren)X]^+} - \varepsilon_{[Cu(Me_6tren)dmf]^{2+}}$)

section 3.3.4, for each of the three anions (Br⁻, N₃⁻ and NCS⁻) systems. The concentration ranges of $[Cu(Me_6tren)dmf]^{2+}$ and X⁻ for each anion system were 2.8×10^{-5} - 2.8×10^{-4} and 2.9×10^{-5} - 2.9×10^{-4} mol dm⁻³ for Br⁻, 3.3×10^{-5} - 3.3×10^{-4} and 3.3×10^{-5} - 3.3×10^{-4} mol dm⁻³ for N₃⁻, and 4.6×10^{-4} - 4.6×10^{-3} and 4.2×10^{-4} - 4.2×10^{-3} mol dm⁻³ for NCS⁻. The ultraviolet/visible absorption spectrum of each solution was recorded at 298.2K for each system and absorbance measured at an appropriate wavelength for that system. These wavelengths were selected as previously described, (see section 4.1.1) and were 315, 410 and 700 nm for Br⁻, N₃⁻ and NCS⁻, respectively.

The results of the Job method analysis (see chapter 2.2) for each system are shown in figure 4.2. The resultant plots are indicative of the formation of a single 1:1 species, $[Cu(Me_6tren)X]^+$ in all cases. The shape of the plots, with particular attention to the very sharply defined apex for each plot, characterizes[2] a high stability constant estimated at ca 10^5 dm³mol⁻¹ in the reaction of $[Cu(Me_6tren)dmf]^{2+}$ with each of the anions Br⁻, N₃⁻ and NCS⁻.

4.1.3 Ligand substitution on $[Cu(Me_6tren)dmf]^{2+}$ in dmf

Ligand substitution of dmf on $[Cu(Me_6tren)dmf]^{2+}$ by the anions Br⁻, N₃⁻ NCS⁻ in dmf solution (adjusted to an ionic strength of 0.5 mol dm⁻³ with sodium perchlorate) was studied at 278.2K, 288.2K and 298.2K, employing stopped-flow spectrophotometric techniques at the same wavelengths as are given in table 4.1. Experimental solutions were prepared as outlined in section 3.3.5. The initial concentrations of $[Cu(Me_6tren)dmf]^{2+}$ varied in the range 5.17×10^{-5} - 8.41×10^{-4} mol dm⁻³ and in all cases never exceeded 10% of the excess anion concentrations which varied in the range 5.17×10^{-4} - 2.59×10^{-2} mol dm⁻³. In this manner, pseudo first-order conditions were maintained throughout.
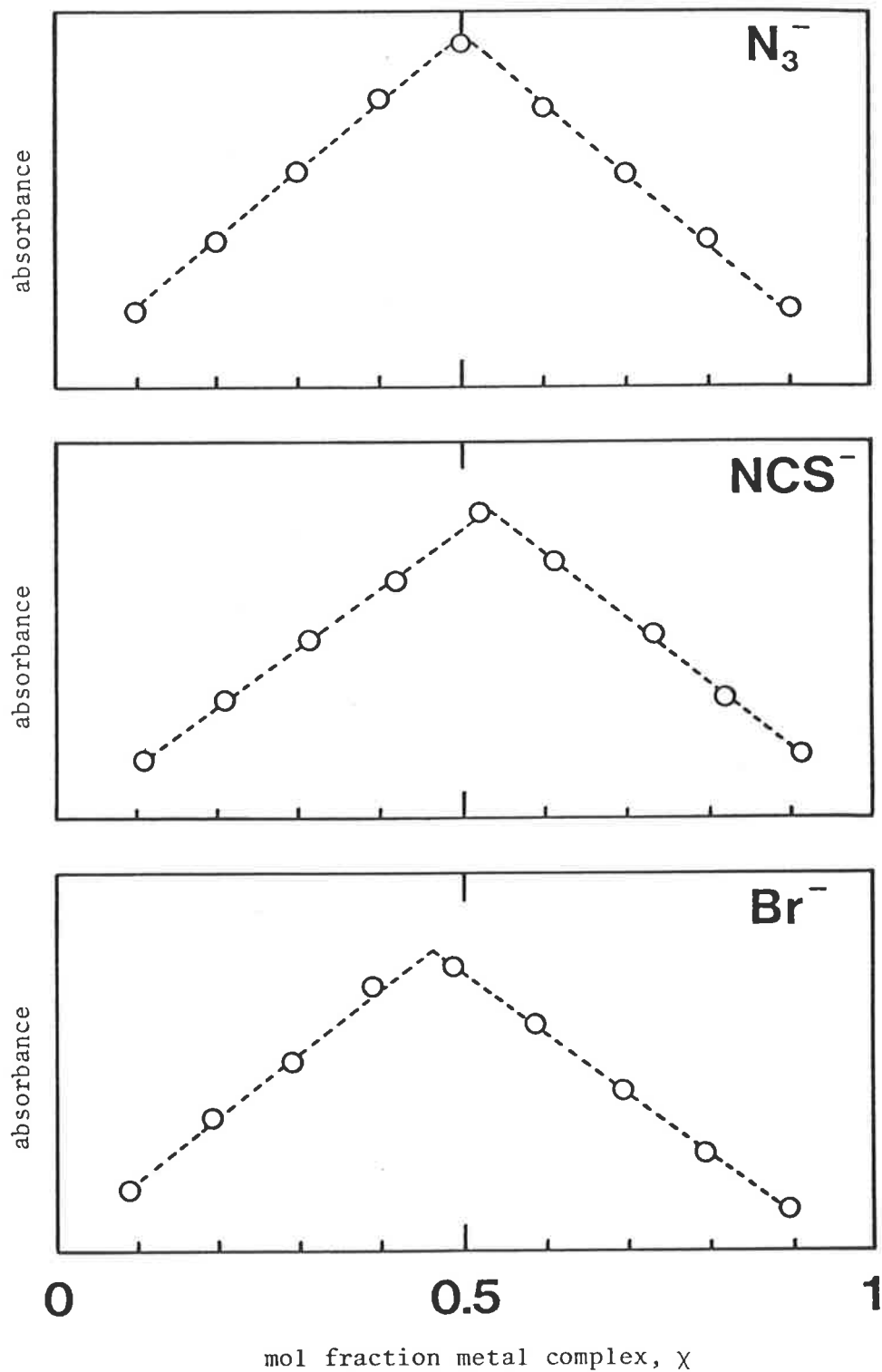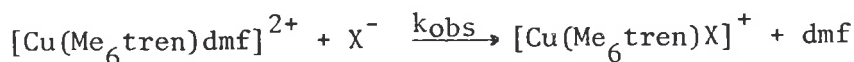
Figure 4.2

Job plots for the formation of $[Cu(Me_6tren)X]^+$ (X^- = N_3^-, NCS^-, Br^-) in dmf solution.

The anation reaction is characterized by a single kinetic process typified by a first-order rate constant, k_{obs}. Values of k_{obs} for each solution were obtained from linear least-squares fitting of strip-chart voltage versus time data quantifying this process (see section 2.3.2). These values appear as an appendix to this thesis.
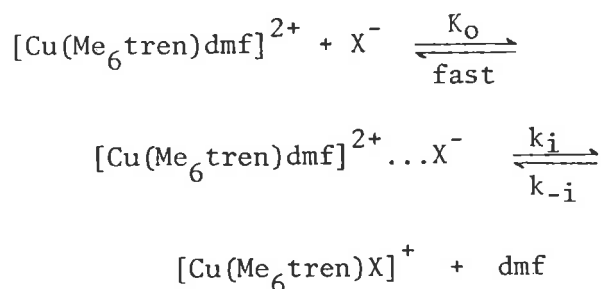
The variation of k_{obs} with excess anion concentration, $[X^-]$, as shown in the kinetic plots (figures 4.3, 4.4, 4.5) for the anation reaction

$$[Cu(Me_6tren)dmf]^{2+} + X^- \xrightarrow{k_{obs}} [Cu(Me_6tren)X]^+ + dmf$$

appears to be consistent with equation 4.1

$$k_{obs} = \frac{k_i K_0 [X^-]}{1 + K_0[X^-]} + k_{-i} \tag{4.1}$$

which typifies (see section 2.1.3) an interchange (I) mechanism[3] proceeding through the following reaction scheme.

$$[Cu(Me_6tren)dmf]^{2+} + X^- \underset{fast}{\overset{K_0}{\rightleftharpoons}}$$

$$[Cu(Me_6tren)dmf]^{2+}...X^- \underset{k_{-i}}{\overset{k_i}{\rightleftharpoons}}$$

$$[Cu(Me_6tren)X]^+ + dmf$$

The parameter K_0 is the equilibrium constant characterizing the rapid formation of the encounter complex in which X^- resides in the second coordination sphere of the solvated complex. Following this process is the slower, rate determining interchange of X^- and coordinated dmf characterized by the forward rate constant, k_i. Inspection of the kinetic plots for each anion reveals that the backward rate constant characterizing the dissociation of X^- from $[Cu(Me_6tren)X]^+$, k_{-i}, reflected in the y-axis intercept of each curve, is too small to be distinguishable from the experimental error in k_{obs}. This, coupled with the fact that due to experimental constraints on $[X^-]$, (in order to maintain pseudo first-order conditions and still have a sufficient metal complex concentration to have
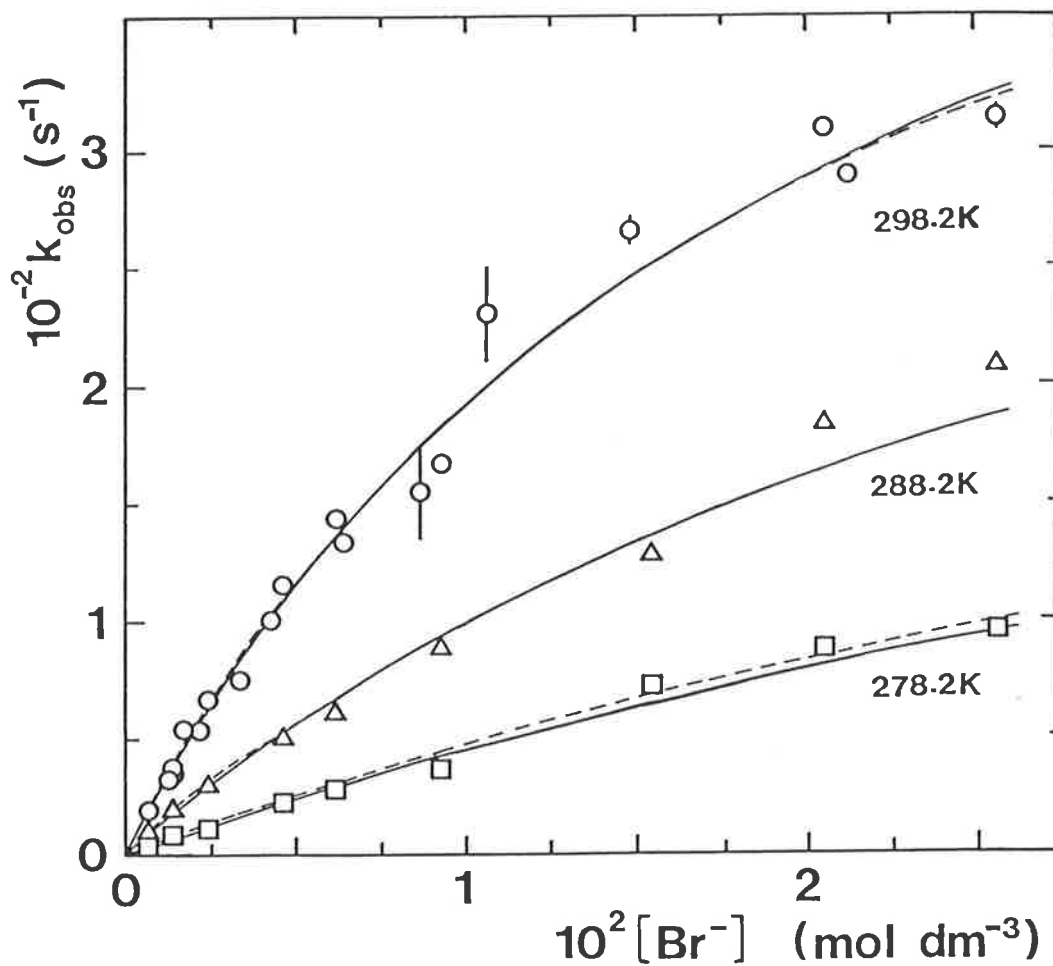
Figure 4.3

Variation of k_{obs} for the anation of $[Cu(Me_6tren)dmf]^{2+}$ by Br^- with temperature and excess $[Br^-]$ in dmf solution. Solid curves represent the simultaneous best fit of the data at 278.2, 288.2 and 298.2K to the appropriate equation, whereas broken lines represent the best fits of the data to equation 4.1 separately at each temperature.
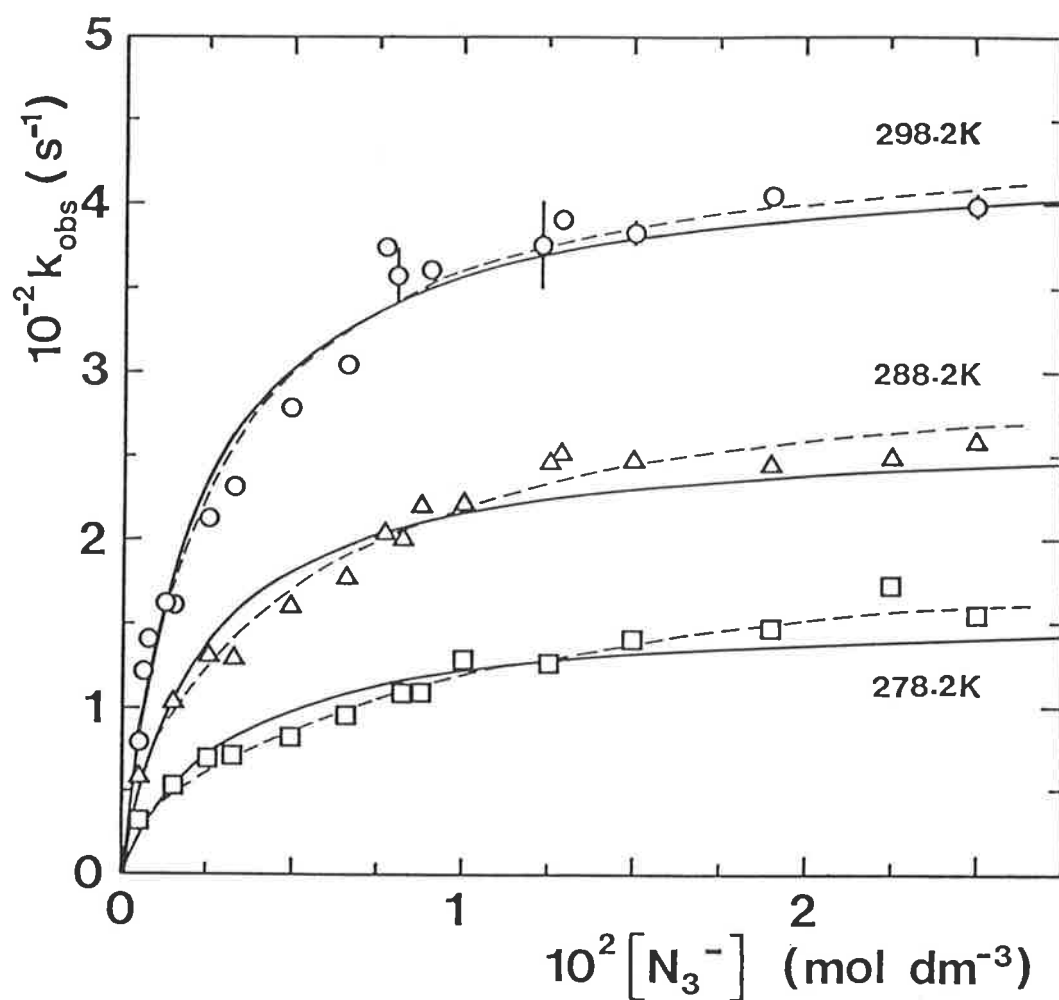
Figure 4.4

Variation of k_{obs} for the anation of $[Cu(Me_6 tren)dmf]^{2+}$ by N_3^- with temperature and excess $[N_3^-]$ in dmf solution. Solid curves represent the simultaneous best fit of the data at 278.2, 288.2 and 298.2K to the appropriate equation, whereas broken lines represent the best fits of the data to equation 4.1 separately at each temperature.

Figure 4.5

Variation of k_{obs} for the anation of $[Cu(Me_6tren)dmf]^{2+}$ by NCS$^-$ with temperature and excess [NCS$^-$] in dmf solution. Solid curves represent the simultaneous best fit of the data at 278.2, 288.2 and 298.2K to the appropriate equation, whereas broken lines represent the best fits of the data to equation 4.1 separately at each temperature.
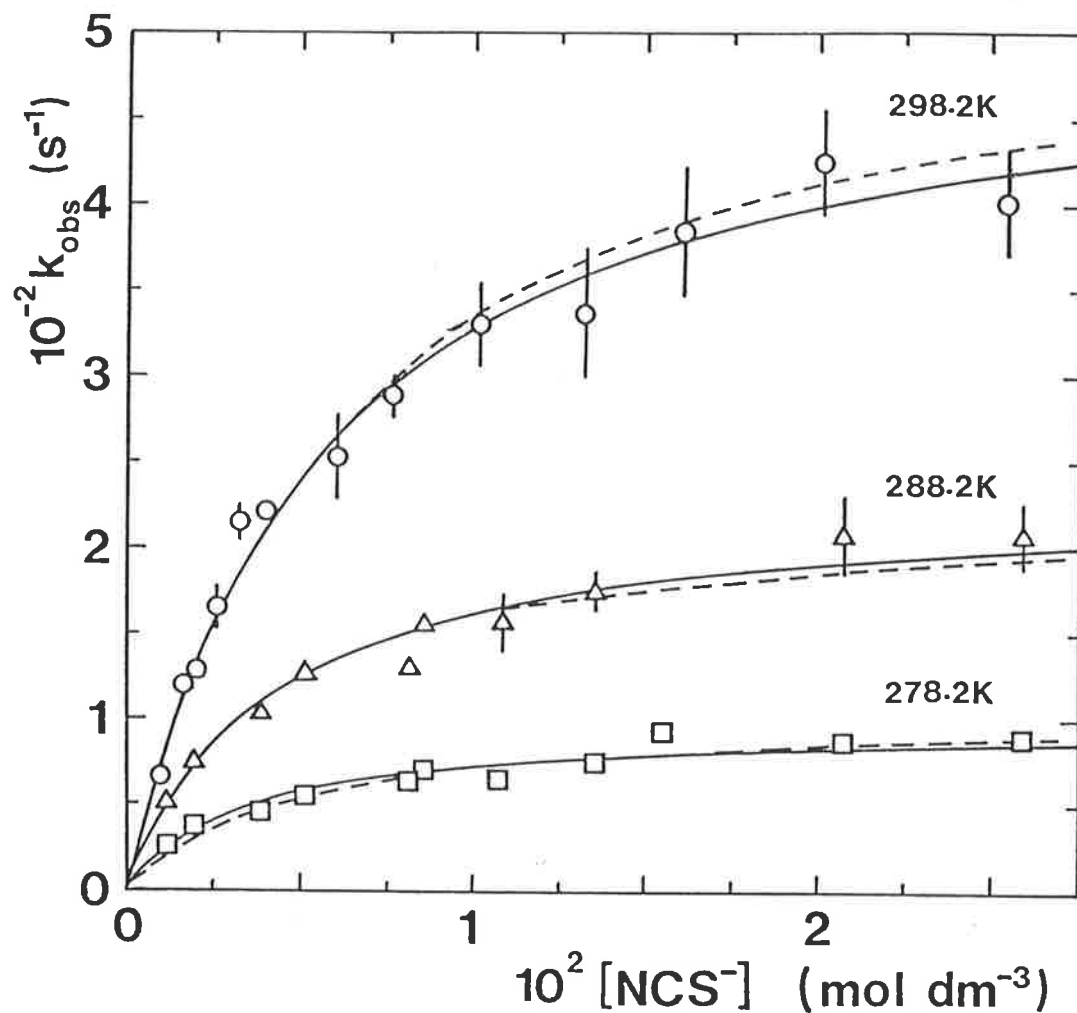
an experimentally measurable reaction trace) means that data points are not attainable at very low excess anion concentrations, which would lead to a more accurate determination of k_{-i}. Therefore, this parameter is not further discussed in any detail, although its existence is recognised.

For each anion, derived kinetic parameters k_i and K_o were attained through non-linear least-squares fitting of experimental k_{obs} and $[X^-]$ data to equation 4.1 on a Cyber 173 computer using the DATAFIT[4] fitting module.

A more statistically reliable method of parameter determination is to combine equation 4.1 with the temperature dependent formulation of k_i from transition state theory[5] given by the Eyring equation, equation 4.2.

$$k_i = \frac{k_b T}{h} \exp(-\Delta H_i^{\#}/RT) \exp(\Delta S_i^{\#}/R) \tag{4.2}$$

where k_b = Boltzmann constant

T = Absolute temperature

h = Plank constant

R = Gas constant

$\Delta H_i^{\#}$ = Enthalpy of activation for the anation reaction

$\Delta S_i^{\#}$ = Entropy of activation for the anation reaction

and fit data obtained at all three experimental temperatures to this model simultaneously. Non-linear least-squares fitting in this manner using DATAFIT gave rise to optimized values for kinetic and activation parameters k_i, K_o and $\Delta H_i^{\#}$, $\Delta S_i^{\#}$, respectively.

The resulting optimized parameters from each of these fitting procedures for anation of $[Cu(Me_6tren)dmf]^{2+}$ by Br^-, N_3^- and NCS^- anions in dmf, appear in table 4.2. The derived parameters from both individual and simultaneous temperature fits show little variation between each other. The best fit lines as a result of fitting procedures for each anion studied are shown also in figures 4.3, 4.4, 4.5.

Table 4.2

Kinetic and activation parameters[a] for anation by X^- in the $[Cu(Me_6tren)dmf]^{2+}$ species in dmf solution at an ionic strength of 0.5 mol dm^{-3} adjusted with $NaClO_4$.

X^-	Br^-	N_3^-	NCS^-
$K_o(298.2K)^{b}(dm^3mol^{-1})$	52 ± 3	403 ± 43	157 ± 16
$K_o(298.2K)^{c}(dm^3mol^{-1})$	49 ± 6	464 ± 15	175 ± 15
$k_i(298.2K)^{b}(s^{-1})$	563 ± 27	451 ± 13	545 ± 38
$k_i(298.2K)^{c}(s^{-1})$	$-$	435 ± 19	529 ± 32
$k_i(288.2K)^{b}(s^{-1})$	433 ± 90	294 ± 11	220 ± 11
$k_i(288.2K)^{c}(s^{-1})$	$-$	263 ± 12	235 ± 10
$k_i(278.2K)^{b}(s^{-1})$	341 ± 119	180 ± 13	107 ± 6
$k_i(278.2K)^{c}(s^{-1})$	$-$	157 ± 7	99 ± 5
$\Delta H_i^{\#c}(kJmol^{-1})$	19.0 ± 10.4	32.1 ± 2.7	43.6 ± 3.2
$\Delta S_i^{\#c}(JK^{-1}mol^{-1})$	-128 ± 36	-86.9 ± 9.4	-56.2 ± 10.9

a   All errors represent one standard deviation from the best fit of the data to the appropriate equation.

b   Parameters derived from data at a single temperature.

c   Parameters derived from a simultaneous fit of data at three temperatures.

For the case $X^- = Br^-$ the expected variation of k_{obs} with $[X^-]$ (see section 2.1.3, particularly figure 2.2) is not fully developed over the anion concentration range studied. These conditions result in optimized derived parameters that are unlikely to be reliable and hence not considered to be of mechanistic significance. This is illustrated by the relatively large errors on each parameter for $X^- = Br^-$.

4.1.4   Ligand exchange on $[Cu(Me_6tren)dmf]^{2+}$ in dmf

Ligand exchange of dmf on $[Cu(Me_6tren)dmf]^{2+}$ in dmf solution was studied over the temperature range 228-381K employing nmr spectroscopy. Three solutions, (i) - (iii), which were 0.164, 0.0547 and 0.0912 mol dm^{-3} in $[Cu(Me_6tren)dmf]^{2+}$ respectively, were prepared in the manner described in section 3.3.3, as were the accompanying $[Zn(Me_6tren)dmf]^{2+}$ reference solutions. The ionic strength of solution (iii) was adjusted to 0.5 mol dm^{-3} with sodium perchlorate.

Kinetic exchange behaviour was followed by monitoring the variation of transverse relaxation time of the formyl proton resonance of bulk solvent dmf, T_2, with temperature in solutions of $[Cu(Me_6tren)dmf]^{2+}$ which is reflected in the change of linewidth at half-maximum intensity of that resonance. Individual nmr absorption spectra for each solution at every temperature studied were hand digitized and computer fitted by the non-linear least-squares fitting module DATAFIT[4] on the Cyber 173 computer to a theoretical Lorentzian lineshape described by equation 4.3.

$$I(\nu) = \frac{T_2 C_n}{1 + T_2^2(\nu_o - \nu)^2} + C_b \qquad (4.3)$$

where $I(\nu)$ = The resonance intensity (in arbitrary units) as a function of spectral frequency ν (in rad s^{-1})

T_2 = The transverse relaxation time of the formyl proton of bulk solvent dmf (in s)

ν_o = The central resonance frequency (rad s^{-1})

C_n, C_b = The normalization and baseline correction constants respectively.

(The experimental nmr lineshape deviates[6,7] slightly from that described by equation 4.3 but this has been found to introduce no significant errors in lineshape analysis[8,9]). The same method was employed for analysis of reference solutions over the same temperature range. Between 20 and 25 (equally spaced along the ν axis) digitized resonance line data points were used for all spectra. It is pertinent to note that within experimental error, the value of T_2 given by this resonance line fitting procedure was in excellent agreement with that calculated from direct measurement of the resonance linewidth at half-maximum intensity from the recorded spectrum.

As has already been discussed (see section 2.4.2) the relaxation parameter, T_{2p}, is determinable through the difference in reciprocal transverse relaxation times of the $[Cu(Me_6tren)dmf]^{2+}$ and $[Zn(Me_6tren)dmf]^{2+}$ reference solutions thus.

$$T_{2p}^{-1} = T_2^{-1} - T_{2ref}^{-1}$$

Resultant T_{2p} data for solutions (i) - (iii) appear as an appendix to this thesis. According to the Swift and Connick treatment (see section 2.4.2) the form of T_{2p} is given by equation 4.4.

$$T_{2p}^{-1} = \frac{P_m}{\tau_m} \left[\frac{T_{2m}^{-2} + (T_{2m}\tau_m)^{-1} + \Delta\omega_m^2}{(T_{2m}^{-1} + \tau_m^{-1})^2 + \Delta\omega_m^2} \right] + \frac{P_m}{T_{2o}} \qquad (4.4)$$

Where all of the symbols have previously been defined. For dmf exchange on $[Cu(Me_6tren)dmf]^{2+}$ equation 4.4, under the limits of slow and very slow exchange, reduces to equation 4.5 where τ_m^{-1} is equated to k_{ex}, the rate constant characterizing dmf exchange on $[Cu(Me_6tren)dmf]^{2+}$,

$$(P_m T_{2p})^{-1} = \tau_m^{-1} + T_{2o}^{-1} = \frac{k_b T}{h} \exp(-\Delta H^{\#}/RT) \exp(\Delta S^{\#}/R) + A_o \exp(-E_o/RT)$$

$$(4.5)$$

and where all other symbols have also been previously defined. The dmf exchange rate on $[Cu(Me_6 tren)dmf]^{2+}$ becomes

$$v_{dmf} = k_{ex} [Cu(Me_6 tren)dmf^{2+}]$$

The temperature variation of $P_m T_{2p}$ for the bulk solvent dmf formyl proton resonance, which characterizes dmf exchange on $[Cu(Me_6 tren)dmf]^{2+}$ is shown in figure 4.6. This variation was found to be reversible over the entire experimental temperature range. The best fit line of the T_{2p} data for solution (i) is shown in the figure and it can be seen that the data for solutions (ii) and (iii) show no significant departure from that best fit curve.

The temperature variation of $P_m T_{2p}$ for solution (i) was fitted to equation 4.5 by a program utilizing the non-linear least-squares fitting module DATAFIT on the Cyber 173 computer optimizing both kinetic and activation parameters. Optimized parameters thus derived for dmf exchange on $[Cu(Me_6 tren)dmf]^{2+}$ in dmf solution are given in table 4.3.

The paramagnetic induced chemical shift of the bulk solvent dmf resonance line, $\Delta\omega$, relative to the internal 2% benzene reference resonance line, was measured by hand directly from nmr absorption spectra. The resultant raw chemical shift data for solution (i), at temperatures over the full temperature range studied, appear as an appendix to this thesis. The temperature variation of $\Delta\omega$ characterizing exchange of dmf on $[Cu(Me_6 tren)dmf]^{2+}$ may be given according to equation 4.6

$$\Delta\omega = \frac{\Delta\omega_m P_m}{(\tau_m/T_{2m} + 1)^2 + \tau_m^2 \Delta\omega_m^2} \qquad (4.6)$$

where all of the symbols have been previously defined. This variation is shown in figure 4.7. The $\Delta\omega$ variation below 320K arises as a result
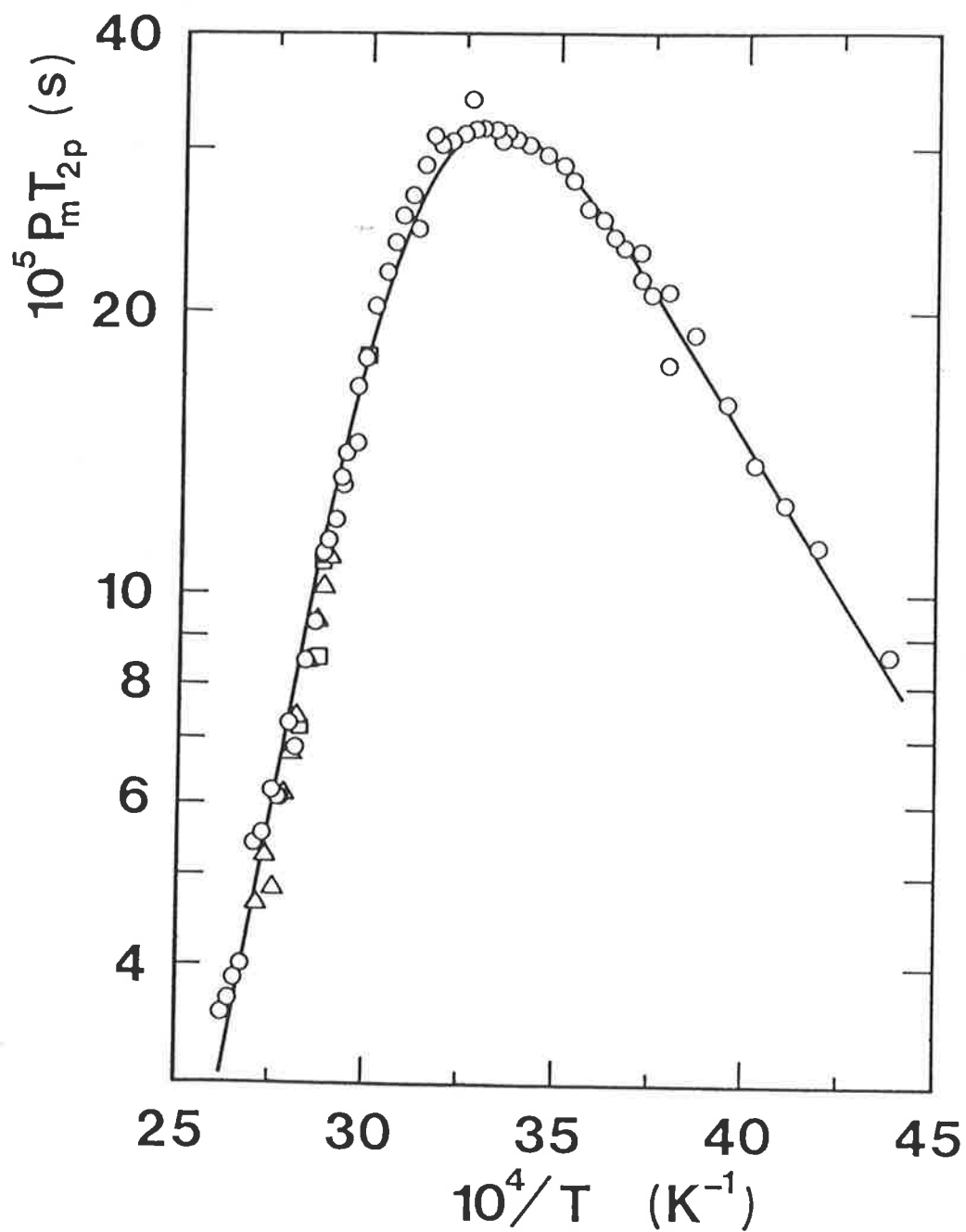
Figure 4.6

Temperature variation of P_mT_{2p} for the bulk solvent dmf formyl proton resonance characterizing dmf exchange on $[Cu(Me_6tren)dmf]^{2+}$. Circles, triangles and squares represent data for solutions (i)-(iii), respectively.

Table 4.3

Parameters[a] for dmf exchange on $[Cu(Me_6tren)dmf]^{2+}$ in dmf solution.

$T(K)$	$k_{ex}(s^{-1})$
278.2	150 ± 10
288.2	298 ± 21
298.2	555 ± 39

$T(K)$	$\Delta V^{\#}(cm^3mol^{-1})$[b]
350K	6.8 ± 0.2
365K	6.1 ± 0.1

$\Delta H^{\#} = 43.3 \pm 1.1 \ kJ \ mol^{-1}$

$\Delta S^{\#} = -47.0 \pm 3.1 \ JK^{-1} \ mol^{-1}$

$A_o = 17.0 \pm 3.0 \ s^{-1}$

$E_o = 12.5 \pm 0.4 \ kJ \ mol^{-1}$

a   All errors represent one standard deviation from the best fit

of the data to the appropriate equation.

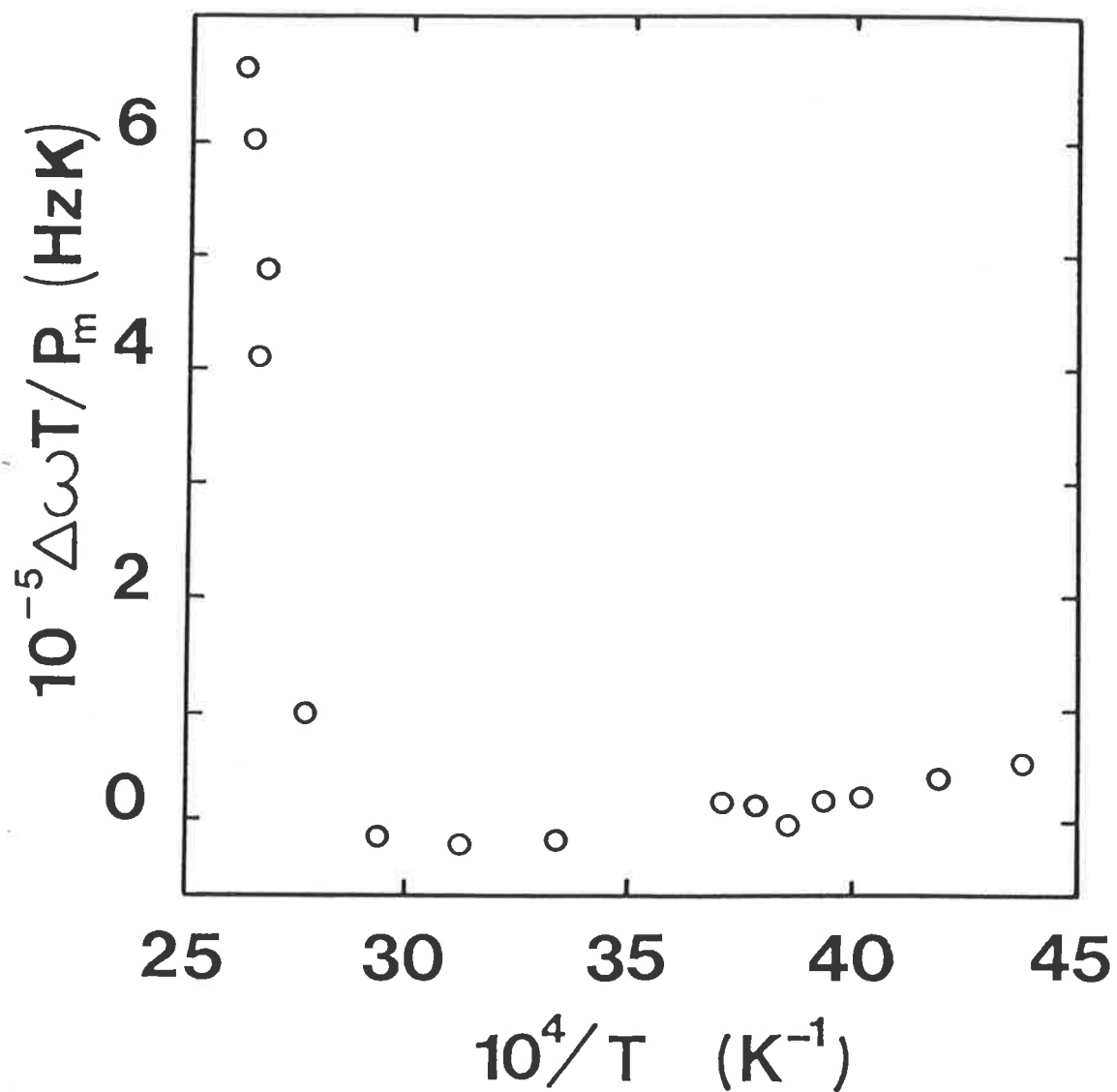b   Parameters from A.E. Merbach, Université de Lausanne.

Figure 4.7

Temperature variation of $\Delta\omega T$ for the bulk solvent dmf formyl

proton resonance characterizing dmf exchange on

$[Cu(Me_6tren)dmf]^{2+}$. The circles represent data for solution

(i) with $P_m = 0.01378$.

of dipolar interactions between $[Cu(Me_6tren)dmf]^{2+}$ and dmf outside the first coordination sphere. Above 320K the temperature variation of $\Delta\omega$ arises from relaxation of coordinated dmf consistent with the interpretation of the T_{2p} data.

Samples of $[Cu(Me_6tren)dmf]^{2+}$ in dmf solution at 0.194 and 0.484 mol dm^{-3} were prepared, sealed in glass under vacuum and shipped to Professor A.E. Merbach at the Université de Lausanne. The effect of pressure on dmf exchange in $[Cu(Me_6tren)dmf]^{2+}$ was determined and the volume of activation, $\Delta V^\#$, calculated (see section 2.4.3). Values of $\Delta V^\#$ as determined by Professor Merbach are given in table 4.3. The activation compressibility, $\Delta\beta^\#$, (see section 2.4.3) was found to be very small; $\Delta\beta^\# = 0.9(\pm0.3) \times 10^{-2}$ cm^3 mol^{-1} $(Nm^{-2})^{-1}$. The pressure dependence of the ratio of k_{ex} at ambient pressure, k_o and under an applied pressure, k_p, is shown in figure 4.8.

4.1.5 Ligand exchange on $[Cu(Me_6tren)def]^{2+}$ in def

Ligand exchange of def on $[Cu(Me_6tren)def]^{2+}$ in def solution was studied over the temperature range 240-402 K employing nmr spectroscopy. Two solutions which were 0.0685 and 0.0228 mol dm^{-3} in $[Cu(Me_6tren)def]^{2+}$ were prepared in the manner described in section 3.3.3, as were the accompanying $[Zn(Me_6tren)def](ClO_4)_2$ reference solutions. The 0.0685 mol dm^{-3} solution represents approximately the limiting solubility of $[Cu(Me_6tren)def](ClO_4)_2$ in def under the experimental conditions of this study.

Kinetic exchange behaviour was followed by monitoring the variation of transverse relaxation time of the formyl proton resonance of bulk solvent def with temperature in each $[Cu(Me_6tren)def]^{2+}$ solution, relative to a $[Zn(Me_6tren)def]^{2+}$ reference solution at an identical concentration. This was effected in precisely the same manner as for dmf
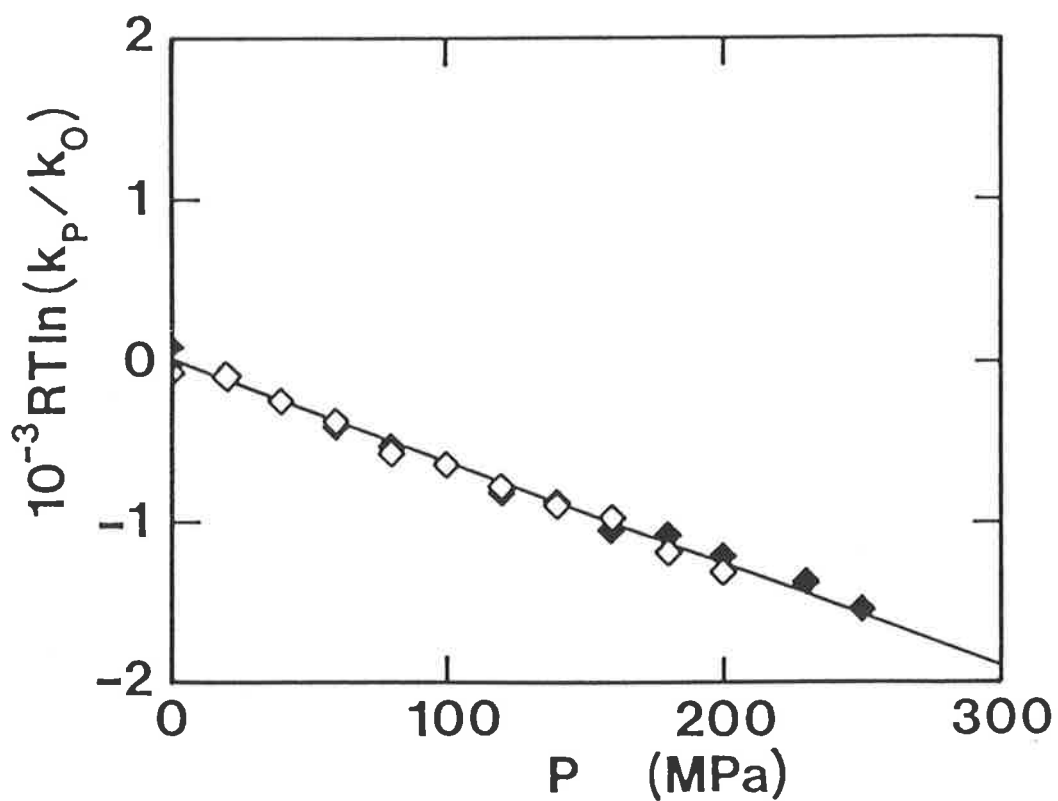
Figure 4.8

Variation of the ratio of k_{ex} at ambient, k_o and applied, k_p, pressure of $[Cu(Me_6tren)dmf]^{2+}$ in dmf solution. The open and filled symbols represent data derived from solutions for which $P_m = 0.0452$ (350.3K) and 0.0166 (364.6K), respectively.

exchange on $[Cu(Me_6tren)dmf]^{2+}$ (see section 4.1.3). Resultant T_{2p} data appear as an appendix to this thesis.

The relationship between T_{2p} and the def exchange process according to the Swift and Connick treatment (see section 2.4.2) is given by equation 4.4. For def exchange on $[Cu(Me_6tren)def]^{2+}$ equation 4.4, under the limits of slow and very slow exchange, reduces to equation 4.5. The def exchange rate on $[Cu(Me_6tren)def]^{2+}$ then becomes

$$- \, ^V\!def = k_{ex} \, [Cu(Me_6tren)def^{2+}]$$

where k_{ex} is the rate constant characterizing exchange and obtainable from the solution to equation 4.5. The temperature variation of P_mT_{2p}, for the bulk solvent def formyl proton resonance characterizing def exchange on $[Cu(Me_6tren)def]^{2+}$ is shown in figure 4.9. This variation is found to be reversible over the full experimental temperature range.

The temperature variation of P_mT_{2p} for the most concentrated solution was fitted to equation 4.5 using the non-linear least-squares DATAFIT fitting module on a Cyber 173 computer optimizing both kinetic and activation parameters. Optimized parameters thus derived for def exchange on $[Cu(Me_6tren)def]^{2+}$ in def solution are given in table 4.4.

The variation in paramagnetic induced chemical shift of the bulk solvent def resonance line, $\Delta\omega$, was determined in the same manner as for dmf in section 4.1.3 and the resultant chemical shift data for the 0.0228 mol dm^3 solution appears as an appendix to this thesis. Whilst the anticipated variation of this chemical shift is given by equation 4.6, the domination of equation 4.6 by the τ_m term over the experimental temperature range caused the magnitude of $\Delta\omega$ to be too small to enable reliable derivation of kinetic parameters. The observed temperature variation of $\Delta\omega$ is shown in figure 4.10.
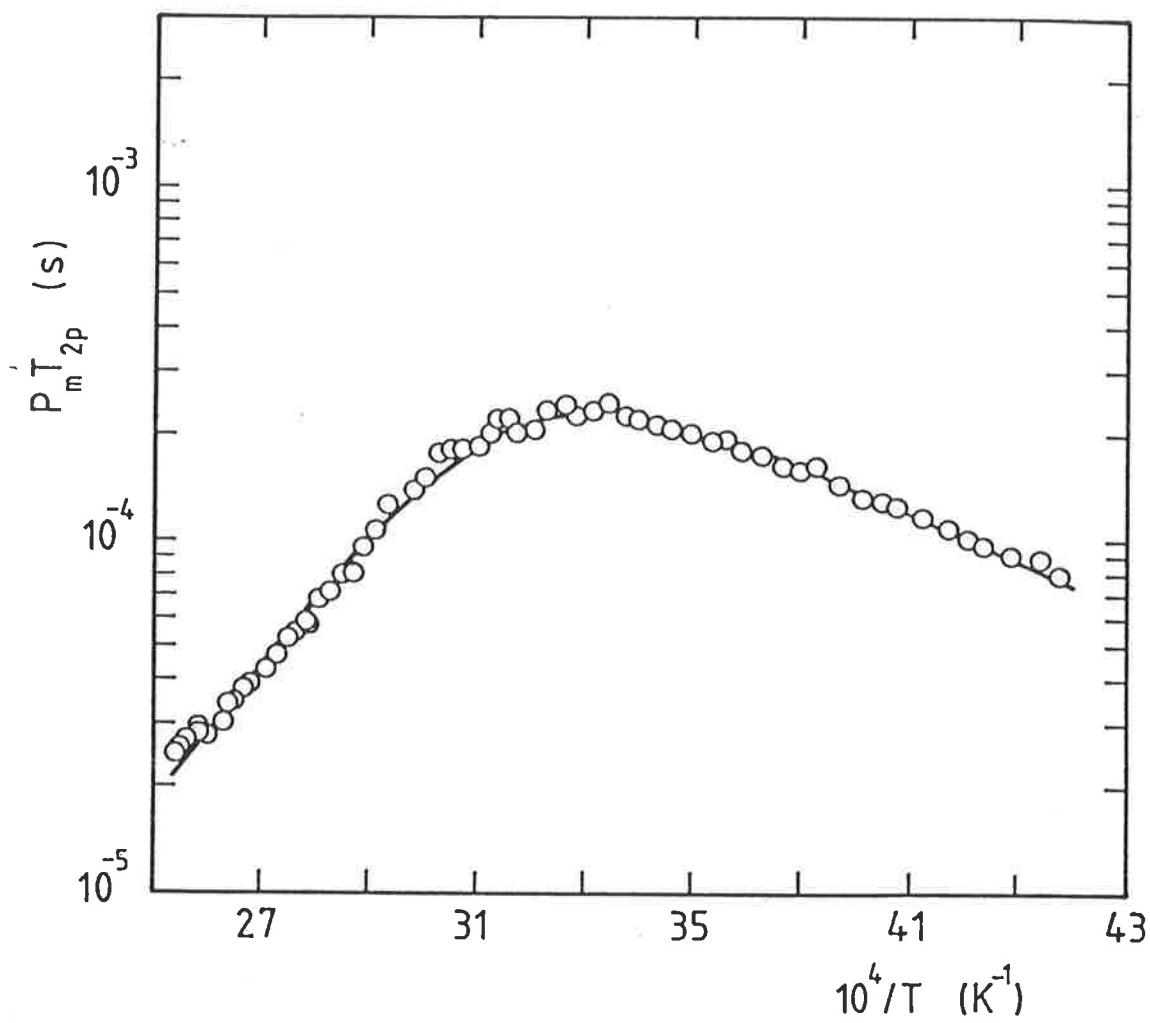
Figure 4.9

Temperature variation of $P_m T_{2p}$ for the bulk solvent def formyl proton resonance characterizing def exchange on $[Cu(Me_6 tren)def]^{2+}$. The circles represent data derived from a solution for which $P_m = 0.008077$.

Table 4.4

Parameters[a] for def exchange on $[Cu(Me_6tren)def]^{2+}$ in def solution.

$k_{ex}(298.2K) = 980 \pm 70 \ s^{-1}$

$\Delta V^{\#}(365.4K)^{b} = 5.3 \pm 0.3 \ cm^3 mol^{-1}$

$[\Delta \beta^{\#} = 0 \ cm^3 \ mol^{-1}(Nm^{-2})^{-1}]$

$\Delta H^{\#} \qquad = 36.3 \pm 0.9 \ kJ \ mol^{-1}$

$\Delta S^{\#} \qquad = -65.9 \pm 2.5 \ JK^{-1} \ mol^{-1}$

$A_o \qquad = 14.0 \pm 3.4 \ s^{-1}$

$E_o \qquad = 13.6 \pm 0.5 \ kJ \ mol^{-1}$

a. All errors represent one standard deviation from the best fit of the data to the appropriate equation.

b. From A.E. Merbach, Université de Lausanne.
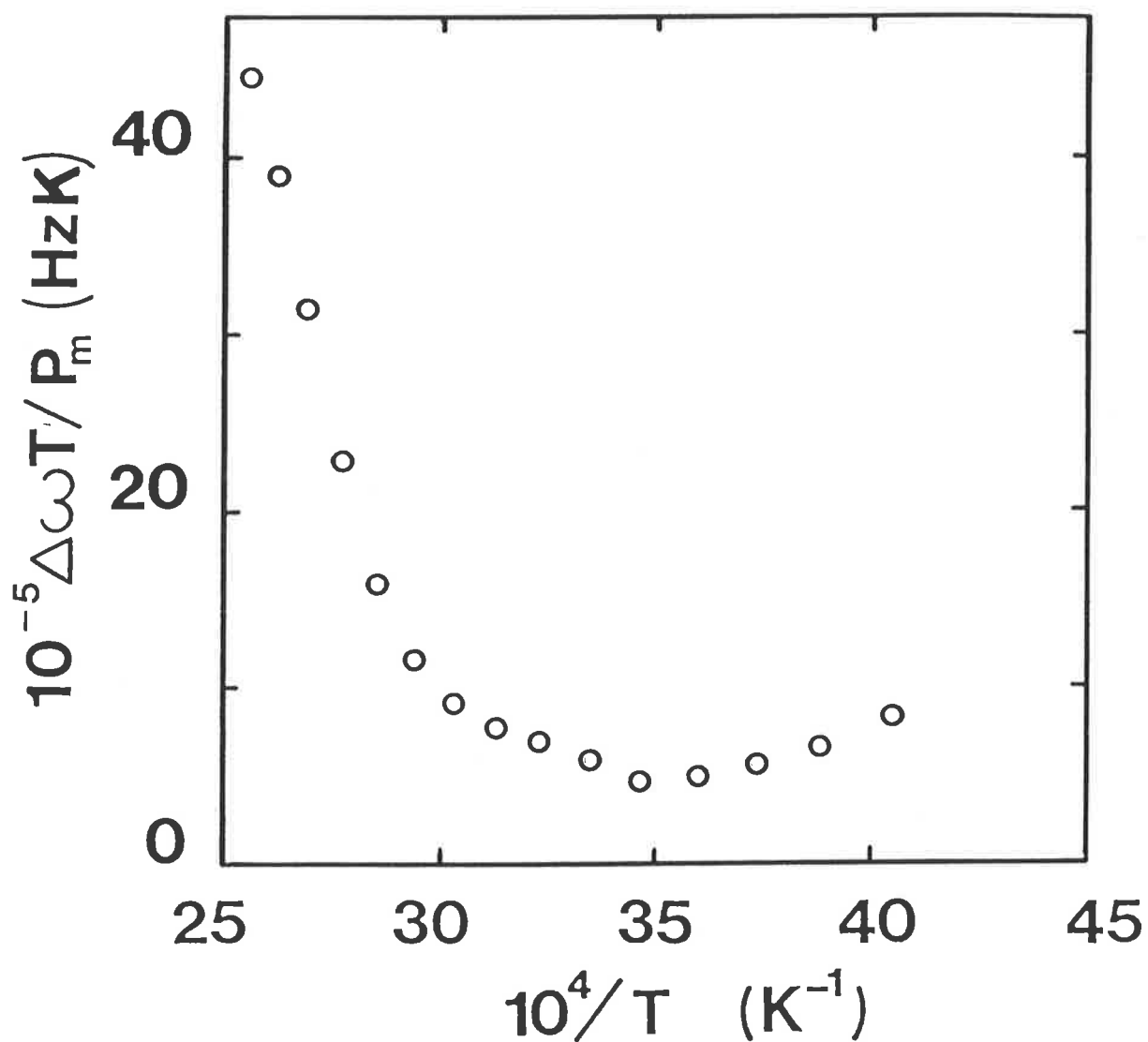
Figure 4.10

Temperature variation of $\Delta\omega T$ for the bulk solvent def formyl proton resonance characterizing def exchange on $[Cu(Me_6tren)def]^{2+}$. The circles represent data derived from a solution for which $P_m = 0.002620$.

The effect of pressure on def exchange in $[Cu(Me_6tren)def]^{2+}$ was undertaken by Professor A.E. Merbach on a sample of concentration 0.0668 mol dm^{-3} in $[Cu(Me_6tren)def]^{2+}$ sent to the Univesité de Lausanne. The pressure dependence of the ratios of k_{ex} at ambient pressure, k_o and under an applied pressure, k_p, is shown in figure 4.11. The calculated volume of activation, $\Delta V^\#$, and activation compressibility, $\Delta \beta^\#$, (see section 2.4.3) are given in table 4.4.

4.1.6 Ligand exchange on $[Cu(Me_6tren)dma]^{2+}$ in dma

Ligand exchange of dma on $[Cu(Me_6tren)dma]^{2+}$ in dma solution was studied over the temperature range 255-369K employing nmr spectroscopy. Two solutions which were 0.132 and 0.211 mol dm^{-3} in $[Cu(Me_6tren)dma]^{2+}$ were prepared in the manner described in section 3.3.3, as were the accompanying $[Zn(Me_6tren)dma]^{2+}$ reference solutions. The 0.211 mol dm^{-3} solution represents approximately the limiting solubility of $[Cu(Me_6tren)-dma](ClO_4)_2$ in dma under the experimental conditions of this study.

Kinetic exchange behaviour was followed by monitoring the variation of the transverse relaxation time of the acetyl proton resonance of bulk solvent dma with temperature in each $[Cu(Me_6tren)dma]^{2+}$ solution, relative to a $[Zn(Me_6tren)dma]^{2+}$ reference solution at an identical concentration. This was undertaken in the same manner as for dmf exchange on $[Cu(Me_6tren)-dmf]^{2+}$ (see section 4.1.3) and the resultant T_{2p} data appears as an appendix to this thesis.

The temperature variation of $P_m T_{2p}$ for the bulk solvent dma acetyl proton resonance characterizing dma exchange on $[Cu(Me_6tren)dma]^{2+}$ is shown in figure 4.12. This variation was found to be reversible over the temperature range studied. The resultant T_{2p} temperature dependent profile shows only a component which is believed to be that arising from exchange under the very slow exchange limit with $\tau_m^{-1} << T_{2m}^{-1}$ and $\Delta \omega_m$. Under this
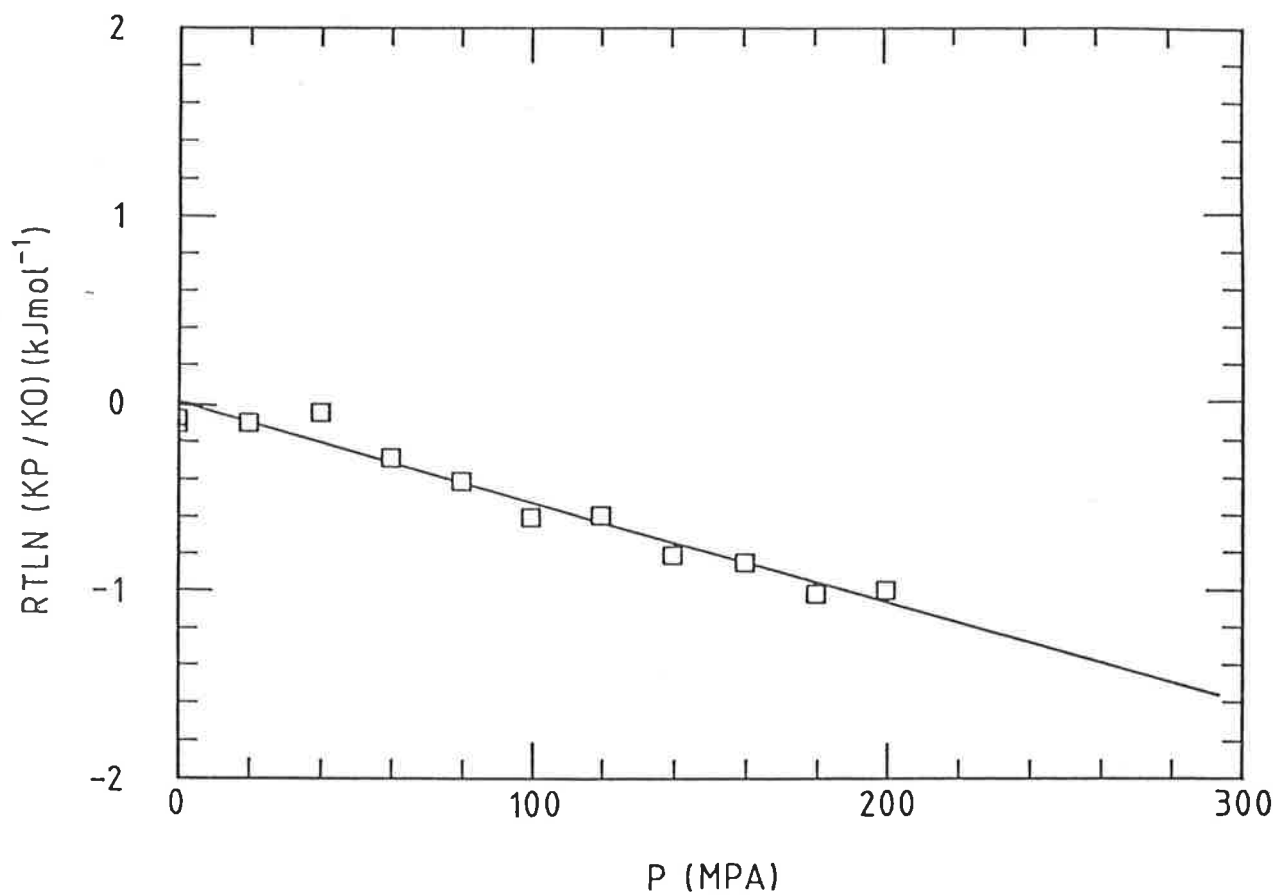
Figure 4.11

Variation of the ratio of k_{ex} at ambient, k_o and applied, k_p, pressure of $[Cu(Me_6tren)def]^{2+}$ in def solution. The squares represent data derived from a solution for which $P_m = 0.0083$ (365.4K).
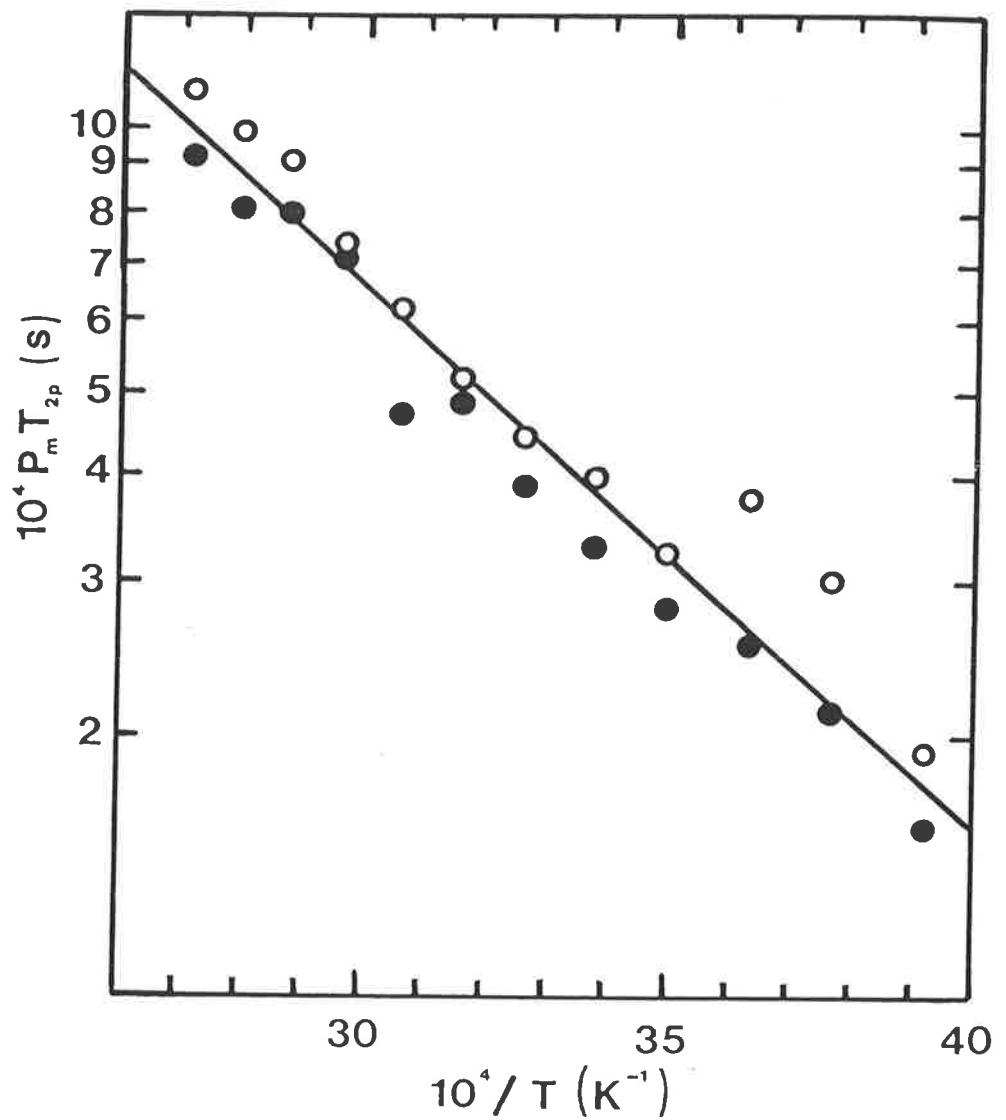
Figure 4.12

Temperature variation of P_mT_{2p} for the bulk solvent dma acetyl proton resonance characterizing dma exchange on $[Cu(Me_6tren)dma]^{2+}$. The open and filled circles represent data derived from solutions for which P_m = 0.01303 and 0.01995, respectively.

condition the Swift and Connick treatment (see section 2.4.2) predicts the form of T_{2p} as given by equation 4.4 to reduce to

$$T_{2p}^{-1} = P_m/T_{2o}$$

and thus the already familiar $P_m T_{2p}$ versus $1/T$ profile is not developed in the case of dma exchange to the same extent as for dmf and def. It is highly likely that the chemical exchange region defined by the experimentally attainable data is in the very slow exchange limit (see section 2.4.2) but this cannot be unequivocally deduced due to the small chemical shifts observed for the acetyl proton resonance of bulk solvent dma (see appendix 1.7).

If this is indeed the case, this region contains no chemical exchange parameters but characterizes outer sphere effects accounting for long-range dipolar magnetic interactions. Clearly, no dma exchange parameters can be derived from the available data but the result is nevertheless significant. The chemical exchange region corresponding to slow exchange, which contains the wealth of chemical exchange kinetic information, is believed to occur at temperatures above those experimentally attainable. This implies that dma exchange on this species is likely to take place at temperatures in excess of 370K and therefore be characterized by a larger exchange rate constant than for def and dmf exchange.

4.2 Ni(II) complexes in solution

4.2.1. Spectral variation on formation of $[Ni(Me_6Tren)X]^+$ in dmf

The ultraviolet/visible absorption spectra in dmf solution (ionic strength adjusted to 0.5 mol dm^{-3} with sodium perchlorate) of the solvated complex $[Ni(Me_6tren)dmf]^{2+}$ and anated species $[Ni(Me_6tren)X]^+$ where $X^- = Br^-$, N_3^-, NCS^- were recorded at 298.2K and the resulting molar absorbance versus wavelength plot is shown in figure 4.13.

The spectrum of $[Ni(Me_6tren)Br]^+$ in dmf as shown in figure 4.13 very closely resembles that observed in dichloromethane (CH_2Cl_2) solution[10] with an absorption band at ca 700nm which may be assigned to the $^3E \rightarrow ^3A_2$ transition[10], indicative of approximately trigonal-bipyramidal geometry. This is consistent with the retention of a five-coordinate structure in solution, given the known approximate C_{3V} symmetry of $[Ni(Me_6tren)Br]Br$ from solid state X-ray studies[11]. The spectra of the azido and thiocyanato complexes are also typical of a five-coordinate structure of C_{3V} symmetry. The solution spectrum of $[Ni(Me_6tren)dmf]^{2+}$ is also as expected for a five-coordinate species but dmf solvent exchange studies, to be discussed later, suggest the possibility of small amounts of six-coordinate $[Ni(Me_6tren)(dmf)_2]^{2+}$ existing in solution. However, a comparison of this spectrum with that of $[Ni(tren)(dmf)_2]^{2+}$, expected to be a six-coordinate complex of similar geometry and therefore be characterized by a similar spectrum to $[Ni(Me_6tren)(dmf)_2]^{2+}$ suggests, since the two spectra are very dissimilar, that $[Ni(Me_6tren)dmf]^{2+}$ is the greatly predominant species in solution. The spectrum of $[Ni(tren)(dmf)_2]^{2+}$ is also shown in figure 4.13.

Primary and secondary kinetic observation wavelengths for substitution of dmf in $[Ni(Me_6tren)dmf]^{2+}$ by each anion were determined subject to the criteria already outlined (see section 4.1.1) and the results are given in table 4.5.
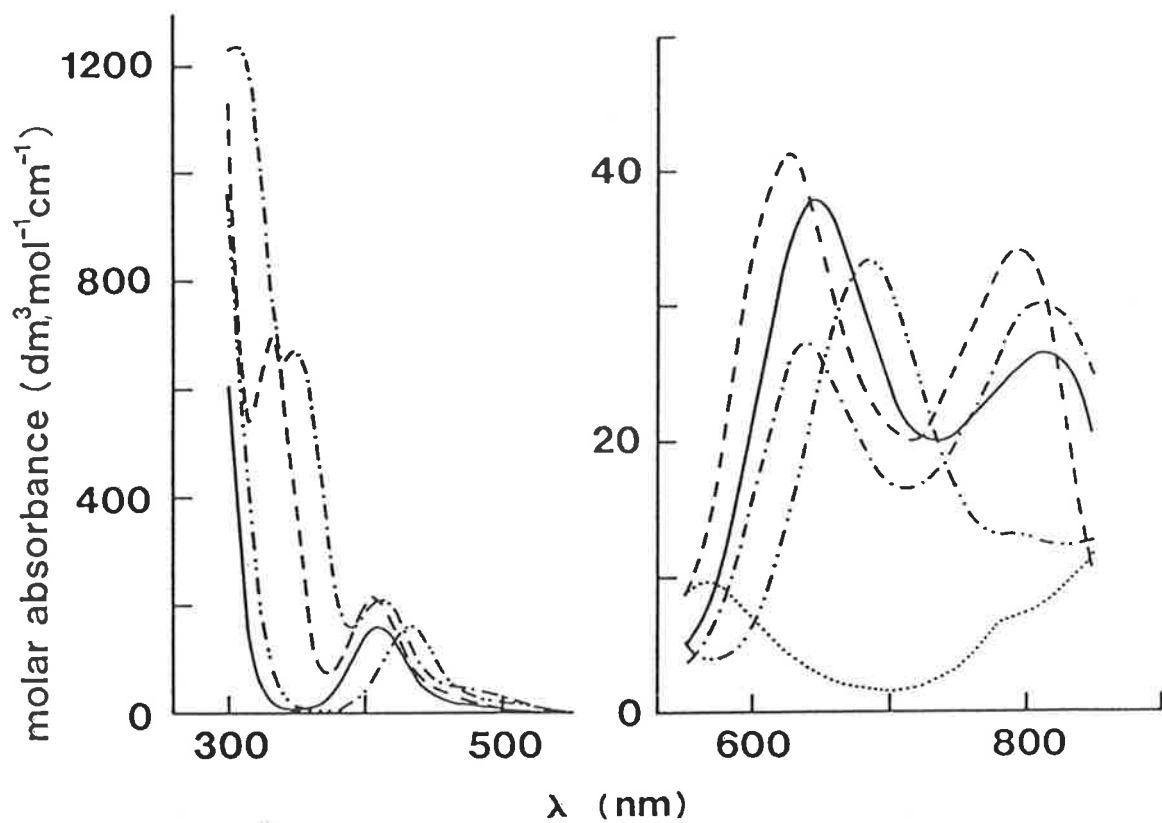
Figure 4.13

Ultraviolet/visible absorption spectra of $[Ni(Me_6tren)dmf]^{2+}$ (———),

$[Ni(Me_6tren)X]^+$ ($X^- = Br^-$ (——··——), N_3^- (——·——), NCS^- (---)) and

$[Ni(tren)(dmf)_2]^{2+}$ (······) in dmf solution.

Table 4.5

Kinetic observation wavelengths for the formation of $[Ni(Me_6tren)X]^+$ in dmf solution (ionic strength adjusted to 0.5 mol dm^{-3} with sodium perchlorate) at 298.2K.

anion X^-	wavelength λ (nm)	change in molar absorbance $\Delta\epsilon^a$ $(dm^3mol^{-1}cm^{-1})$
Br^-	408	-80
	432	80
N_3^-	315	1040
	343	660
NCS^-	332	670
	408	50

(a $\quad \Delta\epsilon = \epsilon_{[Ni(Me_6tren)X]^+} - \epsilon_{[Ni(Me_6tren)dmf]^{2+}}$)

4.2.2 Job plots for [Ni(Me$_6$tren)X]$^+$ formation in dmf

A series of solutions at differing ratios of initial [Ni(Me$_6$tren)dmf]$^{2+}$ concentration to initial anion concentration were prepared as described in section 3.3.4 for each of the three anion (Br$^-$, N$_3^-$ and NCS$^-$) systems. The concentration ranges of [Ni(Me$_6$tren)dmf]$^{2+}$ and X$^-$ used were 8.0 x 10^{-4} - 8.0 x 10^{-3} mol dm^{-3} for Br$^-$, 1.3 x 10^{-4} - 1.3 x 10^{-3} mol dm^{-3} for N$_3^-$ and 6.1 x 10^{-4} - 6.1 x 10^{-3} mol dm^{-3} for NCS$^-$ in the Job method analyses. The ultraviolet/visible absorption spectrum of each solution was recorded at 298.2K for each system and absorbance measured at an appropriate wavelength for that system. These wavelengths were 432, 343 and 610 nm for Br$^-$, N$_3^-$ and NCS$^-$ respectively.

The results of the Job method analysis (see chapter 2.2) for each system are shown in figure 4.14. These results are in each case indicative of the formation of a single 1:1 species, [Ni(Me$_6$tren)X]$^+$. The appearance of a sharply defined apex for each plot is characteristic[2] of a high stability constant estimated at $\sim 10^3$ dm^3 mol^{-1} in the reaction of [Ni(Me$_6$tren)dmf]$^{2+}$ with each of the anions Br$^-$, N$_3^-$ and NCS$^-$.

4.2.3 Ligand substitution on [Ni(Me$_6$tren)dmf]$^{2+}$ in dmf

Ligand substitution of dmf on [Ni(Me$_6$tren)dmf]$^{2+}$ by anions Br$^-$, N$_3^-$ and NCS$^-$ in dmf solution (adjusted to an ionic strength of 0.5 mol dm^{-3} with sodium perchlorate) was studied at 278.2K, 288.2K and 298.2K by stopped-flow spectrophotometry at the same wavelengths as are given in table 4.5. Experimental solutions were prepared (see section 3.3.5) with the initial concentrations of [Ni(Me$_6$tren)dmf]$^{2+}$ varied in the range 4.50 x 10^{-5} - 2.10 x 10^{-3} mol dm^{-3}, in all cases never exceeding 10% of the excess anion concentrations, which varied in the range 5.00 x 10^{-3} - 8.76 x 10^{-2} mol dm^{-3}, at all times maintaining pseudo first-order conditions.
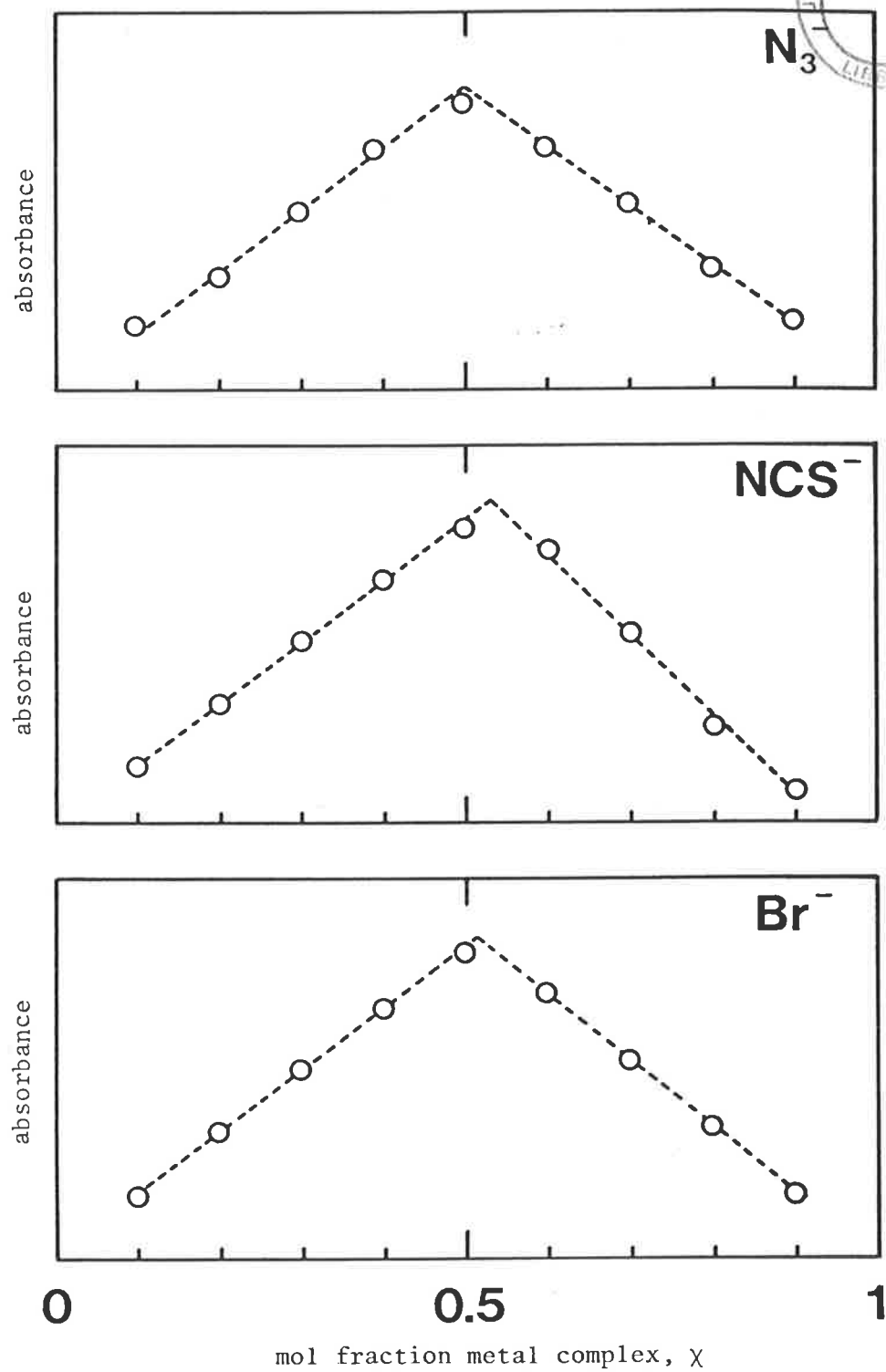
Figure 4.14

Job plots for the formation of $[Ni(Me_6tren)X]^+$ (X =
N_3^-, NCS^-, Br^-) in dmf solution.
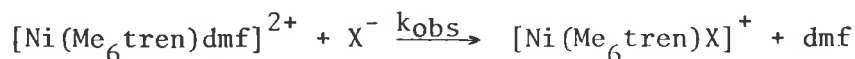
The anation reaction:

$$[Ni(Me_6tren)dmf]^{2+} + X^- \xrightarrow{k_{obs}} [Ni(Me_6tren)X]^+ + dmf$$

is characterized by a single kinetic process, typified by a first-order rate constant, k_{obs}. Experimentally determined values of k_{obs} for each solution were obtained from a non-linear least-squares fit of an averaged digitized reaction trace to a single exponential equation (see section 3.4.4). The resultant values appear as an appendix to this work.

- The variation of k_{obs} with excess anion concentration, $[X^-]$, where $X^- = N_3^-$ and NCS^- is shown in figure 4.15. Inspection of these plots reveals that when $[X^-] = 0$, k_{obs} approaches zero within experimental error and accordingly k_i, the rate constant characterizing dissociation of $[Ni(Me_6tren)X]^+$, is equated to zero in subsequent data treatment and therefore not further considered. Under these circumstances the variation of k_{obs} with $[X^-]$ is consistent with equation 4.7

$$k_{obs} = \frac{k_i K_0 [X^-]}{1 + K_0 [X^-]} \qquad (4.7)$$

which typifies (see section 2.1.3) an interchange (I) mechanism[3] proceeding through the following reaction scheme.

$$[Ni(Me_6tren)dmf]^{2+} + X^- \underset{fast}{\overset{K_0}{\rightleftharpoons}}$$

$$[Ni(Me_6tren)dmf]^{2+}...X^- \underset{k-i}{\overset{k_i}{\rightleftharpoons}}$$
$$\text{(encounter complex)}$$

$$[Ni(Me_6tren)X]^+ + dmf$$
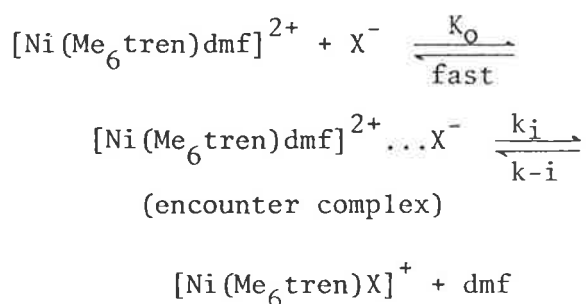
The rapid formation of the encounter complex in which X^- resides in the second coordination sphere of the solvated complex is characterized by K_0, and the subsequent rate determining exchange of X^- between the second and first coordination sphere is characterized by the forward rate constant k_i. When $X^- = Br^-$ the small absorbance change characterizing

Figure 4.15

Variation of k_{obs} for the anation of $[Ni(Me_6tren)dmf]^{2+}$ by N_3^- and NCS^- with temperature and excess anion concentration in dmf solution.

Data at 298.2, 288.2 and 278.2K are represented by circles, triangles and squares respectively. Data points are characterized by open and filled symbols for N_3^- and NCS^-, respectively.
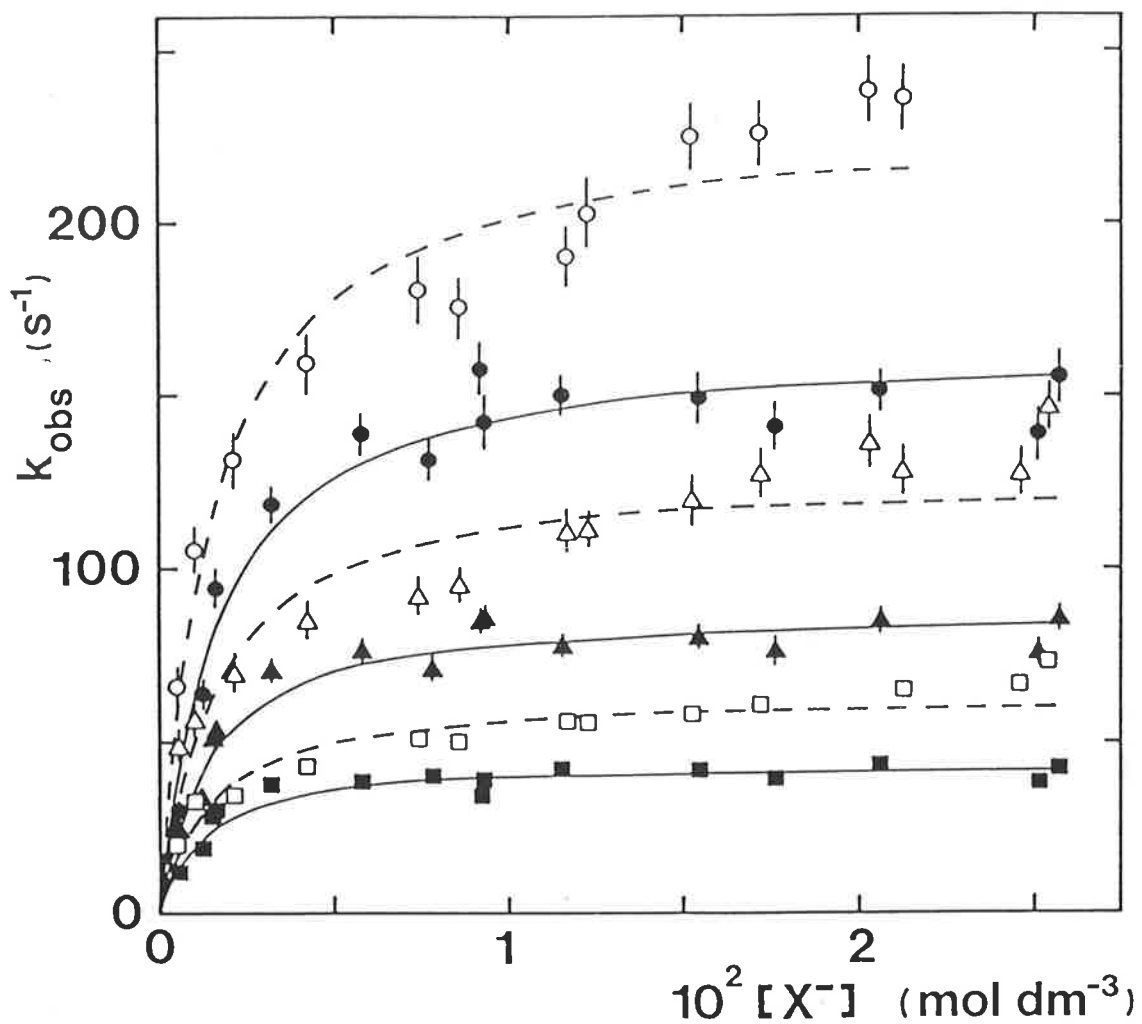
the anation process (see table 4.5) limits kinetic study to $[Br^-] > 0.03$ mol dm^{-3}. The variation of k_{obs} with excess bromide ion concentration is shown in figure 4.16. Under these higher $[Br^-]$ conditions k_{obs} is observed to be independent of $[Br^-]$, this being consistent with the limiting condition $K_o[X^-] \gg 1$ (see section 2.1.3) causing equation 4.7 to reduce to equation 4.8.

$$k_{obs} = k_i \qquad\qquad\qquad (4.8)$$

Kinetic parameters k_i, K_o and activation enthalpy and entropy $\Delta H_i^{\#}$ and $\Delta S_i^{\#}$, respectively, characterizing anation of $[Ni(Me_6tren)dmf]^{2+}$ by N_3^- and NCS^-, were derived by the following procedure. Recalling the temperature dependent formulation of the Eyring equation (equation 4.2),

$$k_i = \frac{k_b T}{h} \exp\left(-\Delta H_i^{\#}/RT\right) \exp\left(\Delta S_i^{\#}/R\right) \qquad\qquad (4.2)$$

combining equations 4.2 and 4.7, and simultaneously fitting experimentally determined data at all three experimental temperatures to this model using the DATAFIT non-linear least-squares fitting module on the Cyber 173 computer, optimized values for k_i, K_o, $\Delta H_i^{\#}$ and $\Delta S_i^{\#}$ can be obtained. A similar method, using a model combining equations 4.2 and 4.8, was employed to obtain optimized values for k_i, $\Delta H_i^{\#}$ and $\Delta S_i^{\#}$ characterizing anation of $[Ni(Me_6tren)dmf]^{2+}$ by Br^-.

These kinetic and activation parameters characterizing anation of $[Ni(Me_6tren)dmf]^{2+}$ in dmf are given in table 4.6. The best fit lines as a result of simultaneous data fitting for each anion studied are shown also in figures 4.15 and 4.16.

4.2.4 Ligand exchange on $[Ni(Me_6tren)dmf]^{2+}$ in dmf

Ligand exchange of dmf on $[Ni(Me_6tren)dmf](ClO_4)_2$ in dmf solution was studied over the temperature range 229-386K employing nmr spectroscopy. Two solutions which were 0.159 and 0.415 mol dm^{-3} in $[Ni(Me_6tren)dmf](ClO_4)_2$
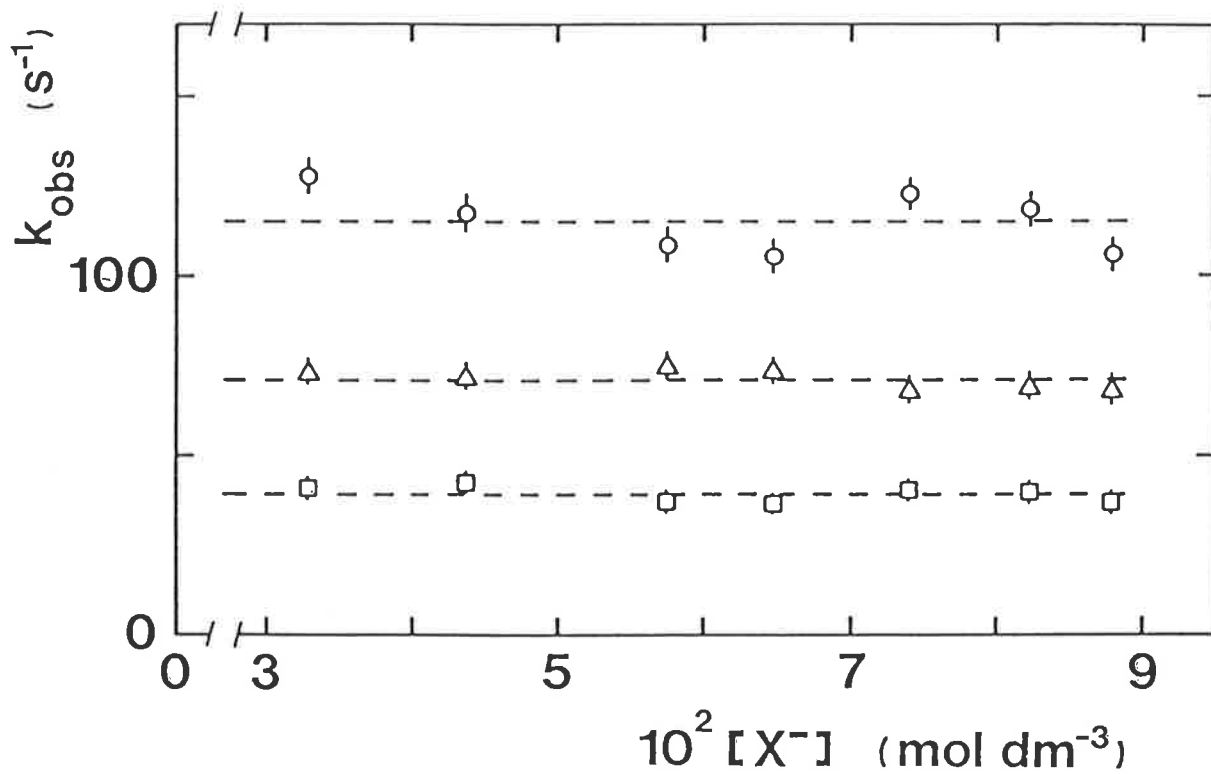
Figure 4.16

Variation of k_{obs} for the anation of $[Ni(Me_6tren)dmf]^{2+}$ by Br^- with temperature and excess $[Br^-]$ im dmf solution. Data at 298.2, 288.2 and 278.2K are represented by circles, triangles and squares, respectively.

Table 4.6

Kinetic and activation parameters[a] for anation by X^- in the $[Ni(Me_6tren)dmf]^{2+}$ species in dmf solution at an ionic strength of 0.5 mol dm^3 adjusted with $NaClO_4$.

X^-	Br^-	N_3^-	NCS^-
$K_o(298.2K)$ (dm^3mol^{-1})	-	758 ± 114	520 ± 60
$k_i(298.2K)$ (s^{-1})	116 ± 3	229 ± 10	170 ± 6
$k_i(288.2K)$ (s^{-1})	68.5 ± 1.6	123 ± 6	88.4 ± 2.3
$k_i(278.2K)$ (s^{-1})	39.2 ± 2.4	63.4 ± 2.8	44.1 ± 1.3
$\Delta H_i^{\#}$ $(kJ\ mol^{-1})$	34.9 ± 1.2	41.8 ± 2.5	44.0 ± 2.1
$\Delta S_i^{\#}$ $(JK^{-1}\ mol^{-1})$	-88.4 ± 4.2	-59.6 ± 8.4	-54.7 ± 7.2

a   Parameters derived from a simultaneous fit of data at three
temperatures. All errors represent one standard deviation from
the best fit of the data to the appropriate equations.

were prepared in the manner described in section 3.3.3, as were the accompanying $[Zn(Me_6tren)dmf](ClO_4)_2$ reference solutions.

For dmf exchange occurring on the paramagnetic metal complex ion $[Ni(Me_6tren)dmf]^{2+}$, the relaxation parameter, T_{2p}, is, the difference in transverse relaxation times of the formyl proton of bulk solvent dmf in solutions of $[Ni(Me_6tren)dmf]^{2+}$, T_2, and that of the reference solutions of $[Zn(Me_6tren)dmf]^{2+}$, T_{2ref}.

$$T_{2p}^{-1} = T_2^{-1} - T_{2ref}^{-1}$$

Experimentally, the transverse relaxation times, T_2 and T_{2ref} are related to the linewidth at half-maximum intensity of the bulk solvent dmf formyl proton resonance (see section 2.4.2). Previous results for Cu(II) exchanging systems (see section 4.1) have shown that within experimental error direct measurement of resonance linewidths was as accurate as that from computer linewidth fitting techniques. Hence, direct measurement of resonance linewidths from spectra was used to determine transverse relaxation times. Resultant T_{2p} data for each solution appear as an appendix to this thesis.

The temperature variation of T_{2p} for the two solutions of $[Ni(Me_6tren)dmf](ClO_4)_2$ is shown in figure 4.17 and appears to be consistent with dmf exchange occurring at two different sites. This temperature variation was found to be reversible over the experimental temperature range.

The temperature variation of T_{2p} characterizing the well established $[Ni(tren)(dmf)_2]^{2+}$ system[12] is consistent with dmf at each of two non-equivalent coordination sites A and B being characterized by different mean residence times, τ_{mA} where
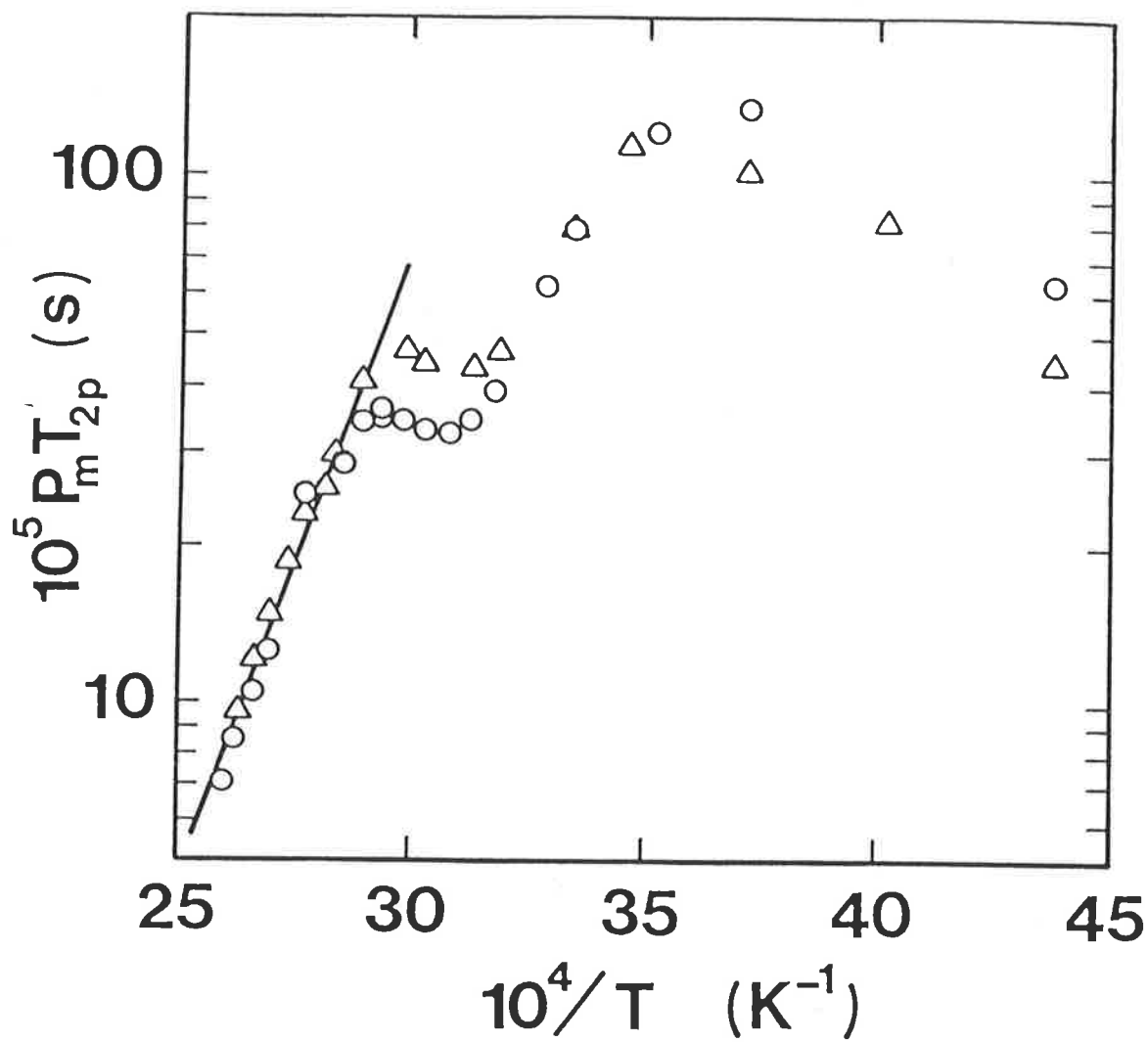
Figure 4.17

Temperature variation of P_mT_{2p} for the bulk solvent dmf formyl

proton resonance characterizing dmf exchange for solutions of

$[Ni(Me_6tren)dmf](ClO_4)_2$ in dmf. The circles and triangles represent

data derived from solutions for which P_m = 0.01291 and 0.03248,

respectively.

$$\tau_{mA} = {}^1\!/k_{exA} = \frac{h}{k_b T}\ \exp(\Delta H_A^{\#}/RT)\ \exp(-\Delta S_A^{\#}/R) \qquad (4.9)$$

with: k_{ex} = first-order dmf exchange rate constant

$\quad\quad$ h $\quad$ = Plank constant

$\quad\quad$ k_b $\quad$ = Boltzmann constant

$\quad\quad$ T $\quad$ = absolute temperature

$\quad\quad$ R $\quad$ = gas constant

$\quad\quad$ $\Delta H^{\#}$ = enthalpy of activation for dmf exchange

$\quad\quad$ $\Delta S^{\#}$ = entropy of activation for dmf exchange

and similarly τ_{mB} ($= 1/k_{exB}$) where subscripts A and B refer to the non-equivalent coordination sites. This temperature variation of T_{2p} may, in principle, be given by equation 4.10.

$$\frac{1}{T_{2p}} = \frac{P_{mA}}{\tau_{mA}} \left[\frac{T_{2mA}^{-2} + (T_{2mA}\,\tau_{mA})^{-1} + \Delta\omega_{mA}^{2}}{(T_{2mA}^{-1} + \tau_{mA}^{-1})^2 + \Delta\omega_{mA}^{2}} \right] + \frac{P_{mA}}{T_{2oA}}$$

$$+ \frac{P_{mB}}{\tau_{mB}} \left[\frac{T_{2mB}^{-2} + (T_{2mB}\tau_{mB})^{-1} + \Delta\omega_{mB}^{2}}{(T_{2mB}^{-1} + \tau_{mB}^{-1})^2 + \Delta\omega_{mB}^{2}} \right] + \frac{P_{mB}}{T_{2oB}} \qquad (4.10)$$

where: P_m = mole fraction of coordinated solvent at each site.

$\quad\quad$ T_m = transverse relaxation time of coordinated solvent at each site.

$\quad\quad$ $\Delta\omega_m$ = chemical shift between coordinated solvent at each site and bulk solvent.

$\quad\quad$ T_{2o} = contribution to T_{2p} arising from relaxation processes outside the first coordination sphere at each site.

with subscripts A and B again referring to the two non-equivalent dmf coordination sites on $[Ni(tren)(dmf)_2]^{2+}$.

Results from the equilibrium ultraviolet/visible study of the spectrum of $[Ni(Me_6tren)dmf](ClO_4)_2$ in dmf solution (see section 4.2.1) indicate that five-coordinate $[Ni(Me_6tren)dmf]^{2+}$ is the predominant species in solution so one may suppose that the observed behaviour of the T_{2p} variation of these solutions is due to the presence of a minor concentration of possibly the six-coordinate $[Ni(Me_6tren)(dmf)_2]^{2+}$ species. One might expect this T_{2p} variation to be a superimposition of the relaxation profiles of the two different species.

The first relaxation profile for dmf exchange occurring at only one site is defined only by terms containing the subscript A on the right-hand side of equation 4.10. Under the conditions of slow and very slow exchange equation 4.10 further reduces to equation 4.11.

$$^1/T_{2p} = \frac{P_{mA}}{\tau_{mA}} + \frac{P_{mA}}{T_{2oA}} \tag{4.11}$$

where the P_{mA}/τ_{mA} term dominates above ca 350K (slow exchange) and the P_{mA}/T_{2oA} term dominates below ca 280K (very slow exchange). Approximate values of kinetic and activation parameters characterizing dmf exchange on $[Ni(Me_6tren)dmf]^{2+}$ were obtained from least-squares fitting of the 13 highest temperature T_{2p} data points (those which form the linear portion of the temperature dependent T_{2p} plot in the slow exchange, τ_m, region) to a model combining the slow exchange component of equation 4.11 with equation 4.9 using the DATAFIT fitting module on the Cyber 173 computer. The regression line of best fit using this approach is shown in figure 4.17 and the corresponding kinetic and activation parameters are given in table 4.7.

It is not possible reliably to determine a relaxation profile for dmf exchange occurring at two non-equivalent sites due to the absence of any precise determination of the concentration ratios of the two nickel-

Table 4.7

Parameters[a] for dmf exchange on $[Ni(Me_6tren)dmf]^{2+}$ in dmf solution.

(i) Calculated assuming $[Ni(Me_6tren)dmf]^{2+}$ provides 100% of sites available for exchange.

$k_{ex}(298.2K) = 203 \pm 20 \text{ s}^{-1}$

$\Delta H^{\#} \qquad = 42.6 \pm 2.0 \text{ kJ mol}^{-1}$

$\Delta S^{\#} \qquad = -58 \pm 8 \quad \text{JK}^{-1} \text{ mol}^{-1}$

(ii) Calculated assuming $[Ni(Me_6tren)dmf]^{2+}$ provides 80% of sites available for exchange.

$k_{ex}(298.2K) = 254 \pm 22 \text{ s}^{-1}$

$\Delta H^{\#} \qquad = 42.6 \pm 2.0 \text{ kJ mol}^{-1}$

$\Delta S^{\#} \qquad = -56 \pm 8 \quad \text{JK}^{-1} \text{ mol}^{-1}$

(II) complexes. However, it is possible to estimate kinetic and activation parameters characterizing dmf exchange on $[Ni(Me_6tren)dmf]^{2+}$, assuming that $[Ni(Me_6tren)dmf]^{2+}$ provides, say, 80% of the sites available for exchange with the other 20% of the sites being provided by, say, $[Ni(Me_6tren)(dmf)_2]^{2+}$. Data treatment was undertaken in a similar manner to that above for $[Ni(Me_6tren)dmf]^{2+}$, except that the model used allowed for the reduced number of available coordination sites and temperature dependence of the equilibrium between the two nickel(II) complexes. The corresponding kinetic and activation parameters are also given in table 4.7.

If $[Ni(Me_6tren)(dmf)_2]^{2+}$ is in fact the second exchanging species then it is expected that 20% $[Ni(Me_6tren)(dmf)_2]^{2+}$ in dmf solutions of $[Ni(Me_6tren)dmf](ClO_4)_2$ would be an upper concentration ratio limit, so the correct value for k_{ex} (298.2K) characterizing dmf exchange on $[Ni(Me_6tren)dmf]^{2+}$ is assumed to lie between the two limiting values given in table 4.7. However, these values together with $\Delta H^{\#}$ and $\Delta S^{\#}$ parameters may be viewed, at best, as only semi-quantitative.

The T_{2p} temperature variation profile in the 280-350K region is believed to include a contribution from exchange on a more labile species, possibly $[Ni(Me_6tren)(dmf)_2]^{2+}$. However, since only two exchange processes are identifiable over the experimental temperature range it may be supposed that either both dmf exchange sites on $[Ni(Me_6tren)(dmf)_2]^{2+}$ exhibit similar labilities, or that a less labile exchange site on $[Ni(Me_6tren)(dmf)_2]^{2+}$ has a similar or far lesser lability (so as not to be detected over the experimental temperature range) than the dmf exchange site on $[Ni(Me_6tren)dmf]^{2+}$. A divergence with experimental $[Ni(Me_6tren)-dmf](ClO_4)_2$ solution concentration of P_mT_{2p} data would seem to be consistent with a concentration or ionic strength dependence of the

equilibrium existing between the five and six-coordinate nickel(II) species.

The paramagnetic induced chemical shift of the bulk solvent dmf resonance line, $\Delta\omega$, relative to the internal 2% benzene reference line, was measured by hand directly from nmr absorption spectra. The resultant chemical shift data for the 0.159 mol dm^{-3} in $[Ni(Me_6tren)dmf]$-$(ClO_4)_2$ solution over the full experimental temperature range appear as an appendix to this thesis. The temperature variation of $\Delta\omega$ characterizing dmf exchange on solvated $[Ni(Me_6tren)dmf](ClO_4)_2$ in dmf is shown in figure 4.18. Dipolar interactions between nickel (II) and dmf outside the first coordination sphere are responsible for the observed temperature variation of $\Delta\omega$ below 300K whilst above 300K this variation is a consequence of relaxation of coordinated dmf consistent with the interpretation of the T_{2p} data.

4.2.5 Ligand exchange on $[Ni(Me_6tren)def]^{2+}$ in def

Ligand exchange of def on $[Ni(Me_6tren)def](ClO_4)_2$ in def solution was studied over the temperature range 216 - 379K employing nmr spectroscopy. Two solutions (i) and (ii) which were 0.0635 and 0.0212 mol dm^{-3} in $[Ni(Me_6tren)def](ClO_4)_2$ respectively were prepared in the manner described in section 3.3.3, as were the accompanying $[Zn(Me_6tren)def](ClO_4)_2$ reference solutions.

Kinetic exchange behaviour was followed by monitoring the variation of transverse relaxation time of the formyl proton resonance of bulk solvent def with temperature in each $[Ni(Me_6tren)def]^{2+}$ solution relative to a $[Zn(Me_6tren)def]^{2+}$ reference solution at an identical concentration. This was undertaken in the same manner as for dmf exchange on solutions of $[Ni(Me_6tren)dmf](ClO_4)_2$ in dmf. The resultant T_{2p} data appear as an appendix to this thesis.

Figure 4.18

Temperature variation of $\Delta\omega T$ for the bulk solvent dmf formyl proton resonance characterizing dmf exchange for solutions of $[Ni(Me_6 tren)dmf]$-$(ClO_4)_2$ in dmf. The inverted triangles represent data derived from a solution for which $P_m = 0.01291$.

According to the Swift and Connick treatment (see section 2.4.2) the relationship between T_{2p} and the def exchange process is given by equation 4.4,

$$T_{2p}^{-1} = \frac{P \cdot m}{\tau_m} \left[\frac{T_{2m}^{-2} + (T_{2m}\tau_m)^{-1} + \Delta\omega_m^2}{(T_{2m}^{-1} + \tau_m^{-1})^2 + \Delta\omega_m^2} \right] + \frac{P_m}{T_{2o}} \qquad (4.4)$$

where all the symbols have previously been defined. Under the limits of slow and very slow exchange, equation 4.4 reduces to equation 4.5, where $\tau_m^{-1} = k_{ex}$, the rate constant characterizing def exchange on $[Ni(Me_6tren)def]^{2+}$

$$(P_m T_{2p})^{-1} = \tau_m^{-1} + T_{2m}^{-1} = \frac{k_b T}{h} \exp(-\Delta H^{\#}/RT) \exp(\Delta S^{\#}/R)$$

$$+ A_o \exp(-E_o/RT) \qquad (4.5)$$

and where all the symbols have also been previously defined. The def exchange rate on $[Ni(Me_6tren)def]^{2+}$ thus becomes

$$v_{def} = k_{ex} [Ni(Me_6tren)def^{2+}]$$

The temperature variation of $P_m T_{2p}$ for the bulk solvent formyl proton resonance characterizing def exchange on $[Ni(Me_6tren)def]^{2+}$ is shown in figure 4.19 and was found to be reversible over the entire experimental temperature range.

The temperature variation of $P_m T_{2p}$ for the more concentrated solution (i) was fitted to equation 4.5 utilizing the non-linear least-squares DATAFIT fitting module on a Cyber 173 computer optimizing both kinetic and activation parameters. The best fit line of the T_{2p} data for solution (i) is shown in figure 4.19 and it can be seen that data for solution (ii) shows no significant departure from that best fit curve. Optimized parameters derived for def exchange on $[Ni(Me_6tren)def]^{2+}$ in def solution are given in table 4.8.
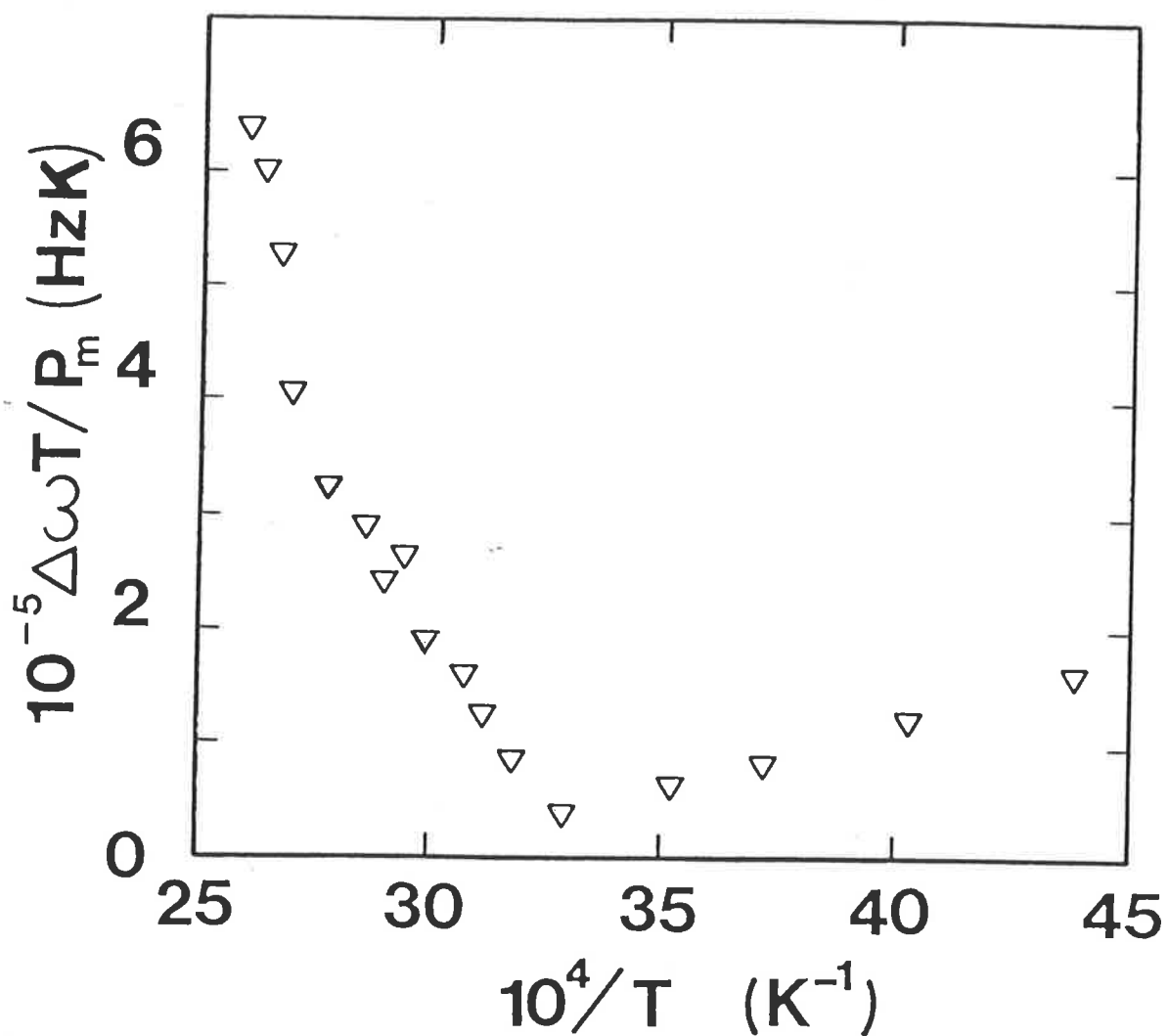
Figure 4.19

Temperature variation of $P_m T_{2p}$ for the bulk solvent def

formyl proton resonance characterizing def exchange on

$[Ni(Me_6 tren) def]^{2+}$. The filled and open circles represent

data derived from solutions for which P_m = 0.007615 and

0.003774, respectively.

Table 4.8

Parameters[a] for def exchange on $[Ni(Me_6tren)def]^{2+}$ in def solution.

$$k_{ex}(298.2K) = 944 \pm 42 \text{ s}^{-1}$$

$$\Delta H^{\#} = 23.1 \pm 0.7 \text{ kJ mol}^{-1}$$

$$\Delta S^{\#} = -111 \pm 2 \quad \text{JK}^{-1} \text{ mol}^{-1}$$

$$A_o = 0.49 \pm 0.26 \text{ s}^{-1}$$

$$E_o = 20.4 \pm 1.0 \text{ kJ mol}^{-1}$$

a.   All errors represent one standard deviation from the best fit of the data to the appropriate equation.

The paramagnetic induced chemical shift of the bulk solvent def resonance line, $\Delta\omega$, relative to the internal 2% cyclohexane reference resonance line was measured by hand directly from charted nmr absorption spectra. The resultant chemical shift data for solution (i) at some temperatures over the full temperature range studied appear as an appendix to this thesis. The temperature variation of $\Delta\omega$ characterizing exchange of def on $[\text{Ni}(\text{Me}_6\text{tren})\text{def}]^{2+}$ is shown in figure 4.20. The anticipated variation of this chemical shift is given by equation 4.12.

$$\Delta\omega = \frac{\Delta\omega_m P_m}{(\tau_m/T_{2m} + 1)^2 + \tau_m^2 \Delta\omega_m^2} + C \Delta\omega_m \qquad (4.12)$$

where C is a constant allowing for interactions outside the first coordination sphere, and where all other symbols have been previously defined. Whilst the variation of $\Delta\omega$ with temperature was qualitatively consistent with equation 4.12 its magnitude was too small to enable a reliable derivation of kinetic parameters. This is a consequence of the domination of the first term, pertaining to interactions occurring inside the first coordination sphere, by τ_m over the observed temperature range.
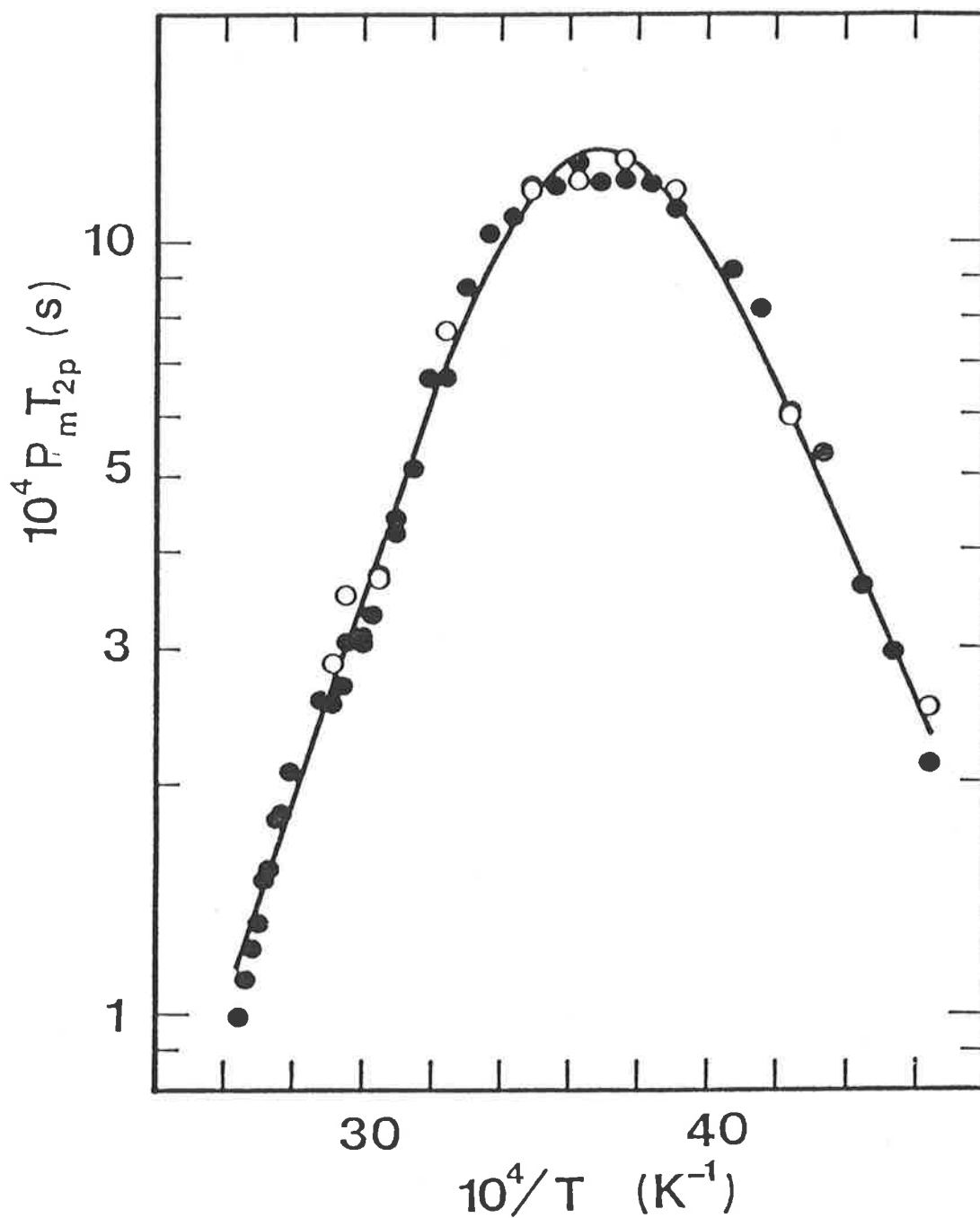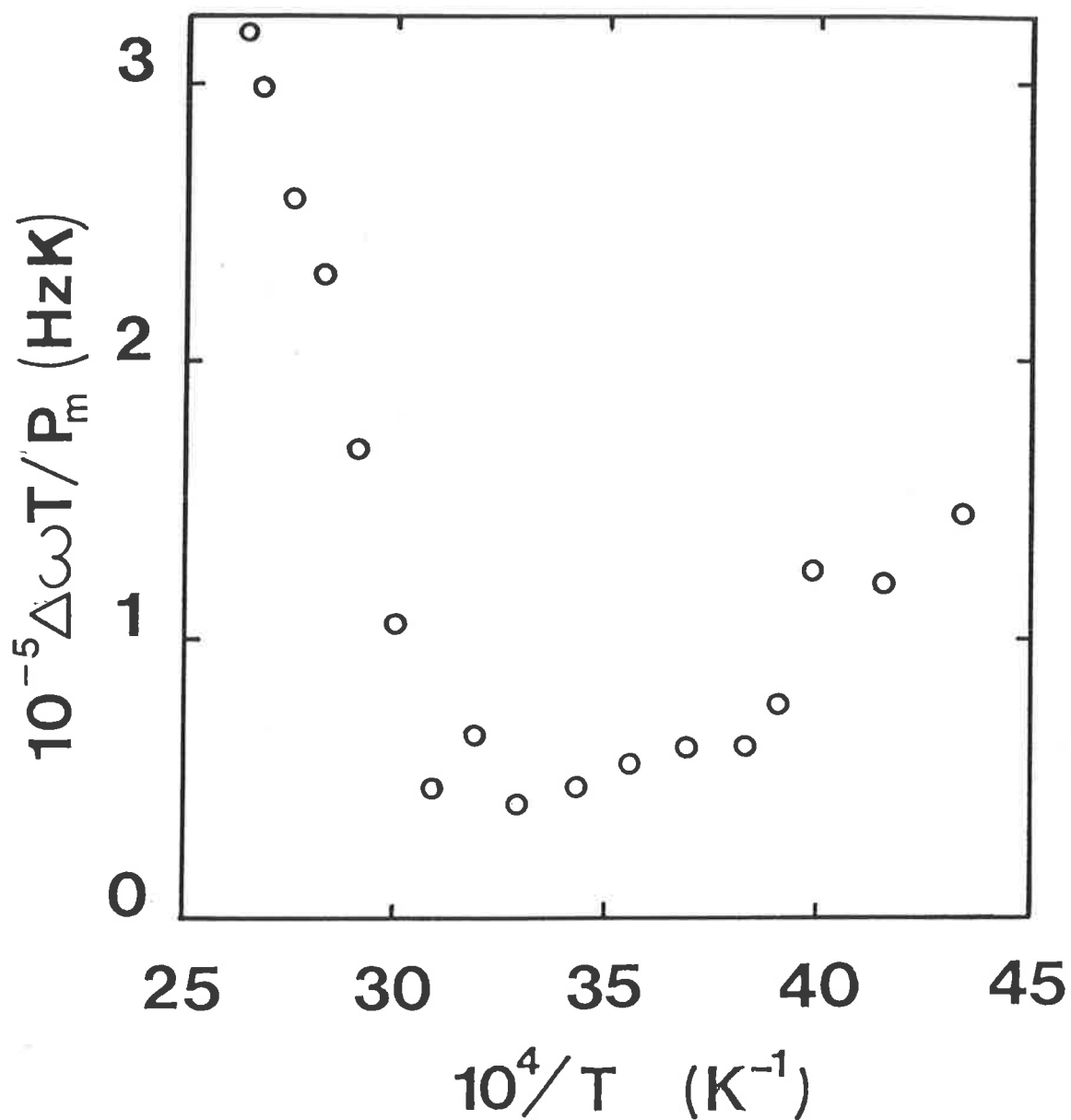
Figure 4.20

Temperature variation of $\Delta\omega T$ for the bulk solvent def formyl proton resonance characterizing def exchange on $[Ni(Me_6tren)def]^{2+}$. The circles represent data derived from a solution for which $P_m = 0.007615$.

4.3   Co(II) complexes in solution

4.3.1   Spectral variation on formation of [Co(Me$_6$tren)X]$^+$ in dmf

The ultraviolet/visible absorption spectra in dmf solution (ionic strength adjusted to 0.5mol dm^{-3} with sodium perchlorate) of the solvated complex [Co(Me$_6$tren)dmf]$^{2+}$ and anated species [Cu(Me$_6$tren)X]$^+$ where X$^-$ = Br$^-$, N$_3^-$, NCS$^-$ were recorded at 298.2K and the resulting molar absorbance versus wavelength plot is shown in figure 4.21.

The spectra in the wavelength range 400 - 900 nm and the observed absorption maxima are indicative of an approximately trigonal-bipyramidal arrangement of C$_{3V}$ symmetry[13]. The absorption spectrum in dmf solution of [Co(Me$_6$tren)Br]$^+$ in figure 4.21 bears very close resemblance to that of [Co(Me$_6$tren)Br]$^+$ in dichloromethane solution for which C$_{3V}$ symmetry is assumed and spectral transition assignments have already been made[10].

Primary and secondary kinetic observation wavelengths for substitution of dmf in [Co(Me$_6$tren)dmf]$^{2+}$ by each anion were determined, subject to the criteria already outlined (see section 4.1.1), and the results are given in table 4.9.

In the presence of oxygen, dmf solutions of [Co(Me$_6$tren)dmf](ClO$_4$)$_2$ slowly darken, probably as the consequence of the formation of a μ-peroxo complex[14]. This process was found to be reversible with the accompanying spectral changes shown in figure 4.22. The formation of molecular dioxygen complexes is not unusual[15], particularly for metal complexes containing divalent cobalt. Structural and thermodynamic studies have been carried out in aqueous solution on μ-peroxo complexes of cobalt (II) containing the closely related tren ligand[16-19]. One might expect cobalt(II) complexes containing Me$_6$tren to behave in a similar manner in the presence of oxygen.
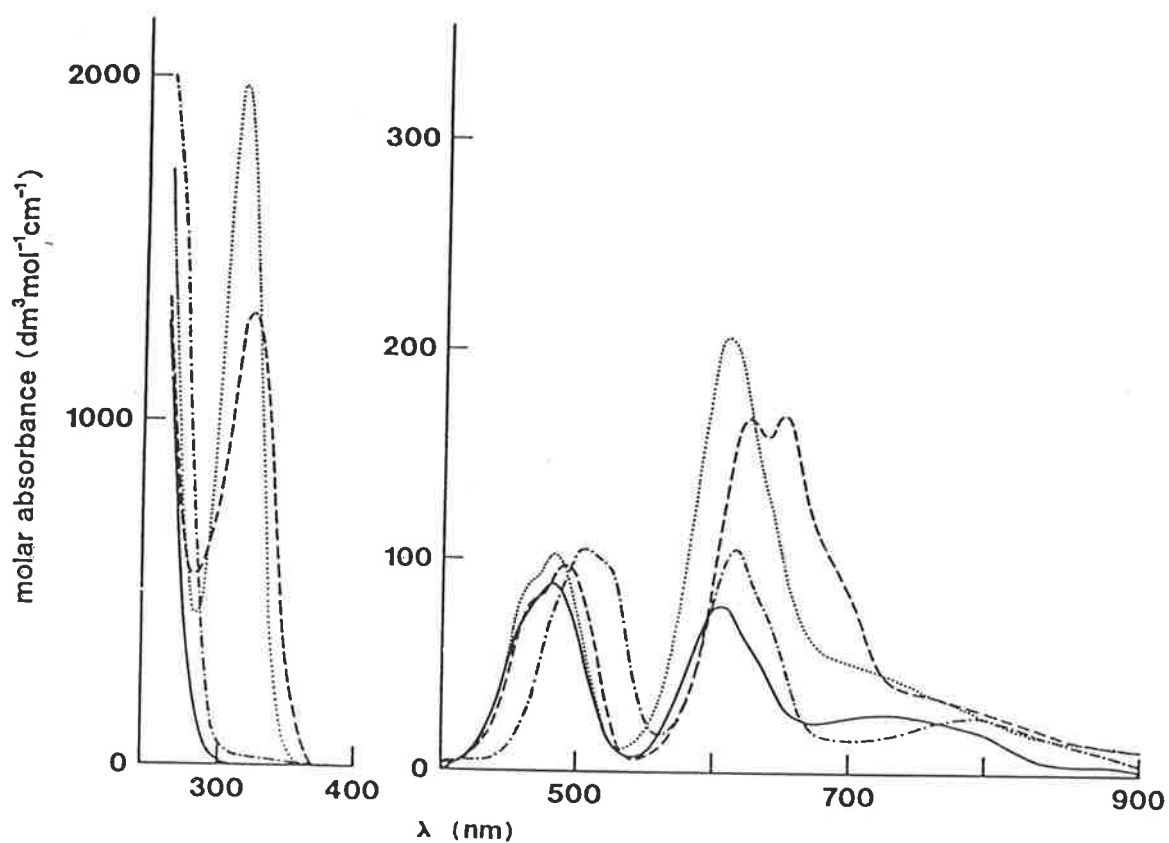
Figure 4.21

Ultraviolet/visible absorption spectra of

$[Co(Me_6tren)dmf]^{2+}$ (——) and $[Co(Me_6tren)X]^+$

($X^- = Br^-$ (—·—), N_3^- (---), NCS^- (···)) in dmf

solution.

Table 4.9

Kinetic observation wavelengths for the formation of $[\text{Co(Me}_6\text{tren)X]}^+$ in dmf solution (ionic strength adjusted to 0.5 mol dm^{-3} with sodium perchlorate) at 298.2K.

anion X^-	wavelength λ (nm)	change in molar absorbance $\Delta\epsilon^a$ (dm^3 mol^{-1} cm^{-1})
Br^-	525	80
	615	30
N_3^-	322	1310
	650	140
NCS^-	312	1970
	608	130

(a $\Delta\epsilon = \epsilon_{[\text{Co(Me}_6\text{tren)X]}^+} - \epsilon_{[\text{Co(Me}_6\text{tren)dmf]}^{2+}}$)
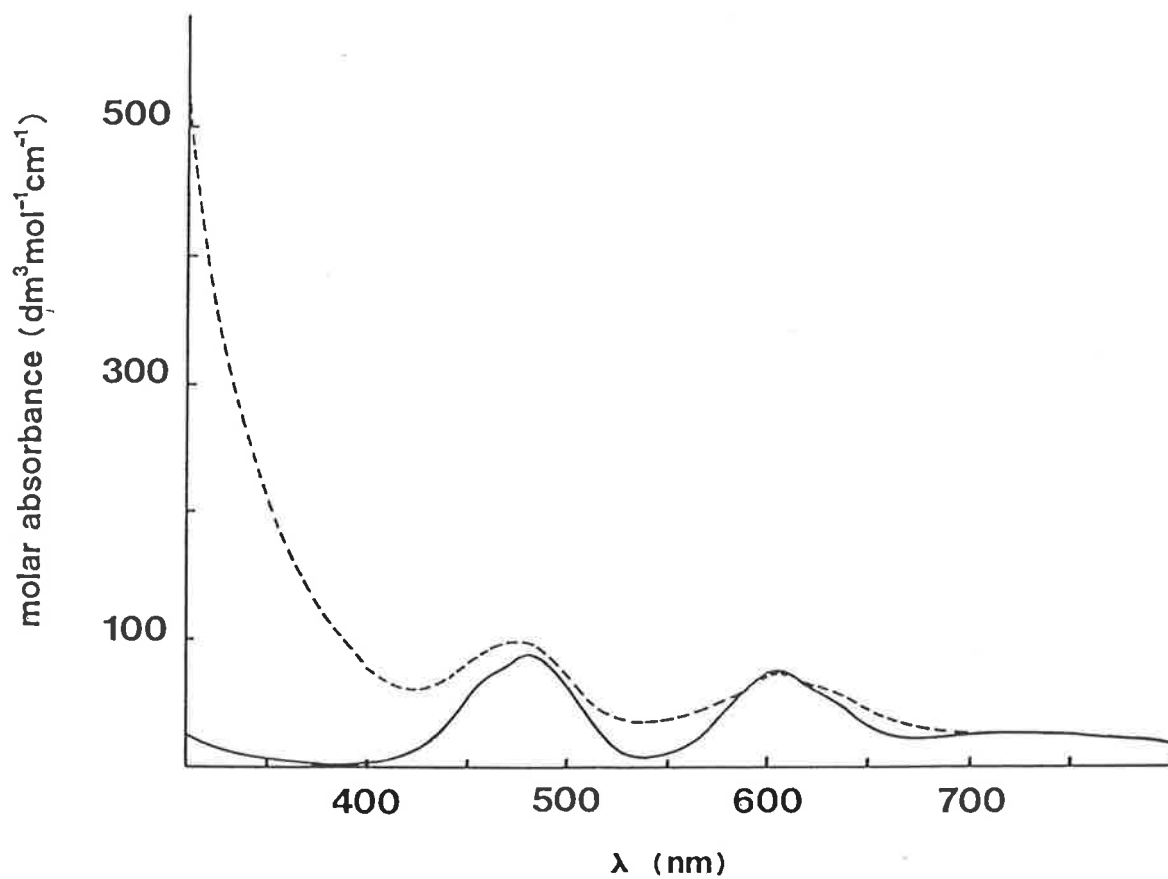
Figure 4.22

Ultraviolet/visible absorption spectra of $[Co(Me_6tren)dmf]^{2+}$ in the absence (——) and presence (---) of oxygen in dmf solution.

4.3.2 Job plots for $[Co(Me_6tren)X]^+$ formation in dmf

A series of solutions at differing ratios of initial $[Co(Me_6tren)dmf]^{2+}$ concentration to initial anion concentration were prepared as described in section 3.3.4 for each of the three anion (Br^-, N_3^- and NCS^-) systems. The concentration ranges of $[Co(Me_6tren)dmf]^{2+}$ and X^- for each anion system were 5.2×10^{-4} - 4.7×10^{-3} and 5.3×10^{-4} - 4.8×10^{-3} mol dm^{-3} for Br^-, 1.2×10^{-4} - 1.1×10^{-3} and 1.3×10^{-4} - 1.2×10^{-3} mol dm^{-3} for N_3^- and 7.6×10^{-5} - 6.0×10^{-4} and 7.3×10^{-5} - 6.4×10^{-4} mol dm^{-3} for NCS^-. The ultraviolet/visible absorption spectrum of each solution was recorded at an appropriate wavelength for that system. These wavelengths were 525, 322 and 312 nm for Br^-, N_3^- and NCS^- respectively.

The results of the Job method analysis (see chapter 2.2) for each system are shown in figure 4.23. The results are indicative of dmf being substituted in $[Co(Me_6tren)dmf]^{2+}$ by Br^-, N_3^- and NCS^- to form a single 1:1 species, $[Co(Me_6tren)X]^+$. The appearance of a sharply defined apex for each plot is characteristic[2] of a high stability constant estimated at ca 10^3 dm^{3}mol^{-1} for the anation reaction.

4.3.3 Ligand substitution on $[Co(Me_6tren)dmf]^{2+}$ in dmf

Ligand substitution of dmf on $[Co(Me_6tren)dmf]^{2+}$ by anions Br^-, N_3^- and NCS^- in dmf solution (adjusted to an ionic strength of 0.5 mol dm^{-3} with sodium perchlorate) was studied at 278.2K, 288.2K and 298.2K by stopped-flow spectrophotometry at the wavelengths given in table 4.9. Experimental solutions were prepared (see section 3.3.5) with the initial concentrations of $[Co(Me_6tren)dmf]^{2+}$ varied in the range 4.74×10^{-5} - 1.39×10^{-3} mol dm^{-3}, in all cases never exceeding 10% of the excess anion concentrations, which varied in the range 5.02×10^{-4} - 7.93×10^{-2} mol dm^{-3}, at all times maintaining pseudo first-order conditions. Particular care was taken to minimize exposure to oxygen of kinetic solutions, which were used immediately after preparation. This was to
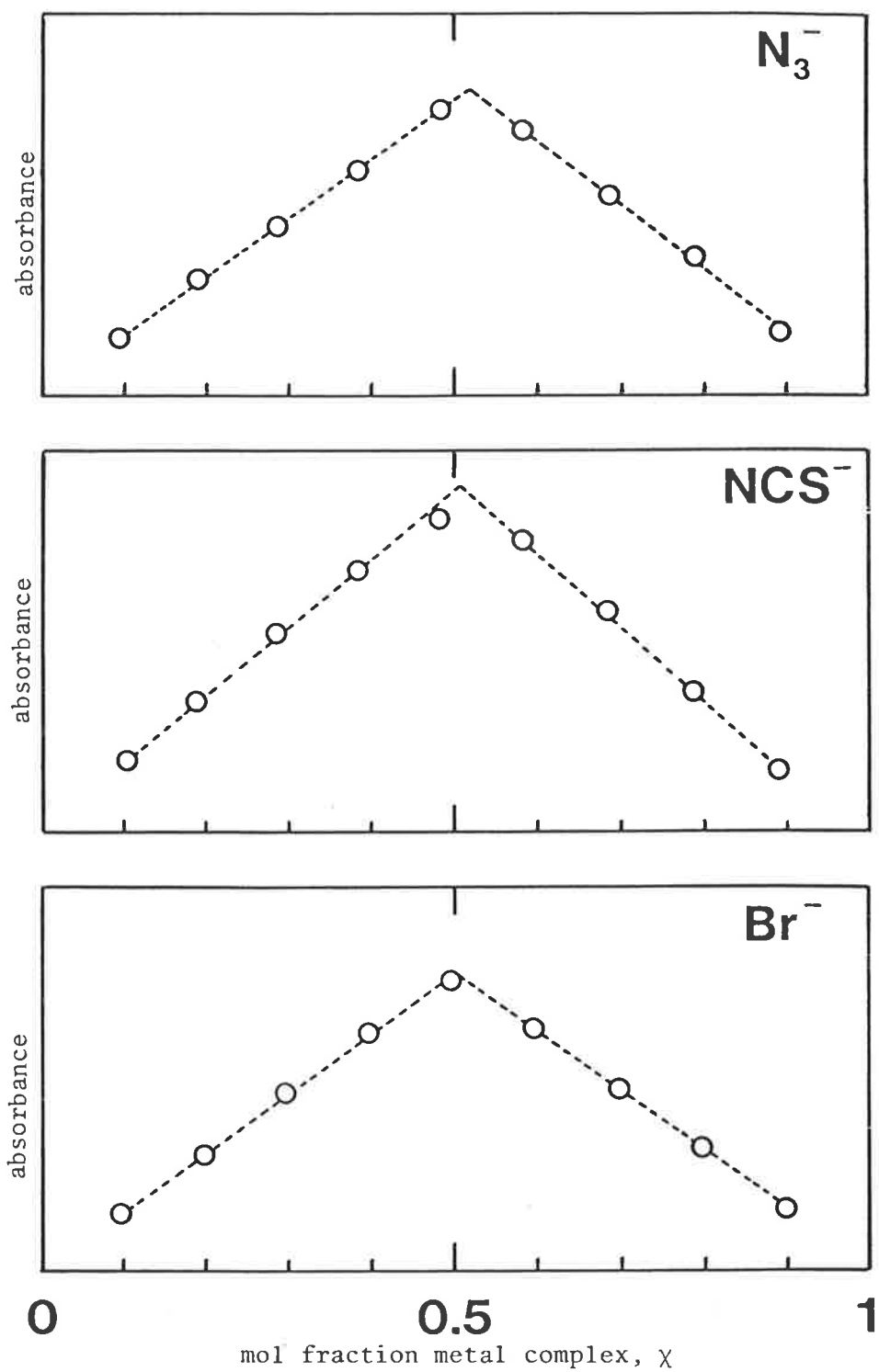
Figure 4.23

Job plots for the formation of $[Co(Me_6tren)X]^+$ (X^- = N_3^-, NCS^-, Br^-) in dmf solution.

prevent the (very slow) formation of any molecular dioxygen complex (see section 4.3.1).

The anation reaction
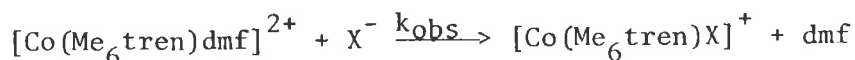
$$[Co(Me_6tren)dmf]^{2+} + X^- \xrightarrow{k_{obs}} [Co(Me_6tren)X]^+ + dmf$$

is characterized by a single kinetic process typified by a first-order rate constant, k_{obs}. Experimentally determined values of k_{obs} for each solution were obtained from a non-linear least-squares fit of averaged digitized reaction traces to a single exponential equation (see section 3.4.4). The resultant values appear as an appendix to this thesis.

The variation of k_{obs} with excess anion concentration, $[X^-]$, where $X^- = N_3^-$ and NCS⁻ is shown in figure 4.24. The moderate size of the spectral change accompanying ligand substitution (see table 4.9) and the instrumental dead time (ca 2ms), combine to cause the experimental error in k_{obs} to increase substantially for $k_{obs} > 300s^{-1}$. As a consequence of these experimental constraints, the $[X^-]$ range was limited when $X^- = N_3^-$ and NCS⁻. The variation of k_{obs} with $[X^-]$ where $X^- = Br^-$ is shown in figure 4.25. The small spectral change accompanying dmf substitution by Br⁻ necessitated working at a greater $[Co(Me_6tren)dmf]^{2+}$ concentration than was applicable for the N_3^- and NCS⁻ systems. However, the comparatively smaller k_{obs} values permitted studies at higher excess Br⁻ concentrations than for N_3^- and NCS⁻, whilst still maintaining pseudo first-order conditions, with no reduction in data reliability.

The variations of k_{obs} with $[X^-]$ in figures 4.24 and 4.25 is consistent with equation 4.1

$$k_{obs} = \frac{k_i K_0 [X^-]}{1 + K_0 [X^-]} + k_{-i} \tag{4.1}$$

which typifies (see section 2.1.3) an interchange (I) mechanism[3] proceeding through the following reaction scheme.
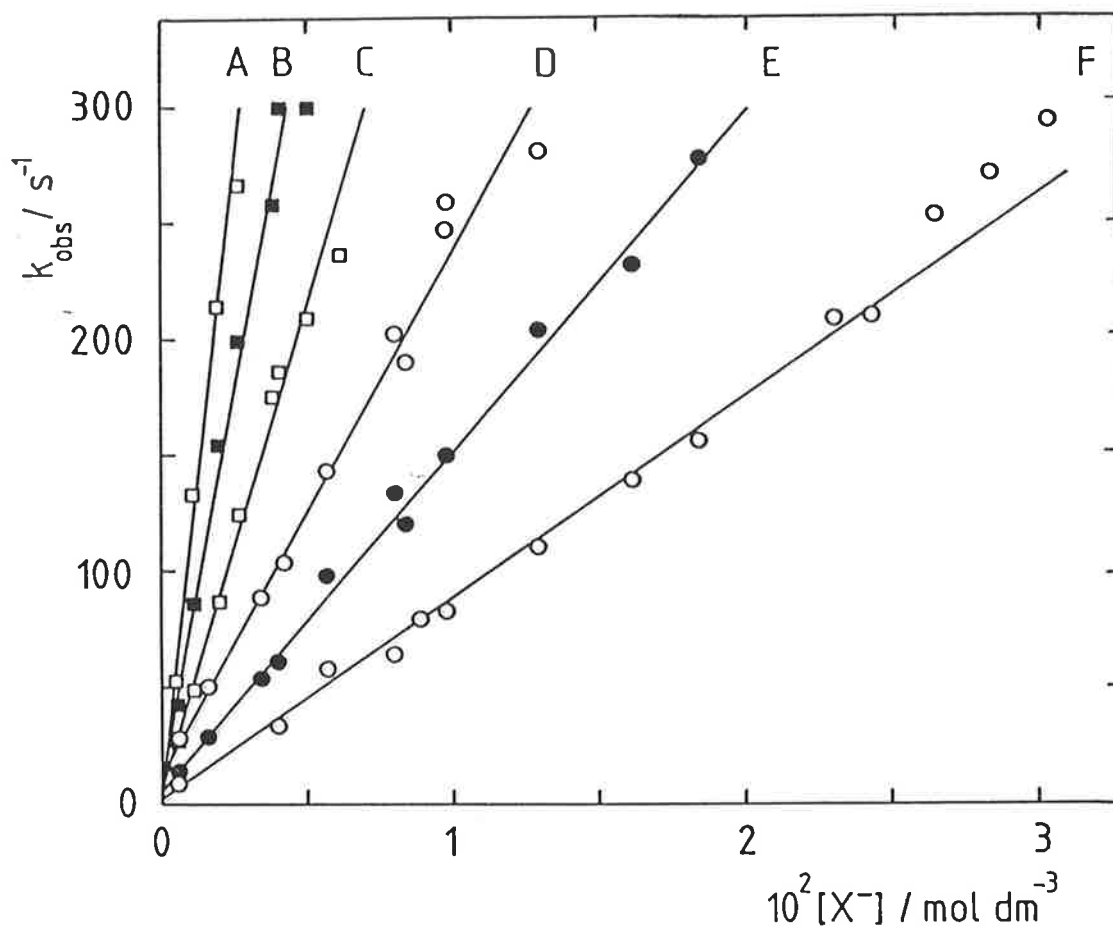
Figure 4.24

Variation of k_{obs} for the anation of $[Co(Me_6 tren)dmf]^{2+}$ by N_3^- and NCS^- with temperature and excess anion concentration in dmf solution. Data for N_3^- and NCS^- are represented by squares and circles respectively, and the temperatures are 298.2 [(A) and (D)], 288.2 [(B) and (E)], and 278.2K [(C) and (F)].
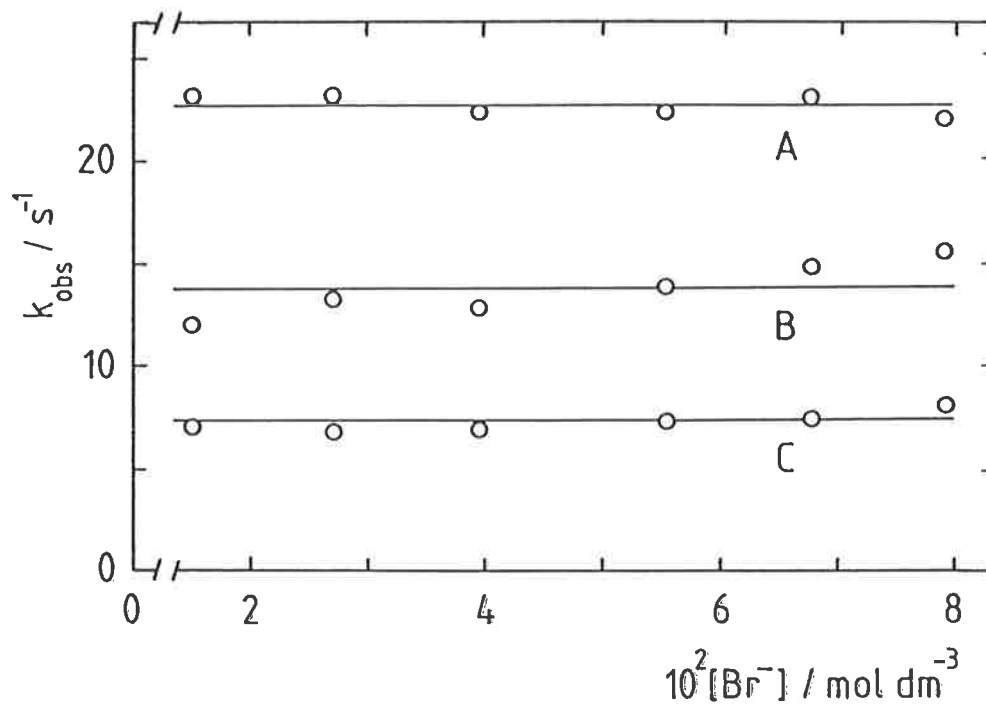
Figure 4.25

Variation of k_{obs} for the anation of $[Co(Me_6tren)dmf]^{2+}$ by Br^- with temperature and excess $[Br^-]$ in dmf solution. The temperatures are 298.2 (A), 288.2 (B) and 278.2K (C).
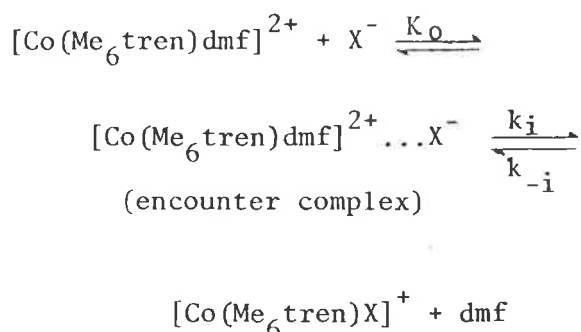
$$[Co(Me_6tren)dmf]^{2+} + X^- \xrightarrow{\quad K_o \quad}$$

$$[Co(Me_6tren)dmf]^{2+}...X^- \; \underset{k_{-i}}{\overset{k_i}{\rightleftharpoons}}$$

(encounter complex)

$$[Co(Me_6tren)X]^+ + dmf$$

The rapid formation of the encounter complex in which X^- resides in the second coordination sphere of the solvated complex is characterized by K_o, and the subsequent rate determining exchange of X^- between the second and first coordination sphere is characterized by the forward rate constant k_i. The reverse process, involving dissociation of $[Co(Me_6tren)X]^+$ is characterized by k_{-i}, the backward rate constant.

The applicability of equation 4.1 to the experimental data is subject to a set of limiting conditions (see section 2.1.3) as follows. The k_{obs} data for the N_3^- and NCS^- systems is consistent with a limiting condition $K_o[X^-] \ll 1$ imposed on equation 4.1 such that the equation reduces to

$$k_{obs} \sim k_i K_o [X^-] + k_{-i} \tag{4.13}$$

a formulation that gives a linear relationship between k_{obs} and $[X^-]$. Data determined at all three experimental temperatures for the N_3^- system were simultaneously fitted to equation 4.13 using the DATAFIT least-squares fitting module on the Cyber 173 computer giving optimized values for $(k_i K_o)$ and k_{-i}. Values characterizing the NCS^- system were similarly obtained and the linear regression lines for the simultaneous fit at the three experimental temperatures for each system are shown in figure 4.24. The derived optimized values of $(k_i K_o)$ appear in table 4.10. As has been the case throughout this study, the k_{-i} values for each system ($X^- = N_3^-$ and NCS^-) are negligible within the limits of experimental error and are therefore not further discussed.

Table 4.10

Kinetic and activation parameters[a] for anation by X^- in the [Co(Me$_6$tren)dmf]$^{2+}$ species in dmf solution at an ionic strength of 0.5 mol dm^{-3} adjusted with NaClO$_4$.

X^-	Br^-	N_3^-	NCS^-
$k_i K_o$ (298.2K) (10^3dm^{3}mol^{-1}s^{-1})	-	111± 9	22.4± 0.7
$k_i K_o$ (288.2K) (10^3dm^{3}mol^{-1}s^{-1})	-	67.2± 3.6	14.6± 0.4
$k_i K_o$ (278.2K) (10^3dm^{3}mol^{-1}s^{-1})	-	41.9± 2.0	8.68± 0.19
k_i (298.2K) (s^{-1})	23.1± 0.6	-	-
k_i (288.2K) (s^{-1})	13.2± 0.3	-	-
k_i (278.2K) (s^{-1})	7.23± 0.19	-	-
$\Delta H_i^{\#}$ (kJ mol^{-1})	38.2± 1.5	-	-
$\Delta S_i^{\#}$ (JK^{-1} mol^{-1})	-90.5± 5.2	-	-

a   All errors represent one standard deviation from the best fit of the data to the appropriate equation.

The invariance of k_{obs} data as a function of $[X^-]$ when $X^- = Br^-$, as shown in figure 4.25, is consistent with another limiting condition $K_0[X^-] \gg 1$ imposed on equation 4.1 such that the equation reduces to

$$k_{obs} \sim k_i + k_{-i}$$

No kinetic data is available to indicate the magnitude of k_{-i} but one might expect that since the overall apparent equilibrium constant is high ca $10^3 \text{ dm}^3 \text{ mol}^{-1}$, k_{-i} is negligibly small and hence

$$k_{obs} \sim k_i \qquad\qquad (4.14)$$

Experimentally determined data at all three experimental temperatures for the Br^- system were simultaneously computer fitted using the DATAFIT fitting module to a model combining equation 4.14 and the Eyring equation (equation 4.2) in a manner already described in this chapter. This process gave rise to optimized values for kinetic (k_i) and activation ($\Delta H_i^{\#}, \Delta S_i^{\#}$) parameters characterizing the Br^- system which appear in table 4.10.

4.3.4 Ligand exchange on $[Co(Me_6tren)dmf]^{2+}$ in dmf

Ligand exchange of dmf on $[Co(Me_6tren)dmf]^{2+}$ in dmf solution was studied over the temperature range 223-384K employing nmr spectroscopy. This work was carried out in conjunction with Dr. D.L. Pisaniello, of the University of Adelaide. Two solutions, for which the mol fraction of coordinated dmf was 0.0191 and 0.0306, were prepared in the manner described in section 3.3.3, as were the accompanying $[Zn(Me_6tren)dmf]^{2+}$ reference solutions.

Kinetic exchange behaviour was followed by monitoring the variation of transverse relaxation time of the formyl proton resonance of bulk solvent dmf with temperature in each $[Co(Me_6tren)dmf]^{2+}$ solution relative to a $[Zn(Me_6tren)dmf]^{2+}$ reference solution at an identical concentration. This

was effected in the same manner as for dmf exchange on solutions of the copper (II) and nickel (II) analogues in dmf already treated in this chapter. The resultant T_{2p} data appear as an appendix to this thesis.

The Swift and Connick treatment (see section 2.4.2) gives the relationship between T_{2p} and the dmf exchange process as equation 4.4,

$$T_{2p}^{-1} = \frac{P_m}{\tau_m} \left[\frac{T_{2m}^{-2} + (T_{2m}\tau_m)^{-1} + \Delta\omega_m^2}{(T_{2m}^{-1} + \tau_m^{-1})^2 + \Delta\omega_m^2} \right] + \frac{P_m}{T_{2o}} \tag{4.4}$$

where all the symbols have previously been defined. Under the limits of slow and very slow exchange, equation 4.4 reduces to equation 4.5, where $\tau_m^{-1} = k_{ex}$, the rate constant characterizing dmf exchange on $[Co(Me_6tren)dmf]^{2+}$,

$$(P_m T_{2p})^{-1} = \tau_m^{-1} + T_{2o}^{-1} = \frac{k_b T}{h} \exp(-\Delta H^{\#}/RT) \exp(\Delta S^{\#}/R)$$

$$+ A_o \exp(-E_o/RT) \tag{4.5}$$

and where all the symbols have also been previously defined. The dmf exchange rate on $[Co(Me_6tren)dmf]^{2+}$ thus becomes

$$v_{dmf} = k_{ex} [Co(Me_6tren)dmf^{2+}]$$

The temperature variation of $P_m T_{2p}$ for the two solutions studied is shown in figure 4.26 and was found to be reversible over the entire experimental temperature range.

The temperature variation of $P_m T_{2p}$ for each solution was fitted to equation 4.5 utilizing the non-linear least-squares DATAFIT fitting module on a Cyber 173 computer, optimizing both kinetic and activation parameters. The best fit line of the T_{2p} data for each solution is shown in figure 4.26 and the optimized parameters derived for dmf exchange on $[Co(Me_6tren)dmf]^{2+}$ in dmf solution are given in table 4.11. It may be seen from figure 4.26 that T_{2o}, the contribution to T_{2p} arising from interactions outside the first coordination sphere, begins to influence T_{2p} at the low temperature

Figure 4.26

Temperature variation of P_mT_{2p} for the bulk solvent dmf formyl proton resonance characterizing dmf exchange on $[Co(Me_6tren)dmf]^{2+}$. The filled and open circles refer to data derived from solutions in which $P_m = 0.01909$ and 0.03059, respectively.

Table 4.11

Parameters[a] for dmf exchange on $[Co(Me_6tren)dmf]^{2+}$ in dmf solution.

$k_{ex}(298.2K) = 51.4\pm4.2\ s^{-1}$

$\Delta H^{\#} = 52.4\pm1.1\ kJ\ mol^{-1}$

$\Delta S^{\#} = -36.5\pm3.0\ JK^{-1}\ mol^{-1}$

$A_o = 28.6\pm4.2^{b}\ s^{-1}$

$= 27.5\pm4.3^{c}\ s^{-1}$

$E_o = 7.3\pm0.3^{b}\ kJ\ mol^{-1}$

$= 7.7\pm0.3^{c}\ kJ\ mol^{-1}$

$\Delta V^{\#}(373.1K) = -2.7\pm0.2\ cm^{3}\ mol^{-1}$

a. All errors represent one standard deviation from the best fit of
the data to an appropriate equation.

b. Value for solution in which $P_m = 0.0306$.

c. Value for solution in which $P_m = 0.0191$.

extreme with the more concentrated solution characterized by a smaller T_{2o}. This is possibly a reflection of greater solution viscosity and consequently shorter correlation time in this case. However, in the high temperature region, where kinetic and activation parameters are derived, there is no significant variation in T_{2p} between the two experimental solutions, and no significant effect on the magnitude of these derived parameters is expected.

The paramagnetic induced chemical shift of the bulk solvent dmf resonance line, $\Delta\omega$, relative to the internal 2% cyclohexane reference resonance line was measured by hand directly from nmr absorption spectra. The resultant chemical shift data for both solutions studied at temperatures covering the full experimental temperature range appear as an appendix to this thesis. The temperature variation of $\Delta\omega$ characterizing exchange of dmf on $[Co(Me_6tren)dmf]^{2+}$ is shown in figure 4.27. Up to 315K no significant chemical shift of the bulk solvent $\Delta\omega$ was observed, but above this temperature $\Delta\omega$ increased with temperature as anticipated from equation 4.6.

$$\Delta\omega = \frac{\Delta\omega_m P_m}{(\tau_m/T_{2m} + 1)^2 + \tau_m^2 \Delta\omega_m^2} \tag{4.6}$$

where all the symbols have been previously defined. However, as a consequence of the domination of equation 4.6 by the relatively large magnitude of τ_m in this case, the magnitudes of $\Delta\omega$ observed were too small to enable a reliable derivation of kinetic parameters from this data.

The effect of pressure on dmf exchange in $[Co(Me_6tren)dmf]^{2+}$ was undertaken by Professor A.E. Merbach at the Université de Lausanne. The high-pressure nmr study was carried out at 371.9K and 373.1K and the calculated volume of activation, $\Delta V^\#$ is given in table 4.11. The activation compressibility, $\Delta\beta^\#$, (see section 2.4.3) was found to be very

Figure 4.27

Temperature variation of $\Delta\omega T$ for the bulk solvent dmf formyl proton resonance characterizing dmf exchange on $[Co(Me_6tren)dmf]^{2+}$. The filled and open circles refer to data derived from solutions for which $P_m = 0.01909$ and 0.03059, respectively.

small; $\Delta\beta^{\#} = 0.2(\pm0.5) \times 10^{-2}$ cm^3 mol^{-1}(Nm^{-2})$^{-1}$. The pressure dependence of the ratio of k_{ex} at ambient pressure, k_o and under an applied pressure, k_p, is shown in figure 4.28.

4.3.5 Ligand exchange on [Co(Me$_6$tren)def]$^{2+}$ in def

Ligand exchange of def on [Co(Me$_6$tren)def]$^{2+}$ in def solution was studied over the temperature range 226-399K employing nmr spectroscopy. This work was carried out in conjunction with Mrs. A.M. Hounslow, of the University of Adelaide. Two solutions, for which the mol fraction of coordinated def was 0.00850 and 0.0125, were prepared in the manner described in section 3.3.3, as were the accompanying [Zn(Me$_6$tren)def]$^{2+}$ reference solutions.

Kinetic exchange behaviour was followed by monitoring the variation of transverse relaxation time of the formyl proton resonance of bulk solvent dmf with temperature in each [Co(Me$_6$tren)def]$^{2+}$ solution relative to a [Zn(Me$_6$tren)def]$^{2+}$ reference solution at an identical concentration. This was undertaken in the same manner as for dmf and def exchange on solutions of [M(Me$_6$tren)(solvent)]$^{2+}$ already treated in this chapter. The resultant T_{2p} data appear as an appendix to this thesis.

The relationship between T_{2p} and the def exchange process according to the Swift and Connick treatment (see section 2.4.2) is given by equation 4.4. For def exchange on [Co(Me$_6$tren)def]$^{2+}$ equation 4.4 reduces to equation 4.5 under the limits of slow and very slow exchange. The def exchange rate on [Co(Me$_6$tren)def]$^{2+}$ then becomes

$$v_{def} = k_{ex} [Co(Me_6tren)def^{2+}]$$

where k_{ex} is the rate constant characterizing the exchange process. The temperature variation of $P_m T_{2p}$ for the two solutions studied was found to be reversible over the entire experimental temperature range and is shown in figure 4.29.
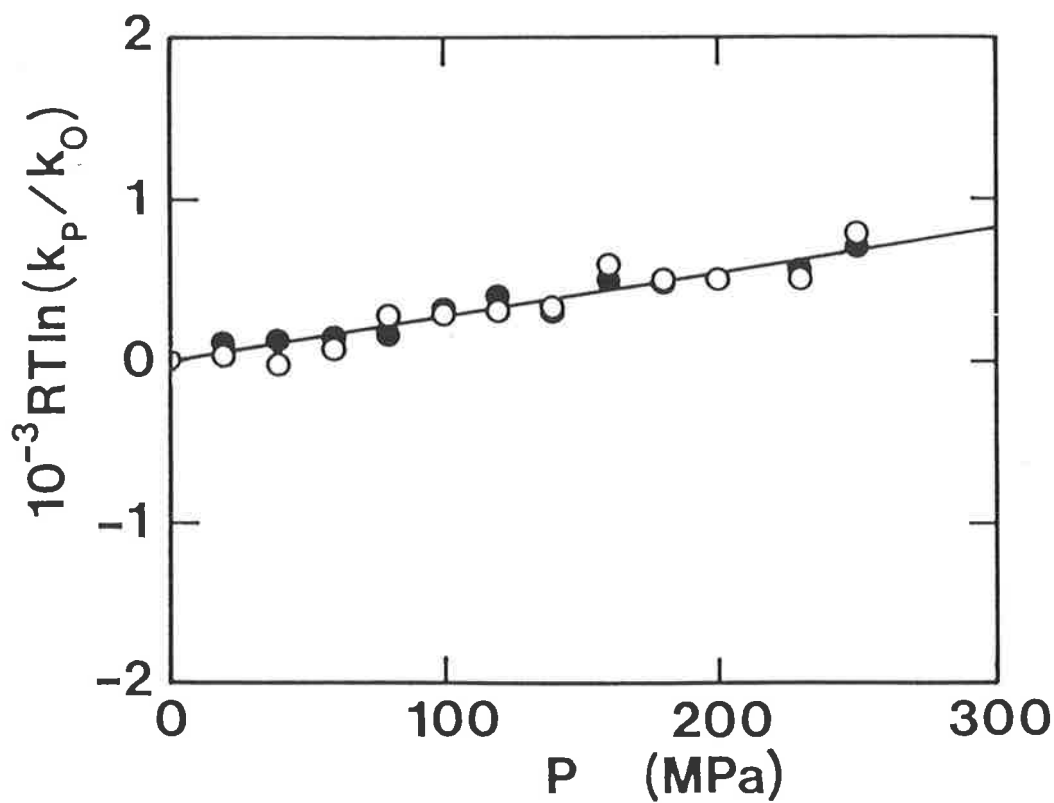
Figure 4.28

Variation of the ratio of k_{ex} at ambient, k_o and applied, k_p, pressure of $[Co(Me_6tren)dmf]^{2+}$ in dmf solution. The open and filled circles represent data derived from solutions for which P_m = 0.0203 (373.1K) and 0.0255 (371.9K), respectively.
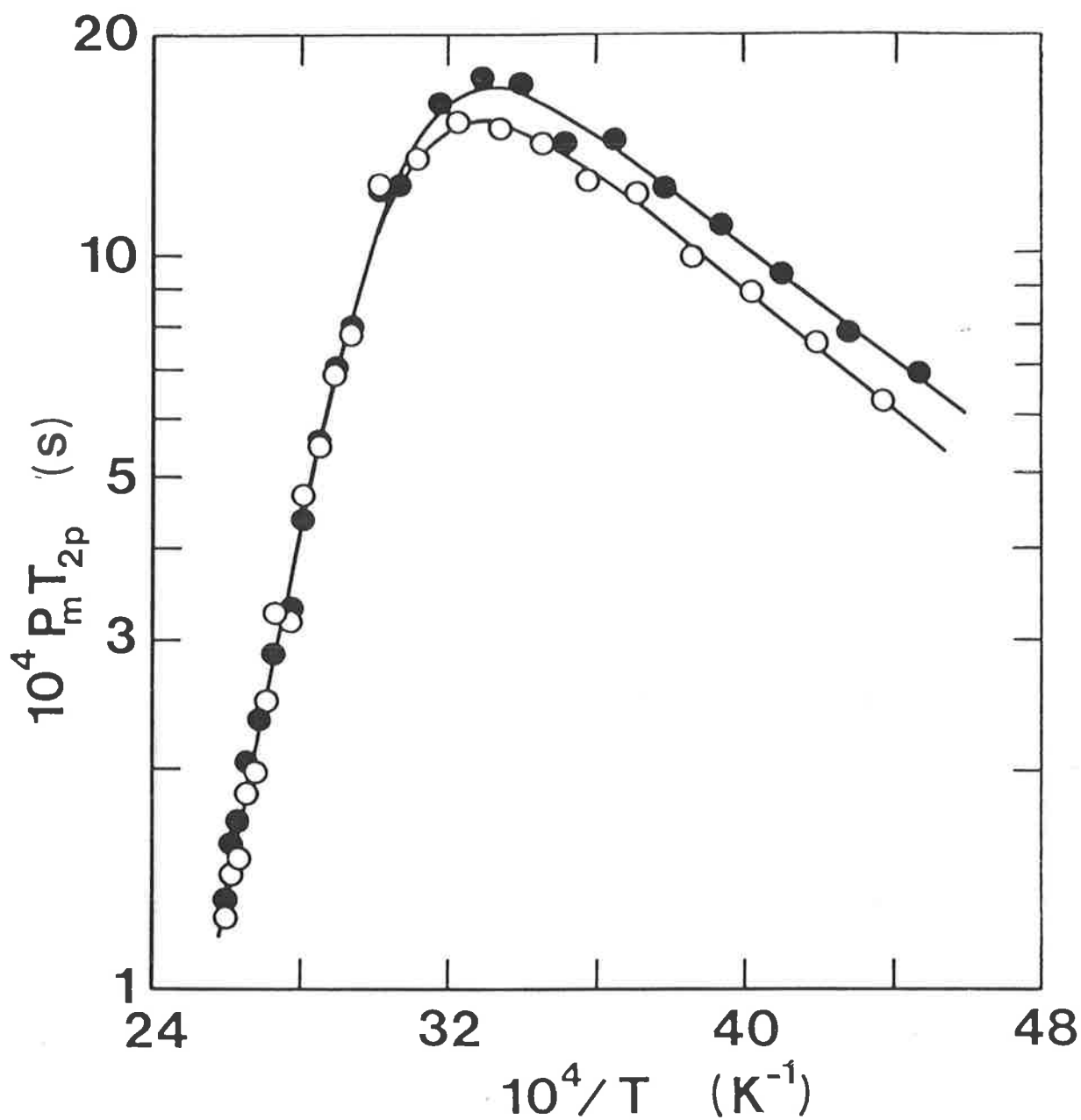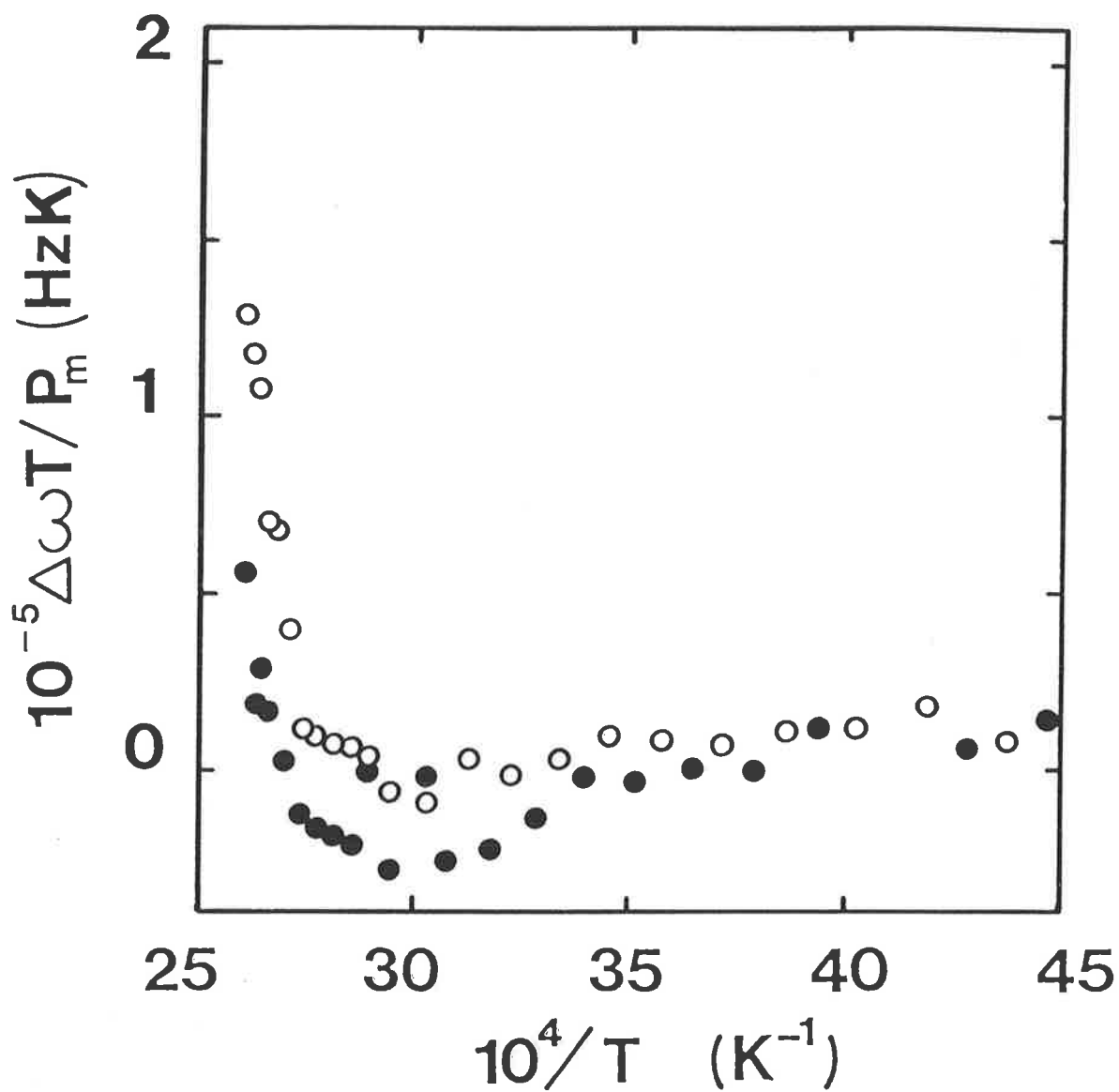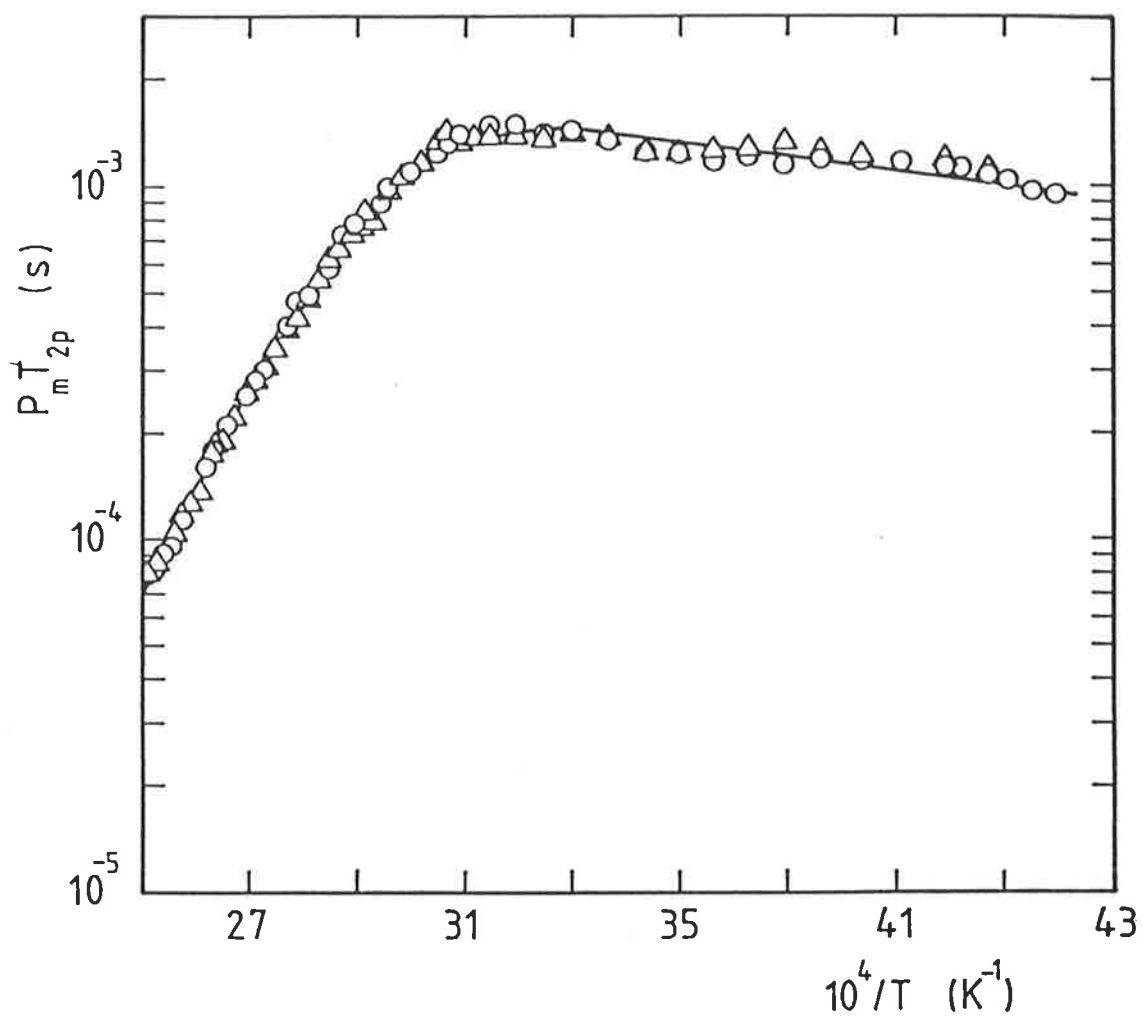
Figure 4.29

Temperature variation of P_mT_{2p} for the bulk solvent def formyl proton resonance characterizing def exchange on $[Co(Me_6tren)def]^{2+}$. The circles and triangles represent data derived from solutions for which $P_m = 0.008500$ and 0.01250, respectively.

From figure 4.29 it can be seen that the temperature dependent P_mT_{2p} profiles for both solutions are essentially superimposible and thus the data from each solution were combined to a single non-linear least-squares fit of equation 4.5 utilizing the DATAFIT fitting module on a Cyber 173 computer, optimizing both kinetic and activation parameters. The best fit line of this T_{2p} data is shown in figure 4.29 and optimized parameters derived for def exchange on $[Co(Me_6tren)def]^{2+}$ in def solution are given in table 4.12.

The paramagnetic induced chemical shift of the bulk solvent def resonance, $\Delta\omega$, relative to an internal 2% cyclohexane reference resonance line was measured by hand directly from nmr absorption spectra. The resultant chemical shift data for both solutions over the temperature range studied appear as an appendix to this thesis. The temperature variation of $\Delta\omega$ characterizing exchange of def on $[Co(Me_6tren)def]^{2+}$ is shown in figure 4.30. Equation 4.6 expresses the anticipated temperature variation of the chemical shift of the bulk solvent def, $\Delta\omega$,

$$\Delta\omega = \frac{\Delta\omega_m P_m}{(\tau_m/T_{2m} + 1)^2 + \tau_m^2 \Delta\omega_m^2} \tag{4.6}$$

where all the symbols have previously been defined. The variation of $\Delta\omega$ with temperature is qualitatively consistent with equation 4.6 but at temperatures above 320K the domination of equation 4.6 by τ_m caused the magnitude of $\Delta\omega$ to be too small to enable reliable incorporation into the derivation of kinetic parameters.

The effect of pressure on def exchange in $[Co(Me_6tren)def]^{2+}$ was undertaken by Professor A.E. Merbach at the Université de Lausanne. The high-pressure nmr study was carried out at 365.6K and 364.5K and the calculated volume of activation, $\Delta V^{\#}$, and activation compressibility,

Table 4.12

Parameters[a] for def exchange on $[Co(Me_6tren)def]^{2+}$ in def solution.

$k_{ex}(298.2K)$ $= 26.3\pm2.2$ s^{-1}

$\Delta H^{\#}$ $= 58.3\pm1.7$ kJ mol^{-1}

$\Delta S^{\#}$ $= -22.2\pm4.6$ JK^{-1} mol^{-1}

A_{o-} $= 123\pm15$ s^{-1}

E_o $= 4.2\pm0.3$ kJ mol^{-1}

$\Delta V^{\#b}$ $= -1.3\pm0.2$ cm^3 mol^{-1}

$[\Delta\beta^{\#}$ $= 0$ cm^3 mol^{-1} (Nm^{-2})$^{-1}]$

a. All errors represent one standard deviation from the best fit
    of the data to an appropriate equation.

b. From A.E. Merbach, Université de Lausanne.
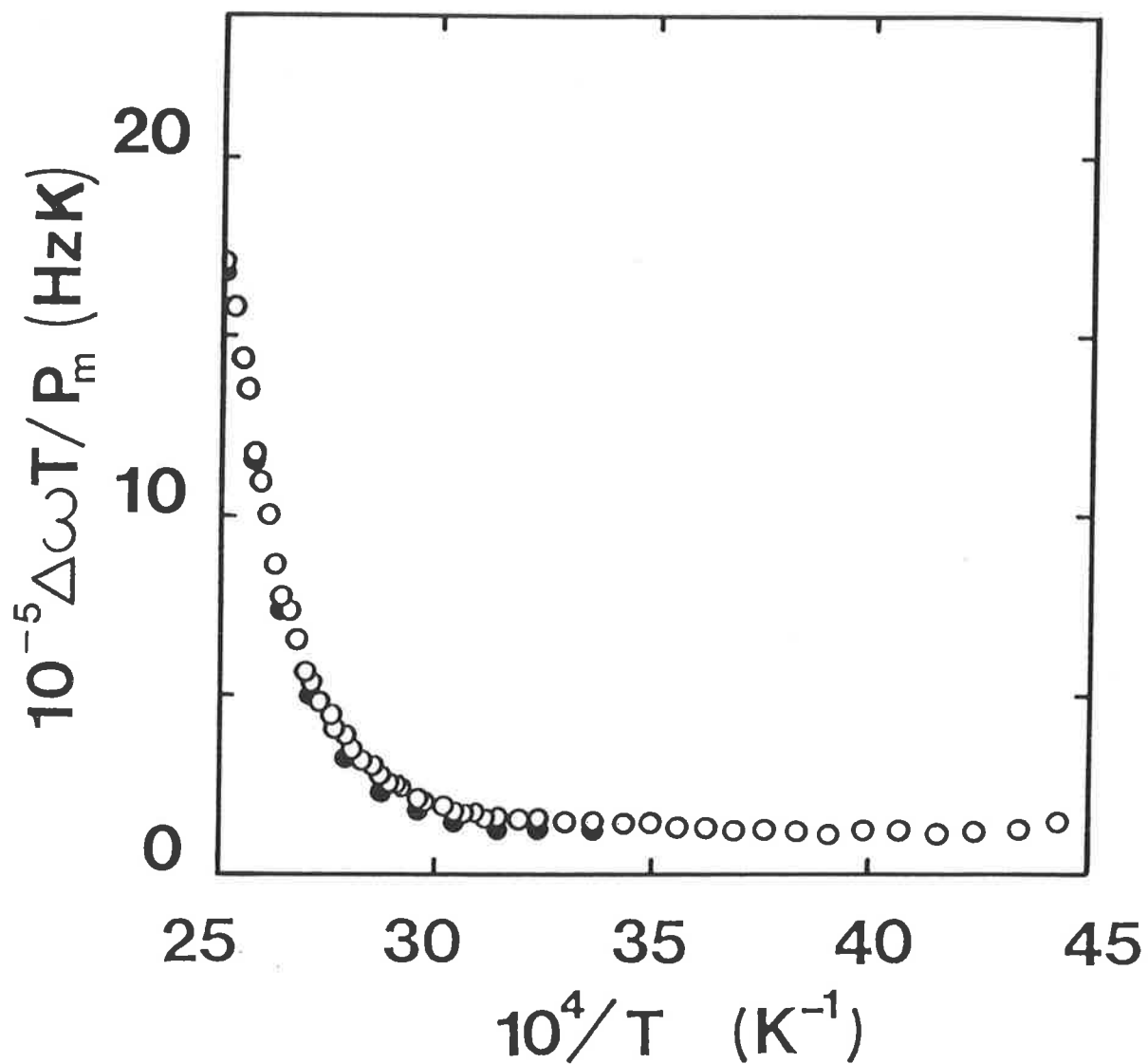
Figure 4.30

Temperature variation of $\Delta\omega T$ for the bulk solvent def formyl

proton resonance characterizing def exchange on

$[Co(Me_6 tren)def]^{2+}$. The open and filled circles refer to

data derived from solutions for which $P_m = 0.008500$ and

0.01250, respectively.

$\Delta\beta^{\#}$, (see section 2.4.3) are given in table 4.12. The pressure dependence of the ratios of k_{ex} at ambient pressure, k_o and under an applied pressure, k_p, is shown in figure 4.31.
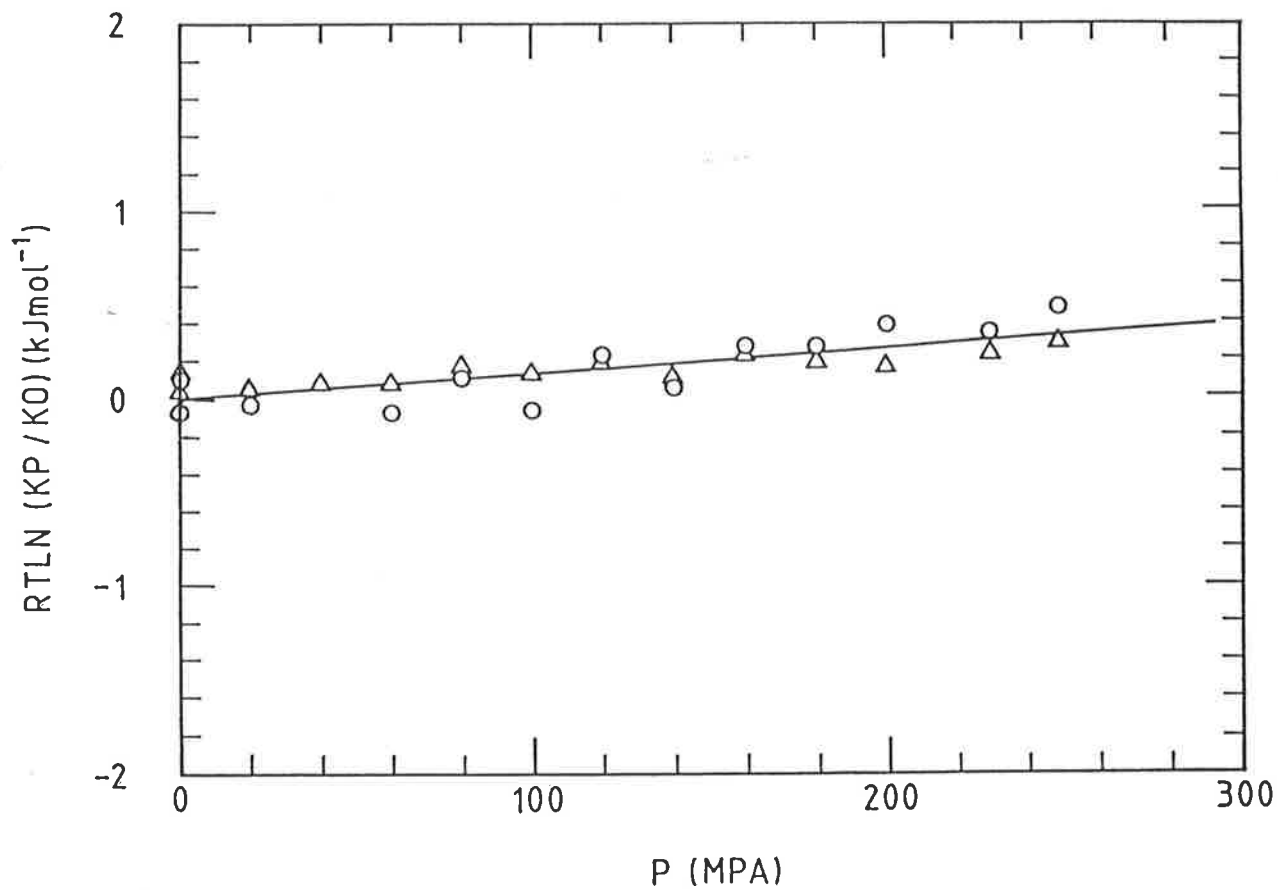
Figure 4.31

Variation of the ratio of k_{ex} at ambient, k_o and applied, k_p, pressure of $[Co(Me_6 tren)def]^{2+}$ in def solution. The circles and triangles represent data derived from solutions for which P_m = 0.0087 (365.6K) and 0.0133 (364.5K), respectively.

4.4 References to chapter 4

1. C. Furlani, Coord. Chem. Rev., 1968, $\underline{3}$, 141.

2. F.J.C. Rossotti, H. Rossotti, in "The Determination of Stability Constants", Chapter 3, McGraw-Hill, N.Y., 1961.

3. C.H. Langford, H.B. Gray, in "Ligand Substitution Processes", W.A. Benjamin, N.Y., 1965.

4. Program DATAFIT, by T. Kurusev, University of Adelaide.

5. S. Glasstone, K.J. Laidler, H. Eyring, in "Thoery of Rate Processes", McGraw-Hill, N.Y., 1941.

6. C.S. Johnson, Adv. Mag. Res., 1965, $\underline{1}$, 33.

7. L.M. Jackman, T.E. Kavanagh, R.C. Haddon, Org. Mag. Res., 1969, $\underline{1}$, 109.

8. F.A.L. Anet, A.J.R. Bourn, J. Amer. Chem. Soc., 1967, $\underline{89}$, 760.

9. D.L. Pisaniello, Ph.D. Thesis, University of Adelaide.

10. M. Ciampolini, Struct.Bonding (Berlin), 1969, $\underline{6}$, 52.

11. M. DiVaira, P.L. Orioli, Acta Crystallogr., Sect. B, 1968, $\underline{24}$, 595.

12. S.F. Lincoln, J.H. Coates, B.G. Doddridge, D.L. Pisaniello, Aust.J.Chem., 1984, $\underline{37}$, 947.

13. M. Ciampolini, I. Bertini, J. Chem. Soc. A, 1968, 2241.

14. J.S. Valentine, Chem. Rev., 1973, $\underline{73}$, 235.

15. E.C. Niederhoffer, J.H. Timmons, A.E. Martell, Chem. Rev., 1984, $\underline{84}$, 137.

16. C.H. Yang, M.W. Grieb, Inorg. Chem., 1973, $\underline{12}$, 663.

17. G. McLendon, A.E. Martell, J. Coord. Chem., 1975, $\underline{4}$, 235.

18. M. Zehnder, U. Thewalt, S. Fallab, Helv.Chim.Acta, 1976, $\underline{59}$, 2290.

19. M. Zehnder, U. Thewalt, S. Fallab, Helv.Chim.Acta, 1979, $\underline{62}$, 2099.

CHAPTER 5 - DISCUSSION

CHAPTER 5 - DISCUSSION

5.1 Copper(II) species in solution

As noted in section 4.1.1, the ultraviolet/visible spectra of the solvated $[Cu(Me_6tren)dmf]^{2+}$ complex and anated species $[Cu(Me_6tren)X]^+$ where $X^- = Br^-$, N_3^- and NCS^- as shown in figure 4.1, are indicative of a five-coordinate species of approximately trigonal-bipyramidal geometry. Other workers have already noted solution and solid state spectra of copper(II) complexes containing the Me_6tren ligand[1-4]. The feature of interest in each spectrum is the two d-d bands in the 600-1100 nm region. The two bands are separated by ca 200nm which is believed to be too large to be attributed solely to spin-orbit coupling[4]. Using a ligand-field interpretation Furlani[5] predicts this to be indicative of pentacoordination involving trigonal-bipyramidal geometry. Energy level diagrams[3,5] are consistent with the two bands being assigned to the $^2E'' \leftarrow {}^2A_1'$ and $^2E' \leftarrow {}^2A_1'$ transitions.

The Job method analysis results (see section 4.1.2) are indicative of the formation of a pentacoordinate species $[Cu(Me_6tren)X]^+$ in the reaction of $[Cu(Me_6tren)dmf]^{2+}$ with $X^- = Br^-$, N_3^- and NCS^-. It is important to note that the high stability constants characterizing the formation of $[Cu(Me_6tren)X]^+$ inferred from the Job analysis results indicate that the equilibrium process forming this species

$$[Cu(Me_6tren)dmf]^{2+} + X^- \rightleftharpoons [Cu(Me_6tren)X]^+ + dmf$$
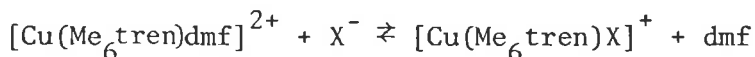
lies almost completely to the right, greatly favouring the formation of the anated product. This result simplifies interpretation of stopped-flow kinetic data.

The rate of solvent exchange, k_{ex} for dmf and other solvents on $[Cu(solvent)_6]^{2+}$ is characterized at 298.2K by values greater than $10^7 \, s^{-1}$, and ligand substitution on this species occurs with similar

rapidity[6-9]. This enhanced lability over that expected for bivalent first-row transition metal ions is due to the Jahn-Teller effect[10,11] a tetragonal distortion that alternates rapidly over all three axes of the solvated metal ion, producing a pairwise labilization of all six solvent molecules[6,7]. This effect is not however, applicable to systems with a non-degenerate electronic ground state such as $[Cu(Me_6tren)dmf]^{2+}$, exhibiting C_{3V} symmetry. The kinetic rate constant values characterizing solvent exchange, k_{ex}, and anation, k_i, for $[Cu(Me_6tren)dmf]^{2+}$ (see table 5.1) indicate a large (ca 10^5-fold) reduction in lability of this species by comparison to those characterizing solvent exchange and ligand substitution for $[Cu(dmf)_6]^{2+}$. The marked reduction in lability of this species, below that expected for other bivalent first-row transition metal ions, suggests that effects other than the removal of Jahn-Teller labilization are responsible. It has been observed that the labilities of six-coordinate cobalt(II) and nickel(II) species usually exhibit substantial increases on coordination of amine groups[8], attributed to electron donation from coordinated nitrogen atoms lowering the effective charge on the central metal ion and thereby labilizing the coordinated solvent molecule[12]. It would then seem that structural effects are an important factor in reducing lability in this case. One can deduce, on the basis of the solid state structure[13] of $[Cu(Me_6tren)Br]^+$, that the dmf coordination site in $[Cu(Me_6tren)dmf]^{2+}$ is in an annulus formed by the three nitrogen $-NMe_2$ groups of Me_6tren and is sterically shielded from interaction with an incoming ligand. In addition, it is probable that when coordinated, the tripodal Me_6tren ligand substantially decreases the degree of flexibility available in forming the transition state for the substitution mechanism by comparison to that available to $[Cu(solvent)_6]^{2+}$. This effect is expected to also reduce lability.

Table 5.1

Parameters[a] for anation and solvent exchange on $[Cu(Me_6tren)(solvent)]^{2+}$.

Anation by X^- on $[Cu(Me_6tren)dmf]^{2+}$

X^-		Br^-	N_3^-	NCS^-
$K_o(298.2K)$	(dm^3mol^{-1})	52 ± 3	464 ± 15	175 ± 15
$k_i(298.2K)$	(s^{-1})	563 ± 27^b	435 ± 19	529 ± 32
$\Delta H_i^{\#}$	$(kJmol^{-1})$	19.0 ± 10.4	32.1 ± 2.7	43.6 ± 3.2
$\Delta S_i^{\#}$	$(JK^{-1}mol^{-1})$	-128 ± 36	-86.9 ± 9.4	-56.2 ± 10.9

Solvent exchange on $[Cu(Me_6tren)(solvent)]^{2+}$

Solvent		dmf	def	dma
$k_{ex}(298.2K)$	(s^{-1})	555 ± 39	980 ± 70	$>>10^3$
$\Delta H^{\#}$	$(kJmol^{-1})$	43.3 ± 1.1	36.3 ± 0.9	-
$\Delta S^{\#}$	$(JK^{-1}mol^{-1})$	-47.0 ± 3.1	-65.9 ± 2.5	-
A_o	(s^{-1})	17.0 ± 3.0	14.0 ± 3.4	-
E_o	$(kJmol^{-1})$	12.5 ± 0.4	13.6 ± 0.5	-
$\Delta V^{\#}$ (365K)	(cm^3mol^{-1})	6.1 ± 0.1	5.3 ± 0.3	-

a. Errors represent one standard deviation.

b. Parameter derived from data at a single temperature.

All other anation parameters derived from a simultaneous fit of data

at three temperatures.

It has already been noted in section 1.3 that persuasive evidence exists that $\Delta V^{\#}$ values are useful in diagnosing reaction activation mode. This is exemplified for dmf exchange on $[Cr(dmf)_6]^{3+}$ with $\Delta V^{\#} = -6.3$ $cm^3 mol^{-1}$ being assigned an associatively activated mechanism[14], and $[Ni(dmf)_6]^{2+}$ with $\Delta V^{\#} = +9.1$ $cm^3 mol^{-1}$ being assigned a dissociatively activated mechanism[15]. As these two species are of similar size to $[Cu(Me_6 tren)dmf]^{2+}$ with $\Delta V^{\#} = +6.1$ $cm^3 mol^{-1}$ (see table 5.1) then exchange on $[Cu(Me_6 tren)dmf]^{2+}$ is interpreted in terms of a dissociatively activated reaction mode. It has been suggested[16] that from the magnitude of $\Delta V^{\#}$ it is possible to discriminate between dissociative (D) and dissociative interchange (I_d) mechanisms but this does not appear to be the case for the structurally complicated dmf molecule[17]. However, the significantly smaller value for $\Delta V^{\#}$ observed for dmf exchange on $[Cu(Me_6 tren)dmf]^{2+}$ by comparison to that observed for $[Ni(dmf)_6]^{2+}$ suggests that it is probable that dmf exchange on $[Cu(Me_6 tren)dmf]^{2+}$ is characterized by an I_d mechanism.

The negative entropy of activation, $\Delta S^{\#}$, value for dmf exchange on $[Cu(Me_6 tren)dmf]^{2+}$ (see table 5.1) at first sight seems contradictory to the operation of a dissociatively activated mechanism. However, if considerations such as vibrational and rotational changes inside the first coordination sphere[18] of the species undergoing solvent exchange and solvent rearrangements occurring outside that first coordination sphere[19] together or separately make significant contributions to this parameter, then its sign becomes of dubious mechanistic consequence.

Bearing in mind that $[Cu(Me_6 tren)dmf]^{2+}$ is not sufficiently substitution labile for selectivity for the entering group to be decreased[20], the relative invariance of k_i values characterizing anation by Br^-, N_3^- and NCS^- and the similarity of these values to k_{ex} (see table 5.1) suggests that the major rate determining step in the anation reaction

mechanism is dissociation of dmf from $[Cu(Me_6tren)dmf]^{2+}$. In view of this and from the variation of k_{obs} for the three anions studied (see figs. 4.3 -5) conforming to equation 4.1 it is probable that the anation of $[Cu(Me_6tren)dmf]^{2+}$ is characterized by an I_d mechanism. This result is consistent with volume of activation data for dmf exchange on $[Cu(Me_6-tren)dmf]^{2+}$ already discussed in this section. It is pertinent to note that although a D mechanism would also be characterized by a rate law similar to equation 4.1, in a solvent of moderately low dielectric constant such as dmf, the opposite charges of $[Cu(Me_6tren)dmf]^{2+}$ and X^- easily facilitate the formation of an encounter complex (ion pair) and make the experimental distinction between the I_d and D mechanisms difficult. The invariance of k_i characterizing anionic substitution on $[Cu(Me_6tren)dmf]^{2+}$ by the designated I_d mechanism may be contrasted with a large variation of k_i characterizing anation of $[Cr(dmf)_6]^{3+}$ by X^- (as shown in table 5.2), a reaction that appears to be a classic example of the operation of an associative interchange, I_a, mechanism[21].

As outlined in the introduction, it is of interest to compare and contrast solvents of similar electron donating characteristics (as evidenced by the Donor Numbers for the solvents of interest in table 1.1) but of differing size, thereby facilitating an assessment of the influence of steric interactions on solvent lability and exchange mechanism.

The rate of def exchange, $k_{ex}(298.2K)$ characterizing $[Cu(def)_6]^{2+}$ is not available but from data on other $[Cu(solvent)_6]^{2+}$ systems[6] it is anticipated to be $\geqslant 10^7$ s^{-1}. On this basis coordination of Me_6tren to form $[Cu(Me_6tren)def]^{2+}$ is also seen to decrease coordinated solvent lability as was the case for dmf exchange on $[Cu(Me_6tren)dmf]^{2+}$. Similarly, this decreased lability for def exchange arises from a combination of effects, steric hindrance imposed by Me_6tren to def exchange and the removal of the Jahn-Teller effect as has already been discussed for dmf exchange on

Table 5.2

Comparison of k_i/k_{ex} values for anation reactions operating through I_d and I_a mechanisms.

	anation of $[Cr(dmf)_6]^{3+}$	anation of $[Cu(Me_6tren)dmf]^{2+}$
	I_a mechanism	I_d mechanism
X^-	k_i/k_{ex} [a]	k_i/k_{ex} [b]
Br^-	0.088	1.01
NCS^-	2.35	0.953
N_3^-	57.5	0.784

a. data from reference 21 at 344.5K .

b. at 298.2K .

$[Cu(Me_6tren)dmf]^{2+}$.

The positive $\Delta V^{\#}$ value observed for $[Cu(Me_6tren)def]^{2+}$ is consistent with a dissociative activation mode. Estimation of $\Delta V^{\#}$ values expected for D and I_d mechanisms for def exchange is not a simple matter due to potential conformational changes in Me_6tren during solvent exchange and the large size of the def molecule. However, the small magnitude of $\Delta V^{\#}$ observed for $[Cu(Me_6tren)def]^{2+}$ suggests the probable operation of an Id mechanism. The similarity of the solvent exchange mechanisms for $[Cu(Me_6tren)dmf]^{2+}$ and $[Cu(Me_6tren)def]^{2+}$ indicates that the increase in size of def over dmf does not generate significant differences in exchange mechanism. In addition, the change in solvent lability between dmf and def analogues of $[Cu(Me_6tren)(solvent)]^{2+}$ is not sufficiently large to suggest a variation in exchange mechanism, with the increased def exchange rate resulting from a decrease in $\Delta H^{\#}$. This change and other accompanying changes in $\Delta S^{\#}$ and $\Delta V^{\#}$ may be indicative of the influence of variation of the size of exchanging solvent molecule on a dissociatively activated mechanism but they are not of sufficient magnitude to warrant extended discussion.

Bearing in mind that both dmf and def coordinate to metal centres by electron density donation from the formyl oxygen atom it appears that substitution of methyl groups on dmf by ethyl groups on def does not introduce steric changes sufficiently close to the metal centre to produce a significant mechanistic variation. However, in the absence of any quantitative data for dma exchange on $[Cu(Me_6tren)dma]^{2+}$ (see section 4.1.6), the introduction of steric crowding much closer to the metal centre in dma solvent is believed to influence exchange kinetics to a much greater extent as illustrated by the substantial increase in k_{ex} (see section 4.1.6 and table 5.1) expected for that system.

5.2 Nickel(II) species in solution

It has already been noted in section 4.2.1 that the ultraviolet/ visible spectra of $[Ni(Me_6tren)dmf]^{2+}$ and its anation products indicate retention in dmf solution of the five-coordinate, distorted trigonal-bipyramidal geometry previously[13] shown to exist in the solid state by X-ray methods. The observation of C_{3V} symmetry is consistent with that for the analogous copper(II) system as previously discussed. Other researchers have already noted absorption spectra of $[Ni(Me_6tren)Br]^{+}$ [3-5,22], $[Ni(Me_6tren)Cl]^{+}$ [23] and the single-crystal polarized electronic absorption spectrum of $[Ni(Me_6tren)(NCS)]^{+}$ [24]. These spectra show marked similarity to those obtained for nickel(II) complexes in this study and the absorption peak in the 600-700nm region, assigned to the $^3E \rightarrow {}^3A_2$ transition on the basis of energy level diagrams[3,4], is clearly indicative of the assumed geometry.

The ultraviolet/visible spectrum of the def analogue, $[Ni(Me_6tren)-def]^{2+}$ in def solution is characterized[25] by absorption bands at 404 nm (with a molar absorptivity of 240 $dm^3mol^{-1}cm^{-1}$), 647 nm (32 $dm^3mol^{-1}cm^{-1}$) and 826 nm (23 $dm^3mol^{-1}cm^{-1}$). On the basis of the previous results the similarity of this spectrum to that of $[Ni(Me_6tren)dmf]^{2+}$ in dmf solution suggests that a similar geometry exists also for $[Ni(Me_6tren)def]^{2+}$ in def solution.

The stoichiometry of the product of the anation of $[Ni(Me_6tren)dmf]^{2+}$ by $X^- = Br^-$, N_3^- and NCS^- in dmf solution has already been shown to be $[Ni(Me_6tren)X]^{2+}$ (see section 4.2.2) by the Job method of continuous variations. As was the case for anation by $X^- = Br^-$, N_3^- and NCS^- of $[Cu(Me_6tren)dmf]^{2+}$ previously, the inferred high stability constants characterizing the formation of $[Ni(Me_6tren)X]^{+}$ are consistent with the position of the equilibrium anation process greatly favouring the (anion substituted) product.

The solvent exchange kinetics of this system are complicated due to what is believed to be the presence of a minor nickel(II) species. This has already been treated in some detail in section 4.2.4. The existence of two nickel(II) species in dmf solution appears to be a result of steric considerations, as solvent exchange on $[Ni(Me_6tren)def]^{2+}$ in def solution shows no evidence of more than one exchanging species. Bearing in mind that the minor nickel(II) species in dmf solution is believed to account for only a small percentage of the total solution composition with respect to nickel(II), the fact that substitution for dmf by def, already shown not to significantly influence coordination and exchange mechanism of solvent on copper(II) species in solution, may still reflect the enhanced sensitivity to steric factors of nickel(II) species in solution. It seems that steric changes in solvent structure quite some distance removed from the solvent coordination site still are of sufficient influence to illustrate a preference for nickel(II) to be six-coordinate[26] as has already been illustrated for some less sterically hindered nickel(II) -tren complexes[27-31].

Variable pressure nmr studies involving solvent exchange[16] on $[Ni(solvent)_6]^{2+}$ have resulted in volume of activation, $\Delta V^{\#}$, values indicative of the operation of a dissociative interchange (I_d) mechanism. This mechanistic assignment is consistent with results from ligand substitution studies[8] on these complexes and on $[NiY(solvent)_{6-n}]^{2+}$ (where Y is an n-dentate amine). It is therefore probable that $[Ni(Me_6tren)dmf]^{2+}$ and its def analogue undergo solvent exchange though an I_d mechanism also.

Solvent exchange on $[Ni(dmf)_6]^{2+}$ in dmf solution is characterized[32] by an exchange rate constant (at 298.2K), k_{ex}, of 3.8×10^3 s^{-1}. The order of magnitude decrease in solvent lability of $[Ni(Me_6tren)dmf]^{2+}$ (also observed[33] for $[Ni(Me_6tren)(CH_3CN)]^{2+}$ in CH_3CN solution compared to that for $[Ni(CH_3CN)_6]^{2+}$) may be attributed to the decreased coordination number

of this species and the increased steric crowding about the site of exchange caused by the close proximity of the six bulky methyl groups. This steric effect is expected on the basis of the X-ray crystallographic structure[13] determined for $[Ni(Me_6tren)Br]^+$ which shows the bromo ligand occupying an annulus formed by the six methyl groups of Me_6tren and the presumed similar placement of dmf in $[Ni(Me_6tren)dmf]^{2+}$. The dmf coordination site is therefore expected to be more protected from dmf molecules occupying the second coordination sphere, which are potential ligands as a result of the exchange process, and hinder involvement of either the entering ligand or general solvation effects in the exchange mechanism transition state. This low lability for dmf on $[Ni(Me_6tren)dmf]^{2+}$ should be contrasted with the very high lability observed[31] for each of the two coordinated solvent dmf molecules on $[Ni(tren)(dmf)_2]^{2+}$ for which the abovementioned steric constraints are much reduced. This observed solvent lability difference is possibly also induced by the increased steric crowding in $[Ni(Me_6tren)dmf]^{2+}$ over $[Ni(tren)(dmf)_2]^{2+}$ reducing the structural flexibility available in approaching a transition state geometry.

It has previously been noted that experimental observations in this study have indicated the (minor) existence of another nickel(II) species in the dmf solutions of $[Ni(Me_6tren)dmf](ClO_4)_2$, possibly being $[Ni(Me_6tren)-(dmf)_2]^{2+}$. If this is indeed the case, then the possibility exists that $[Ni(Me_6tren)dmf]^{2+}$ undergoes solvent exchange through an associatively activated mechanism or alternatively exchange occurring in parallel through associatively and dissociatively activated mechanisms, which has already been observed in solvent exchange processes involving other species[34,35]. It may be important to note that the inferred greater lability of the more sterically crowded $[Ni(Me_6tren)(dmf)_2]^{2+}$ species (see table 4.7) may ostensibly contradict the previous discussion concerning the influence of steric factors on coordinated solvent lability. However, it has been

observed in $[M(\text{solvent})_n]^{m+}$ systems that for a given metal ion, M, coordinated solvent lability tends to increase as n increases presumably due to greater electron density donation by the increased number of coordinated solvent molecules lowering the effective charge on the central metal ion and consequently weakening the metal - solvent bond[34,36]. Thus it may be assumed that increased coordination also enhances lability.

The rate constants characterizing anation of $[\text{Ni}(\text{Me}_6\text{tren})\text{dmf}]^{2+}$ by Br^-, N_3^- and NCS^- are shown in table 5.3 and appear remarkably low by comparison to observed rates for other, six-coordinate nickel(II) complexes[8]. It can be deduced that the factors responsible for slow dmf exchange are also influential for anation. The broad similarity of the exchange rate and activation parameters with those characterizing anation (see table 5.3) suggest the operation of an I_d mechanism for dmf exchange and anionic substitution on this species. As was the case with copper(II) species treated earlier, negative $\Delta S^{\#}$ values characterize exchange and anation on $[\text{Ni}(\text{Me}_6\text{tren})\text{dmf}]^{2+}$. It is assumed that the same considerations (see section 5.1) are applicable to this system in accounting for this obser-vation. A discernable difference (though not of sufficient magnitude to indicate a significant departure from the assigned mechanism) does exist for parameters characterizing anation of $[\text{Ni}(\text{Me}_6\text{tren})\text{dmf}]^{2+}$ by Br^- suggesting some involvement of X^- in the transition state energetics. As outlined in section 2.1.3, the predominant energetic step in an I_d mechanism is the breaking of the bond between the central metal ion and the outgoing ligand. The influence of the incoming ligand varies from substantial to negligible as the mechanism becomes more dissociative (D) in nature. It is therefore, in principle, possible for an incoming ligand to contribute to the energetics of an I_d mechanism to an extent varying with the nature of that ligand. The rod-like anions N_3^- and NCS^- are of similar geometry, size and charge distribution and would be expected to

Table 5.3

Parameters[a] for anation on solvent exchange on $[Ni(Me_6tren)-(solvent)]^{2+}$.

Anation by X^- on $[Ni(Me_6tren)dmf]^{2+}$

X^-	Br^-	N_3^-	NCS^-
$K_o(298.2K)$ $(dm^3mol^{-1})^b$	-	758 ± 114	520 ± 60
$k_i(298.2K)$ (s^{-1})	116 ± 3	229 ± 10	170 ± 6
$\Delta H_i^\#$ $(kJmol^{-1})$	34.9 ± 1.2	41.8 ± 2.5	44.0 ± 2.1
$\Delta S_i^\#$ $(Jk^{-1}mol^{-1})$	-88.4 ± 4.2	-59.6 ± 8.4	-54.7 ± 7.2

Solvent exchange on $[Ni(Me_6tren)dmf]^{2+}$

Solvent	dmf^c	def
$k_{ex}(298.2K)$ (s^{-1})	203 ± 20	944 ± 42
$\Delta H^\#$ $(kJmol^{-1})$	42.6 ± 2.0	23.1 ± 0.7
$\Delta S^\#$ $(JK^{-1}mol^{-1})$	-58 ± 8	-111 ± 2
A_o (s^{-1})	-	0.49 ± 0.26
E_o $(kJmol^{-1})$	-	20.4 ± 1.0

a. Errors represent one standard deviation.

b. No data is available for $X^- = Br^-$ as the reaction was studied over a limited anion concentration range (see section 4.2.3).

c. Parameters calculated assuming $[Ni(Me_6tren)dmf]^{2+}$ provides 100% of sites available for exchange.

make any contributions to the I_d activation energetics to a similar extent. However, Br$^-$ differs considerably in these respects.

In spite of this small dissimilarity when X$^-$ = Br$^-$ the overall relative invariance of k_i characterizing anionic substitution on [Ni(Me$_6$tren)dmf]$^{2+}$ by the designated I_d mechanism may be contrasted (as was done for that on copper(II) operating through a similar mechanism) with a classic case of an I_a mechanism[21], [Cr(dmf)$_6$]$^{3+}$, where the incoming ligand is expected to make a dominant contribution to transition state energetics. This contrast is shown in table 5.4.

As only one kinetic process was experimentally observed for anation it is concluded that anation of the minor nickel(II) species shown to exist from nmr studies is characterized by either a spectral change insufficient for detection or by rates outside of the stopped-flow spectrophotometric time scale.

It appears that from the data in table 5.3, replacing methyl groups on dmf by ethyl groups on def does not introduce steric changes sufficiently close to the metal centre to produce any significant kinetic variation, as was the case in the analogous copper(II) systems studied. However, there does appear to be some inconsistency in comparison with the copper(II) systems already discussed. Solvent exchange on [Ni(def)$_6$]$^{2+}$ is characterized[37] by k_{ex} (at 298.2K) = 1.15 x 10^3 s^{-1} which differs little from that characterizing solvent exchange on [Ni(Me$_6$tren) - def]$^{2+}$ (k_{ex} at 298.2K = 0.944 x 10^3 s^{-1}) despite the major change in the composition of the first coordination sphere of nickel(II). This is in stark contrast to the change from six to five-coordination in the analogous cobalt(II) and copper(II) species producing a major decrease in k_{ex}. This will be discussed in more detail in section 5.4. No data is available for dma exchange on [Ni(Me$_6$tren)dma]$^{2+}$ to make any further inferences concerning the effects of solvent stereochemistry on exchange

Table 5.4

Comparison of k_i/k_{ex} values for anation reactions operating through I_d and I_a mechanisms.

	anation of $[Cr(dmf)_6]^{3+}$	anation of $[Ni(Me_6tren)dmf]^{2+}$
	I_a mechanism	I_d mechanism
X^-	k_i/k_{ex} [a]	k_i/k_{ex} [b]
Br^-	0.088	0.571
NCS^-	2.35	0.837
N_3^-	57.5	1.13

a. data from reference 21 at 344.5K .

b. at 298.2K assuming $k_{ex} = 203$ s^{-1}.

kinetics for these nickel(II) systems.

5.3 Cobalt(II) species in solution

The ultraviolet/visible spectra of $[Co(Me_6tren)dmf]^{2+}$ and its anation products $[Co(Me_6tren)X]^+$ (where $X^- = Br^-$, N_3^- and NCS^-) in dmf solution have already been shown (see section 4.3.1) to characterize a five-coordinate species of approximately trigonal-bipyramidal geometry. The X-ray crystallographic structure of $[Co(Me_6tren)Br]Br$ has been determined[38] and assigned a trigonal-bipyramidal structure with C_{3V} symmetry. The absorbance spectra characterizing cobalt(II) species obtained in this study show marked similarity to spectra in the literature characterizing $[Co(Me_6tren)Cl]Cl$ in the solid state[1,2] and in chloroform solution[2,5], as well as those characterizing $[Co(Me_6tren)Br]Br$ in the solid state[3] and in dichloromethane solution[4]. A ligand-field interpretation[38] of the absorbance spectra of these cobalt(II) species suggests the observed bands in the 400-900 nm wavelength range to be indicative of penta-coordination of an approximately trigonal-bipyramidal structure with C_{3V} symmetry. On the basis of energy level diagrams[2,4,39] the three absorption bands in the 400-900 nm wavelength region have been assigned, in increasing order of energy, to the $^4A_2'(F) \rightarrow {}^4E'(F)$, $^4A_2'(F) \rightarrow {}^4A_2'(P)$ and $^4A_2'(F) \rightarrow {}^4E''(P)$ transitions. The observation of C_{3V} symmetry for cobalt(II) complexes involving the Me_6tren ligand in solution is consistent with the copper(II) and nickel(II) - Me_6tren systems previously discussed.

The stoichiometry of the product of the anation of $[Co(Me_6tren)dmf]^{2+}$ by $X^- = Br^-$, N_3^- and NCS^- in dmf solution has already been shown to be $[Co(Me_6tren)X]^+$ (see section 4.3.2) by the Job method of continuous variations. Consistent with previous results for the analogous copper(II) and nickel(II) systems, the inferred high stability constants characterizing the formation of $[Co(Me_6tren)X]^+$ cause the position of the equilibrium for the anation process,

$$[Co(Me_6tren)dmf]^{2+} + X^- \rightleftharpoons [Co(Me_6tren)X]^+ + dmf$$
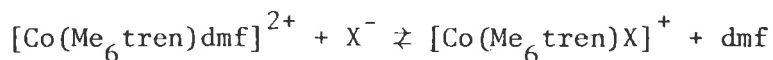
to greatly favour the (anion substituted) product.

The rate of solvent exchange, k_{ex}, for dmf on $[Co(dmf)_6]^{2+}$ is characterized at 298.2K by $k_{ex} = 3.9 \times 10^5 \text{ s}^{-1}$. The kinetic rate constant characterizing solvent exchange on $[Co(Me_6tren)dmf]^{2+}$ at 298.2K is $k_{ex} = 51.4 \text{ s}^{-1}$ indicating a large reduction in lability of this species by comparison to that for $[Co(dmf)_6]^{2+}$. This effect is consistent with that observed for the analogous copper(II) and nickel(II) systems previously treated and it is presumed that the same structural effects already discussed in this chapter are responsible.

The significance of $\Delta V^{\#}$ values derived from high-pressure nmr studies has already been discussed in detail. The exchange of dmf on $[Co(Me_6tren)dmf]^{2+}$ is characterized by $\Delta V^{\#} = -2.7 \text{cm}^3\text{mol}^{-1}$. The negative sign in this case is interpreted as being characteristic of an associatively activated mechanism for dmf exchange on this species. It has already been noted that within the simple theory applied to the interpretation of $\Delta V^{\#}$ values, a significantly smaller $\Delta V^{\#}$ magnitude observed for $[Co(Me_6tren)dmf]^{2+}$, compared to a species of similar size, $[Cr(dmf)_6]^{3+}$, with $\Delta V^{\#} = -6.3 \text{cm}^3\text{mol}^{-1}$ and thought to undergo exchange through an associative activation mode[14], suggests that it is possible that dmf exchange on $[Co(Me_6tren)dmf]^{2+}$ is characterized by an I_a mechanism.

The experimental constraints on the stopped-flow study of ligand substitution on $[Co(Me_6tren)dmf]^{2+}$ and the significance of these constraints with respect to the data appearing in table 5.5 have previously been discussed in section 4.3.3. The k_iK_o values characterizing substitution of N_3^- for dmf on $[Co(Me_6tren)dmf]^{2+}$ (see table 5.5) are substantially greater than those for NCS^- but it cannot be determined from the available data whether this discrepency is a consequence of differences in k_i, K_o or

Table 5.5

Parameters[a] for anation and solvent exchange on $[Co(Me_6tren)(solvent)]^{2+}$.

Anation by X^- on $[Co(Me_6tren)dmf]^{2+}$

X^-	Br^-	N_3^-	NCS^-
$10^3 k_i K_o(298.2K)$ $(dm^3 mol^{-1}s^{-1})$	-	111 ± 9	22.4 ± 0.7
$k_i(298.2K)$ (s^{-1})	23.1 ± 0.6	-	-
$k_i(298.2K)$ $[K_o = 50 \ dm^3 mol^{-1}](s^{-1})$	-	2220	448
$k_i(298.2K)$ $[K_o = 100 \ dm^3 mol^{-1}](s^{-1})$	-	1110	224
$k_i(298.2K)$ $[K_o = 200 \ dm^3 mol^{-1}](s^{-1})$	-	555	-

Solvent exchange on $[Co(Me_6tren)(solvent)]^{2+}$

solvent		dmf	def
$k_{ex}(298.2K)$	(s^{-1})	51.4 ± 4.2	26.3 ± 2.2
$\Delta H^{\#}$	$(kJmol^{-1})$	52.4 ± 1.1	58.3 ± 1.7
$\Delta S^{\#}$	$(JK^{-1}mol^{-1})$	-36.5 ± 3.0	-22.2 ± 4.6
A_o	(s^{-1})	28.6 ± 4.2	123 ± 15
E_o	$(kJmol^{-1})$	7.3 ± 0.3	4.2 ± 0.3
$\Delta V^{\#}$	$(cm^3 mol^{-1})$	-2.7 ± 0.2	-1.3 ± 0.2

a. Errors represent one standard deviation.

both parameters. It is possible to estimate values of k_i for

substitution by N_3^- and NCS^-, assuming values for K_o within limits that

do not introduce a substantial deviation from the observed linear

dependence of k_{obs} on $[X^-]$ over the experimental $[X^-]$ range. Using this

approach a range of k_i values may be derived as shown in table 5.5. In

the case of $X^- = Br^-$, K_o values in the range 200-400 dm^3mol^{-1} would

effect, within experimental error, the observed invariance of k_{obs} with

$[Br^-]$ over the experimental $[Br^-]$ range. All of the possible K_o values

considered fall within the 52-464 dm^3mol^{-1} range indirectly determined

for anation of $[Cu(Me_6tren)dmf]^{2+}$ by Br^-, N_3^- and NCS^- (see section 4.1.3)

for which the full k_{obs} variation with $[X^-]$ predicted by equation 4.7 was

observed. The Fuoss equation (see equation 2.2 in section 2.1.3) may be

used to estimate a value at 298.2K of $K_o = 101$ dm^3mol^{-1} for $[Co(Me_6tren)-$

$dmf]^{2+}$ and X^- considered as perfect spheres at an interaction distance of

56.5 pm in a medium of dielectric constant 36.71. As discussed in

section 2.1.3, the applicability of the Fuoss equation to this system is

in some doubt but the value for K_o estimated approximates K_o values

indirectly determined for the ligand substitution of $[Ni(Me_6tren)dmf]^{2+}$ by

Br^-, N_3^- and NCS^- (see table 4.6) and also falls within the range

characterizing anation of $[Cu(Me_6tren)dmf]^{2+}$ noted above.

Despite the fact that precise k_i values characterizing substitution

of dmf in $[Co(Me_6tren)dmf]^{2+}$ by N_3^- and NCS^- cannot be determined from

the present experimental data it can be seen from table 5.5 that these

values are substantially greater than k_i characterizing substitution by

Br^-. Calculating k_i values characterizing substitution by N_3^- and NCS^-

on the basis of K_o being 100 dm^3mol^{-1}, as derived from the Fuoss equation,

a substantial range of k_i parameters characterizing anionic substitution

for dmf on $[Co(Me_6tren)dmf]^{2+}$ develops, these being 23.1 s^{-1} for Br^-,

224 s^{-1} for NCS^- and 1110 s^{-1} for N_3^-. This significant variation in rate

constant is consistent with the operation of an associatively activated mechanism. This is in turn consistent with the interpretation of volume of activation data for dmf exchange on $[Co(Me_6tren)dmf]^{2+}$ already discussed in this section. The variation in rate constant observed for ligand substitution occurring on $[Co(Me_6tren)dmf]^{2+}$ may be compared and contrasted with substitution occurring via a classic I_a mechanism[21] on $[Cr(dmf)_6]^{2+}$ and substitution occurring on $[Cu(Me_6tren)dmf]^{2+}$ supposedly via an I_d mechanism, respectively, as is shown in table 5.6. It is of interest to note that for both systems purported to undergo ligand substitution (and exchange) through an associatively activated, I_a mechanism, k_i increases in the same sequence this being $Br^- <$ dmf $< NCS^- < N_3^-$.

From the data in table 5.5 it appears that substitution of methyl groups on dmf by ethyl groups on def does not introduce steric changes sufficiently close to the metal centre to produce any significant kinetic variation. There is also a marked decrease in solvent lability of def in $[Co(Me_6tren)def]^{2+}$ with respect to that observed[37] for $[Co(def)_6]^{2+}$ where k_{ex} (at 298.2K) $= 1.20 \times 10^5 \, s^{-1}$. These observations are consistent with the analogous copper(II) system treated in this study and it is expected that again similar structural factors are responsible.

Table 5.6

Comparison of k_i/k_{ex} values for anation reactions operating through I_d and I_a mechanisms.

anation of :	$[Co(Me_6tren)dmf]^{2+}$	$[Cr(dmf)_6]^{3+}$	$[Cu(Me_6tren)dmf]^{2+}$
mechanism :	I_a	I_a	I_d
X^-	k_i/k_{ex} [a]	k_i/k_{ex} [b]	k_i/k_{ex} [a]
Br^-	0.449	0.088	1.01
NCS^-	4.36	2.35	0.953
N_3^-	21.6	57.5	0.784

a. at 298.2K.

b. data from reference 21 at 344.5K.

5.4 General Conclusions

Evidence obtained in this study indicates that complexes of the type $[M(Me_6tren)L](ClO_4)_n$ (where M = Co(II), Ni(II), Cu(II), Zn(II); L = solvent molecule or anion) which have been shown by X-ray crystallographic methods to be pentacoordinate complexes of C_{3V} symmetry in the solid state, retain this geometry in solution. A possible exception is $[Ni(Me_6tren)(solvent)](ClO_4)_2$ which appears to have some tendency to form a six-coordinate species in dmf solution. However, by introducing steric changes in solvent structure (substituting def for dmf) the experimental evidence suggests that only one, five-coordinate def-bound species results. These observations serve to illustrate the influence that even subtle steric changes to labile coordinating ligands can have over the coordination geometry of a metal complex made sensitive to steric crowding around the labile coordination site by the choice of a less labile and bulky multidentate ligand such as Me_6tren.

There is no evidence in this study to suggest that the anation products of these complexes in dmf solution $[M(Me_6tren)X]^+$ (where M = Co(II), Ni(II), Cu(II); X = Br^-, NCS^-, N_3^-) are anything other than five-coordinate. These complexes are all characterized by large stability constants. This is probably due to the strong electrostatic attraction between the charge on the central metal ion of the complex and the substituting anion, somewhat facilitated by the relatively low charge separation characteristics of the dmf solvent.

There has throughout this study been an excellent correlation between the mechanistic interpretations derived from variable temperature and pressure nmr results and those derived from stopped-flow spectrophotometric results, as exemplified by ligand exchange and substitution on $[Cu(Me_6tren)dmf]^{2+}$ in dmf solution. It is to be expected for the I_d

mechanism assigned to the ligand exchange and anionic substitution processes on this species in dmf solution that the rate constant characterizing anation k_i, should be of similar magnitude to the rate constant characterizing dmf exchange, k_{ex}, modified by a competition ratio reflecting the relative abilities of the anion and dmf solvent to compete for a vacant site in the first coordination sphere of the encounter complex. Under the experimental conditions of this study, purely electrostatic grounds would favour substitution by the negatively charged species and one might expect the competition ratio to approach unity. As none of the $[M(Me_6tren)(solvent)]^{2+}$ species examined in this study are sufficiently substitution labile for selectivity for the entering group to be decreased[20], the quite reasonable agreement between k_{ex} and k_i for several anions is consistent with the assigned mechanism.

It has already been noted that coordination of Me_6tren causes a substantial decrease in the lability of $[M(Me_6tren)(solvent)]^{2+}$, attributed to several structural factors which have previously been discussed in detail. This trend is illustrated in table 5.7. The Me_6tren ligand appears, by way of the three bulky nitrogen-donor $-NMe_2$ groups forming an annulus about the labile coordination site, to hinder sterically that site from interaction with an incoming ligand. The constraining influence of the coordinated Me_6tren upon the approach to a transition state for ligand substitution is also expected to reduce lability. In addition, the lower coordination number about the central metal ion in $[M(Me_6tren)(solvent)]^{2+}$ is expected to result in a lower lability for coordinated solvent. In the specific case of copper(II), removal of effects due to Jahn-Teller distortions further reduces lability relative to $[Cu(solvent)_6]^{2+}$.

Some exceptions to this trend do however, exist. Results from an nmr study[40] on $[Mn(Me_6tren)dmf]^{2+}$ show very little change in lability of dmf

Table 5.7

Comparison of parameters for solvent exchange.

M	$[M(Me_6tren)dmf]^{2+}$			
	Mn^a	Co	Ni	Cu
$k_{ex}(298.2K)$ (s^{-1})	2.7×10^6	51.4	203	555
$\Delta H^{\#}(kJmol^{-1})$	18.0	52.4	42.6	43.3
$\Delta S^{\#}(JK^{-1}mol^{-1})$	-61.2	-36.5	-58	-47.0
$\Delta V^{\#}(cm^3mol^{-1})$	-6	- 2.7	-	6.1

M	$[M(dmf)_6]^{2+}$			
	Mn^b	Co^c	Ni^d	Cu
$k_{ex}(298.2K)$ (s^{-1})	2.4×10^6	3.9×10^5	3.8×10^3	$>10^7$
$\Delta H^{\#}(kJmol^{-1})$	-3.1	52.7	15.0	-
$\Delta S^{\#}(JK^{-1}mol^{-1})$	37.2	56.9	8.0	-
$\Delta V^{\#}(cm^3mol^{-1})$	-	6.7	-	-

M	$[M(Me_6tren)def]^{2+}$		
	Co	Ni	Cu
$k_{ex}(298.2K)$ (s^{-1})	26.3	944	980
$\Delta H^{\#}(kJmol^{-1})$	58.3	23.1	36.3
$\Delta S^{\#}(JK^{-1}mol^{-1})$	-22.2	-111	-65.9
$\Delta V^{\#}(cm^3mol^{-1})$	- 1.3	-	5.3

M	$[M(def)_6]^{2+}$		
	Co^e	Ni^e	Cu
$k_{ex}(298.2K)$ (s^{-1})	1.20×10^5	1.15×10^3	$>10^7$
$\Delta H^{\#}(kJmol^{-1})$	51.4	74.2	-
$\Delta S^{\#}(JK^{-1}mol^{-1})$	24.8	62.6	-
$\Delta V^{\#}(cm^3mol^{-1})$	-	-	-

Table 5.7 cont...

a. data from reference 40.

b. data from reference 41.

c. data from references 15 and 32.

d. data from reference 32.

e. data from reference 37.

in that species by comparison to $[Mn(dmf)_6]^{2+}$. Solid-state X-ray crystallographic studies[13,38,42,43] of the trigonal-bipyramidal series $[M(Me_6tren)Br]^+$ (where M = Mn(II), Fe(II), Co(II), Ni(II), Cu(II), Zn(II)) illustrate that the effects of steric constraints due to Me_6tren and of orbital occupancy are superimposed on the expected decrease in bond distances with increase in atomic number. This is shown in table 5.8. In all cases the bromine atom occupies an axial position with the three $-NMe_2$ groups occupying equatorial positions. If one assumes that dmf would also occupy an axial position in $[M(Me_6tren)dmf]^{2+}$ and that the bond distance variations exhibited by this species are similar to those of the bromo analogue then the $M-N_{equatorial}$ distances determine the radius of the annulus formed by the six methyl groups about the labile coordination site occupied by dmf. Increases in the $M-N_{equatorial}$ and M-dmf distances should serve to increase the accessibility of M to an entering ligand and also weaken the M-dmf interaction. This is indeed observed for $[Mn(Me_6tren)dmf]^{2+}$ (see table 5.8) and also on the basis of d orbital occupancy, to be discussed in more detail later, this species ought to favour an associative mode for dmf exchange and be more labile than its cobalt(II), nickel(II) and copper(II) analogues. This greater lability of $[Mn(Me_6tren)dmf]^{2+}$ is reflected in a smaller $\Delta H^{\#}$ (see table 5.7) as a consequence of the greater accessibility of the manganese(II) centre to dmf exchange.

The other exception concerns the values of k_{ex}(at 298.2K) characterizing def exchange on $[Ni(def)_6]^{2+}$ and $[Ni(Me_6tren)def]^{2+}$ being somewhat similar, in contrast to the change from six to five coordination in the analogous cobalt(II) and copper(II) species producing a major decrease in k_{ex}. This effect arises as a result of the combination of two contributing effects. Solvent exchange on $[Ni(solvent)_6]^{2+}$ proceeding through a dissociatively activated mechanism is characterized by a substantial crystal field

Table 5.8

X-ray crystallographic bond distances[a] in $[M(Me_6tren)Br]^+$.

M	M-Br $\overset{\circ}{A}$	M-N$_{equatorial}$ $\overset{\circ}{A}$	M-N$_{axial}$ $\overset{\circ}{A}$
Mn[b]	2.49 (6)	2.27 (2)	2.19 (3)
Fe[b]	2.48 (3)	2.15 (1)	2.21 (1)
Co[c]	2.43 (4)	2.08 (2)	2.15 (2)
Ni[d]	2.47 (2)	2.13 (1)	2.10 (1)
Cu[d]	2.39 (3)	2.14 (1)	2.07 (1)
Zn[b]	2.44 (3)	2.11 (2)	2.19 (2)

a. the number in brackets refers to atoms related to the reference atom by the threefold axis.

b. data from reference 42.

c. data from reference 38.

d. data from reference 13.

activation energy (CFAE) contribution to $\Delta H^{\#}$ increasing its magnitude

whereas the CFAE contribution to the analogous cobalt(II) species, also

believed to undergo solvent exchange through a dissociatively activated

mechanism[16], is smaller, resulting in the latter species being usually

more labile[44]. These CFAE contributions involving octahedral ground

states and (reaction intermediate of reduced coordination number)

trigonal-bipyramidal transition states may be calculated as 5.76 Dq and

1.72 Dq for nickel(II) and cobalt(II) species respectively assuming

$\rho = 1.0$[45,46] and d orbital energies from the literature[47]. Thus the

substantially higher $\Delta H^{\#}$ characterizing def exchange on $[Ni(def)_6]^{2+}$ (see

table 5.7) is, at least in part, responsible for the lower lability of

this species. Obviously, the very high lability of the $[Cu(def)_6]^{2+}$ species

is a consequence of the Jahn-Teller effect[7]. It is difficult to apply

reliably CFAE calculations to the $[Ni(Me_6tren)def]^{2+}$ species due to the

approximate nature of the trigonal-bipyramidal geometry, the differences

in bond lengths to M and the differences in the donor atoms coordinating

to M, therefore no such calculations have been attempted. However, the

value of $\Delta H^{\#}$ characterizing solvent exchange on $[Ni(Me_6tren)def]^{2+}$ is

significantly smaller (see table 5.7) than that characterizing the

cobalt(II) and copper(II) analogues as well as $[Ni(def)_6]^{2+}$. Yet this

ordinarily labilizing effect is largely compensated for by a largely

negative $\Delta S^{\#}$ (see also table 5.7) to give a value for k_{ex} (at 298.2K) =

944 s^{-1}. The observed similarity of this value to that characterizing

$[Ni(def)_6]^{2+}$ is a direct result of the somewhat complex combination of

effects just discussed and may be considered to illustrate the sensitive

nature of these species to such considerations.

In solutions of the solvents of interest in this study,

$[M(Me_6tren)(solvent)]^{2+}$ appears to undergo solvent exchange and anation

through an I_a mechanism when M = Mn(II) and Co(II) and an I_d mechanism

when M = Ni(II) and Cu(II). Studies involving solvent exchange of $[M(solvent)_6]^{2+}$ in a wider range of solvents indicate[16,48,49] that an I_a mechanism operates only when M = V(II) and Mn(II) with an I_d mechanism operating when M = Fe(II), Co(II), Ni(II) and Cu(II). Both of these mechanistic trends are consistent with the hypothesis that increased d orbital occupancy results in increased electrostatic repulsion between the metal centre of the complex and an entering solvent molecule in an I_a mechanism, with a consequent tendency for an I_d mechanism for solvent exchange to become increasingly favoured with increase in atomic number[8]. This consequence is illustrated for $[M(Me_6tren)dmf]^{2+}$ in figure 5.1. In an associatively activated mechanism, the substituting ligand, L, approaches the metal centre through the trigonal face of the trigonal-bipyramidal complex. The progressive filling of the d_{xz} and d_{yz} orbitals in particular and the d_{xy} orbital to a lesser extent (as shown in figure 5.2) is expected to electrostatically hinder the approach of L to any of the three faces of the trigonal-bipyramid adjacent to the coordinated dmf molecule. Thus the associative activation mode tendency is decreased, with a complementary increase in dissociative activation mode tendency, as the number of d electrons increases.

The inconsistency of the exchange mechanism for cobalt(II) complexes above, may reflect the sensitivity of the coordinatively unsaturated nature of five-coordinate $[Co(Me_6tren)(solvent)]^{2+}$ towards mechanism of solvent exchange, despite obvious changes in the environment surrounding the labile coordination site caused by the coordination of the Me_6tren ligand. The enhanced ability to form a new bond in the transition state of $[Co(Me_6tren)dmf]^{2+}$ (having a lower coordination number) favours an associative activation mode whereas the greater electronic occupancy of the d orbitals in the case of $[Co(dmf)_6]^{2+}$ is probably the dominant factor favouring a dissociative activation mode.

$[M(Me_6tren)dmf]^{2+}$
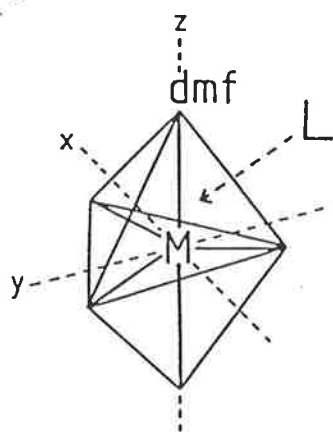
a activation mode L approaches trigonal face

(energies: $d_{z^2} > d_{x^2-y^2} = d_{xy} > d_{xz} = d_{yz}$)

$Mn^{2+}d^5$; $Fe^{2+}d^6$; $Co^{2+}d^7$; $Ni^{2+}d^8$; $Cu^{2+}d^9$.

—electronic repulsion between d_{xy}, d_{xz}, d_{yz} and L increases →

———a activation tendency decreases ⟶

———d "   "   "   " increases ⟶

Figure 5.1

Ligand substitution by L on $[M(Me_6tren)dmf]^{2+}$.
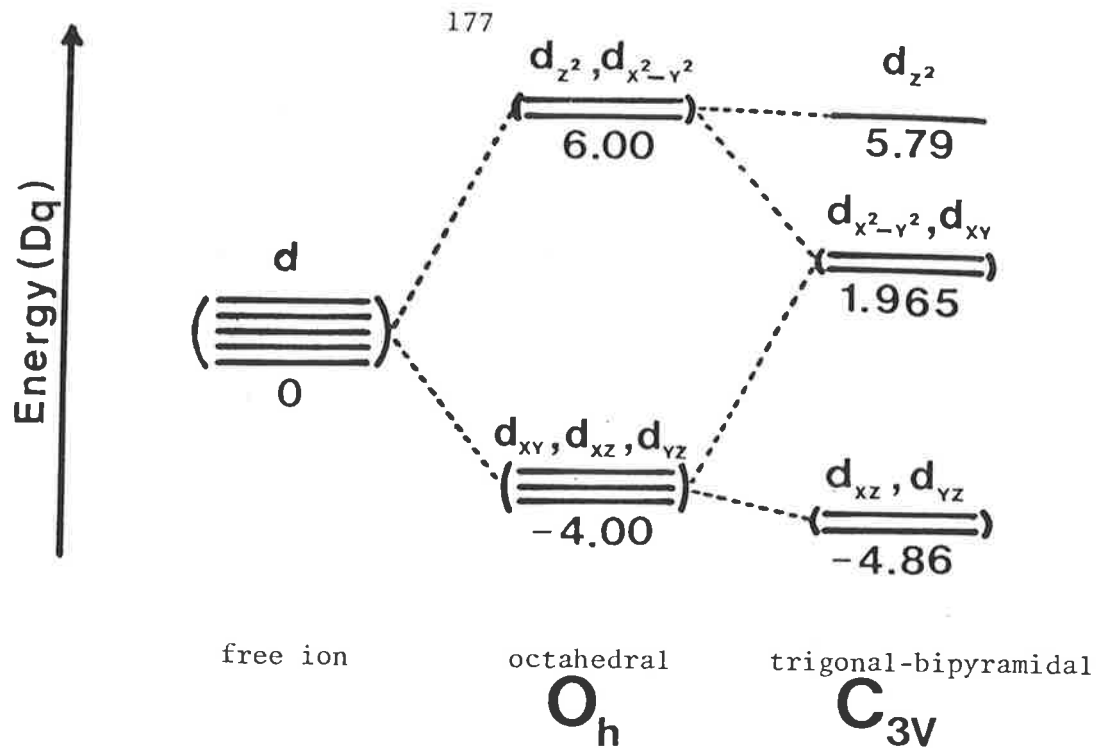
Figure 5.2.(i)

Orbital splitting for a metal ion in the free state and in octahedral and trigonal-bipyramidal fields.
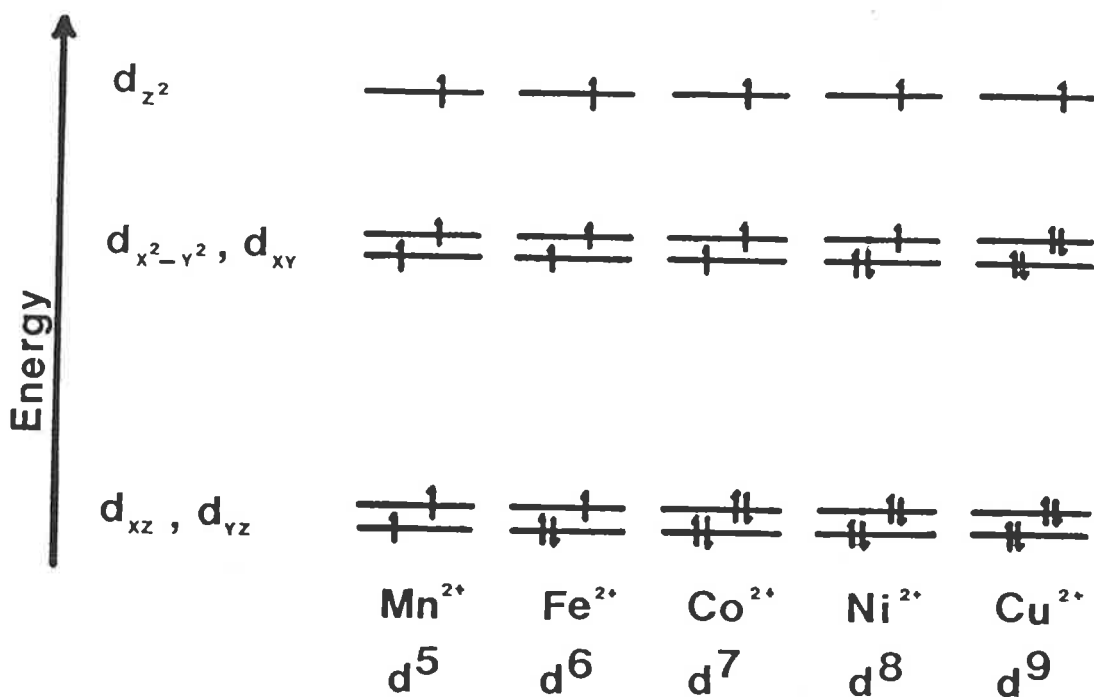
Figure 5.2.(ii)

Ground state electronic occupancy of energy levels of a divalent metal ion, M^{2+}, in a trigonal-bipyramidal, C_{3V}, coordination geometry as a function of the number of d electrons (high-spin).

5.5　References to Chapter 5

1.　M. Ciampolini, N. Nardi, Inorg. Chem., 1966, 5, 41.

2.　M. Ciampolini, N. Nardi, Inorg. Chem., 1966, 5, 1150.

3.　L. Sacconi, in "Coordination Chemistry X, Plenary lectures of X ICCC, Tokyo.", 1967; Pure.Appl.Chem., 1968, 17, 95.

4.　M. Ciampolini, Struct.Bond., 1969, 6, 52.

5.　C. Furlani, Coord.Chem.Rev., 1968, 3, 141.

6.　R. Poupko, Z.Luz, J.Chem.Phys., 1972, 57, 3311.

7.　R.J. West, S.F. Lincoln, J.Chem.Soc., Dalton Trans., 1974, 281.

8.　D.W. Margerum, G.R. Gayley, D.C. Weatherburn, G.K. Pagenkopf, in "Coordination Chemistry", A.E. Martel, ed., vol.2., American Chemical Society, Washington D.C., 1978.

9.　D.P. Rablen, H.W. Dodgen, J.P. Hunt, J.Amer.Chem.Soc., 1972, 94, 1771.

10.　H.A. Jahn, E. Teller, Proc.Roy.Soc., 1937, A161, 220.

11.　H.A. Jahn, Proc.Roy.Soc., 1938, A164, 117.

12.　D.J. Hewkin, R.H. Prince, Coord.Chem.Rev., 1970, 5, 64.

13.　M. Di Vaira, P.L. Orioli, Acta Cryst., 1968, B24, 595.

14.　S.T.D. Lo, T.W. Swaddle, Inorg.Chem., 1975, 14, 1878.

15.　F.K. Meyer, K.E. Newman, A.E. Merbach, Inorg.Chem., 1979, 18, 2142.

16.　A.E. Merbach, Pure Appl.Chem., 1982, 54, 1479.

17.　T.W. Swaddle, Rev.Phys.Chem.Jpn, 1980, 50, 230.

18.　P. Fischer, H. Hoffman, G. Platz, Ber.Bunsenges. Phys.Chem., 1972, 76, 1060.

19.　E.F. Caldin, H.P. Bennetto, J.Solution Chem., 1973, 2, 217.

20.　J.E. Leffler, E. Grunwald, in "Rates and Equilibria of Organic Reactions", Wiley, N.Y., 1965.

21.　S.T.D. Lo, T.W. Swaddle, Inorg.Chem., 1976, 15, 1881.

22.　M. Ciampolini, N. Nardi, Inorg.Chem., 1967, 6, 445.

23. M. Ciampolini, N. Nardi, G.P. Speroni, Coord.Chem.Rev., 1966, 1, 222.

24. I. Bertini, M. Ciampolini, P. Dapporto, D. Gatteschi, Inorg.Chem., 1972, 11, 2254.

25. A.M. Hounslow, University of Adelaide, Private Communication.

26. M. Ciampolini, N. Nardi, Inorg.Chem., 1967, 6, 1261.

27. C.K. Jorgensen, Acta Chem.Scand., 1956, 10, 887.

28. R.W. Asmussen, O. Bostrup, Acta Chem.Scand., 1957, 11, 1097.

29. D. Hall, M.D. Woulfe, Proc.Chem.Soc., 1958, 346.

30. S.E. Rasmussen, Acta Chem.Scand., 1959, 13, 2009.

31. S.F. Lincoln, J.H. Coates, B.G. Doddridge, D.L. Pisaniello, Aust.J.Chem., 1984, 37, 947.

32. N.A. Matwiyoff, Inorg.Chem., 1966, 5, 788.

33. R.J. West, S.F. Lincoln, Inorg.Chem., 1973, 12, 494.

34. D.L. Pisaniello, S.F. Lincoln, Inorg.Chem., 1981, 20, 3689.

35. S.F. Lincoln, M.N. Tkaczuk, Ber.Bunsenges. Phys.Chem., 1982, 86, 221.

36. D.L. Pisaniello, S.F. Lincoln, E.H. Williams, A.J. Jones, Aust.J.Chem., 1981, 34, 495.

37. S.F. Lincoln, A.M. Hounslow, A. Boffa, unpublished results.

38. M. DiVaira, P.L. Orioli, Inorg.Chem., 1967, 6, 955.

39. M. Ciampolini, I. Bertini, J.Chem.Soc. (A), 1968, 2241.

40. S.F. Lincoln, A.M. Hounslow, D.L. Pisaniello, B.G. Doddridge, J.H. Coates, A.E. Merbach, D. Zbinden, Inorg.Chem., 1984, 23, 1090.

41. T. Chen, L.O. Morgan, J.Chem.Phys., 1972, 76, 1973.

42. M. DiVaira, P.L. Orioli, Acta Cryst., 1968, B24, 1269.

43. P.L. Orioli, Coord.Chem.Rev., 1971, 6, 285.

44. A.J. Companion, J.Phys.Chem., 1969, 73, 739.

45. W. Hatfield, T.S. Piper, Inorg.Chem., 1964, 3, 841.

46. P. Day, Proc.Chem.Soc., 1964, 18.

47. R. Krishnamurthy, W.B. Schaap, J.Chem.Ed., 1969, 46, 799.

48. F.K. Meyer, K.E. Newman, A.E. Merbach, J.Amer.Chem.Soc., 1979, 101, 5588.

49. S.F. Lincoln, A.E. Merbach, unpublished results, observing a large positive activation volume for methanol exchange on $[Cu(MeOH)_6]^{2+}$ consistent with the operation of a D activation mode.

Appendices

A.1 Copper(II) species in solution

Appendix 1.1

Stopped-flow spectrophotometric k_{obs} data for anation of $[Cu(Me_6tren)dmf]^{2+}$ by X^- in dmf solution (ionic strength adjusted to 0.5 mol dm^{-3} with sodium perchlorate).

$X^- = Br^-$
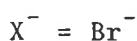
$[Cu(Me_6tren)dmf^{2+}]_o$ (x 10^4mol dm^{-3})	$[Br^-]_o$ (x 10^3mol dm^{-3})	k_{obs}(278.2K) (s^{-1})	k_{obs}(288.2K) (s^{-1})	k_{obs}(298.2K) (s^{-1})
0.5174 (±0.0128)	0.6881 (±0.0055)	4.54 (±0.05)	9.60 (±0.12)	18.9 (±0.3)
0.6781 (±0.0082)	1.274 (±0.014)			32.2 (±3.5)
0.5174 (±0.0128)	1.376 (±0.009)	8.63 (±0.10)	19.2 (±0.2)	37.5 (±0.1)
1.654 (±0.0279)	1.418 (±0.022)			34.3 (±2.4)
0.8218 (±0.0220)	1.693 (±0.018)			53.6 (±2.5)
1.654 (±0.0279)	1.773 (±0.013)			55.8 (±4.3)
0.7406 (±0.0160)	2.162 (±0.019)			52.9 (±2.0)
0.5174 (±0.0128)	2.408 (±0.023)	11.0 (±0.2)	29.9 (±0.4)	65.9 (±0.9)
0.8218 (±0.0220)	3.385 (±0.063)			74.4 (±2.6)
0.6781 (±0.0082)	4.245 (±0.028)			100 (±2)
0.8167 (±0.0152)	4.631 (±0.027)	22.1 (±0.3)	49.6 (±0.6)	115 (±2)
0.8167 (±0.0152)	6.175 (±0.033)	27.8 (±0.3)	60.3 (±0.8)	143 (±2)
0.8218 (±0.0220)	6.347 (±0.036)			133 (±3)
0.7406 (±0.0160)	8.647 (±0.045)			155 (±19)
0.8167 (±0.0152)	9.263 (±0.082)	36.3 (±0.5)	88.7 (±1.9)	167 (±3)
0.6781 (±0.0082)	10.61 (±0.05)			230 (±19)
0.8218 (±0.0220)	14.81 (±0.12)			265 (±7)
0.8167 (±0.0152)	15.44 (±0.03)	72.2 (±0.9)	128 (±2)	
4.393 (±0.033)	20.50 (±0.16)	87.7 (±1.3)	183 (±3)	309 (±5)
0.6781 (±0.0082)	21.23 (±0.03)			290 (±5)
4.393 (±0.033)	25.62 (±0.04)	95.4 (±1.4)	208 (±4)	313 (±6)

$X^- = N_3^-$
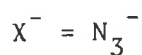
$[Cu(Me_6tren)dmf^{2+}]_o$ $(\times10^4 mol\ dm^{-3})$	$[N_3^-]_o$ $(\times10^3 mol\ dm^{-3})$	$k_{obs}(278.2K)$ (s^{-1})	$k_{obs}(288.2K)$ (s^{-1})	$k_{obs}(298.2K)$ (s^{-1})
0.4261($\pm$0.0194)	0.5168($\pm$0.0076)	32.2($\pm$0.4)	58.6($\pm$0.9)	79.7($\pm$2.7)
0.5367($\pm$0.0228)	0.6473($\pm$0.0006)			122 ($\pm$4)
0.5367($\pm$0.0228)	0.8091($\pm$0.0007)			141 ($\pm$6)
0.5367($\pm$0.0228)	1.295 ($\pm$0.020)			162 ($\pm$3)
0.4261($\pm$0.0194)	1.551 ($\pm$0.018)	53.4($\pm$0.9)	103 ($\pm$2)	161 ($\pm$3)
0.4261($\pm$0.0194)	2.584 ($\pm$0.029)	69.7($\pm$1.2)	131 ($\pm$2)	213 ($\pm$3)
1.202 ($\pm$0.016)	3.307 ($\pm$0.019)	70.9($\pm$1.3)	130 ($\pm$2)	232 ($\pm$4)
1.202 ($\pm$0.016)	4.961 ($\pm$0.048)	85.3($\pm$1.6)	161 ($\pm$3)	278 ($\pm$5)
1.202 ($\pm$0.016)	6.614 ($\pm$0.054)	95.5($\pm$1.5)	188 ($\pm$3)	305 ($\pm$5)
3.840 ($\pm$0.040)	7.734 ($\pm$0.077)		204 ($\pm$4)	375 ($\pm$5)
0.5367($\pm$0.0228)	8.091 ($\pm$0.015)			357 ($\pm$21)
1.202 ($\pm$0.016)	8.268 ($\pm$0.016)	109 ($\pm$2)	201 ($\pm$3)	
1.202 ($\pm$0.016)	8.804 ($\pm$0.073)	190 ($\pm$2)	221 ($\pm$3)	
1.836 ($\pm$0.014)	9.084 ($\pm$0.051)			361 ($\pm$7)
1.202 ($\pm$0.016)	10.06 ($\pm$0.08)	129 ($\pm$2)	223 ($\pm$3)	
3.744 ($\pm$0.013)	12.32 ($\pm$0.08)			376 ($\pm$30)
1.202 ($\pm$0.016)	12.58 ($\pm$0.02)	127 ($\pm$2)	246 ($\pm$3)	
3.840 ($\pm$0.040)	12.89 ($\pm$0.03)		252 ($\pm$5)	390 ($\pm$8)
1.491 ($\pm$0.016)	15.01 ($\pm$0.09)	141 ($\pm$2)	248 ($\pm$4)	384 ($\pm$11)
1.491 ($\pm$0.016)	19.02 ($\pm$0.31)	147 ($\pm$2)	246 ($\pm$4)	405 ($\pm$7)
1.491 ($\pm$0.016)	22.52 ($\pm$0.26)	172 ($\pm$2)	250 ($\pm$4)	
1.491 ($\pm$0.016)	25.02 ($\pm$0.03)	155 ($\pm$2)	259 ($\pm$4)	399 ($\pm$11)

$X^- = NCS^-$
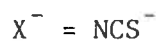
$[Cu(Me_6tren)dmf^{2+}]_o$ ($\times 10^4 mol\ dm^{-3}$)	$[NCS^-]_o$ ($\times 10^3 mol\ dm^{-3}$)	$k_{obs}(278.2K)$ (s^{-1})	$k_{obs}(288.2K)$ (s^{-1})	$k_{obs}(298.2K)$ (s^{-1})
0.9892 (±0.0285)	0.9797 (±0.0069)			66.7 (±5.6)
0.9283 (±0.0201)	1.164 (±0.010)	25.9 (±1.2)	51.8 (±2.7)	
0.9892 (±0.0285)	1.633 (±0.011)			120 (±4)
0.9283 (±0.0201)	1.940 (±0.015)	37.2 (±3.0)	75.1 (±2.5)	
1.791 (±0.014)	2.011 (±0.018)			129 (±2)
0.9892 (±0.0285)	2.613 (±0.018)			166 (±13)
0.9892 (±0.0285)	3.266 (±0.009)			215 (±11)
0.9283 (±0.0201)	3.880 (±0.016)	45.6 (±0.8)	103 (±4)	
1.791 (±0.014)	4.021 (±0.027)			222 (±7)
3.865 (±0.012)	5.136 (±0.050)	56.9 (±2.4)	127 (±5)	
1.791 (±0.014)	6.032 (±0.035)			254 (±25)
4.824 (±0.013)	7.638 (±0.043)			289 (±14)
5.418 (±0.025)	8.159 (±0.046)	63.5 (±4.6)	130 (±8)	
3.865 (±0.012)	8.560 (±0.021)	71.5 (±3.6)	156 (±5)	
4.824 (±0.013)	10.18 (±0.05)			331 (±25)
5.418 (±0.025)	10.88 (±0.06)	65.6 (±3.3)	157 (±17)	
4.824 (±0.013)	13.24 (±0.23)			337 (±38)
5.418 (±0.025)	13.60 (±0.07)	75.7 (±4.0)	176 (±11)	
8.410 (±0.016)	15.55 (±0.14)	93.1 (±4.2)		
1.791 (±0.014)	16.09 (±0.09)			384 (±39)
1.791 (±0.014)	20.11 (±0.03)			425 (±31)
8.410 (±0.016)	20.73 (±0.16)	87.1 (±2.2)	208 (±23)	
4.824 (±0.013)	25.46 (±0.04)			402 (±81)
8.410 (±0.016)	25.92 (±0.04)	88.8 (±3.1)	208 (±20)	

Appendix 1.2

^{1}H line broadening measurements on solutions of $[Cu(Me_6tren)dmf](ClO_4)_2$ in dmf (the experimental error in individual P_mT_{2p} values is ca $\pm5\%$)

solution (i) 0.164 mol dm^{-3}, $P_m = 0.01378$

T(K)	$10^5P_mT_{2p}$(s)	T(K)	$10^5P_mT_{2p}$(s)	T(K)	$10^5P_mT_{2p}$(s)
228.5	8.70	298.1	31.5	340.1	14.0
238.6	11.5	299.2	30.5	340.4	13.0
243.7	12.5	300.3	31.5	342.2	13.5
248.8	14.0	303.6	31.5	343.2	12.0
253.9	16.0	305.8	31.5	345.3	11.5
259.0	19.0	306.1	34.5	347.4	11.0
264.1	17.5	308.1	31.0	349.5	9.40
264.1	21.0	311.2	30.5	352.6	8.50
267.2	21.0	314.2	30.5	355.8	6.85
269.2	21.5	316.3	31.0	357.9	7.30
269.3	22.0	318.3	29.0	360.6	6.10
272.5	23.5	320.0	24.5	361.1	6.10
274.6	24.0	321.4	27.0	363.2	6.20
276.5	25.5	324.5	25.5	366.5	5.60
279.9	26.0	326.6	24.0	368.5	5.40
283.1	28.0	328.7	22.0	373.9	4.00
285.2	29.0	331.8	20.5	375.9	3.90
288.5	29.5	334.9	18.0	378.9	3.70
292.8	30.5	337.0	16.5	381.0	3.60
296.0	31.0	337.0	14.5		

solution (ii) 0.0547 mol dm^{-3}, P_m = 0.004259

T(K)	$10^5 P_m T_{2p}$(s)	T(K)	$10^5 P_m T_{2p}$(s)	T(K)	$10^5 P_m T_{2p}$(s)
344.3	10.5	354.8	7.25	365.3	5.15
346.3	9.95	356.9	6.65	367.5	4.55
348.4	9.15	359.0	6.00		
350.5	8.30	362.1	4.70		

solution (iii) 0.0912 mol dm^{-3}, P_m = 0.007383

333.8	18.0	348.4	8.75	368.5	5.00
347.4	11.0	353.7	7.35		

Appendix 1.3

Paramagnetic induced chemical shift measurements on solutions of
$[Cu(Me_6tren)dmf](ClO_4)_2$ in dmf. The error in chemical shift does not
exceed the digital resolution of 0.5 Hz. Downfield shifts are positive.

solution (i) 0.164 mol dm^{-3}, P_m = 0.01378.

T(K)	$\Delta\omega$(Hz)	T(K)	$\Delta\omega$(Hz)	T(K)	$\Delta\omega$(Hz)
228.5	3.1	264.1	0.6	360.6	3.6
238.6	2.2	269.2	0.8	374.0	17.7
248.8	1.2	299.2	-0.7	376.0	14.8
253.9	1.0	320.0	-0.8	379.0	21.5
259.0	-0.2	340.4	-0.5	381.0	23.7

Appendix 1.4

[1]H line broadening measurements on solutions of $[Cu(Me_6tren)def](ClO_4)_2$ in def (the experimental error in individual P_mT_{2p} values is ca $\pm5\%$).

solution (i) 0.0685 mol dm^{-3}, P_m = 0.008077

T(K)	$10^5P_mT_{2p}$(s)	T(K)	$10^5P_mT_{2p}$(s)	T(K)	$10^5P_mT_{2p}$(s)
239.5	7.95	299.4	24.6	356.1	6.84
241.6	8.86	301.4	23.2	358.2	5.76
244.7	9.16	304.5	22.6	359.2	5.86
247.8	9.70	306.6	24.1	361.3	5.55
249.8	10.0	309.7	23.3	363.3	5.26
251.9	10.9	311.7	20.5	366.4	4.69
255.0	11.6	314.8	20.3	368.5	4.26
258.1	12.6	316.9	22.2	371.6	3.98
260.1	12.7	319.0	22.2	373.6	3.95
262.2	13.1	320.0	20.9	374.7	3.79
265.3	14.3	322.1	18.4	376.7	3.41
268.4	16.1	325.1	18.1	378.8	3.43
270.5	15.9	327.2	18.3	379.8	3.03
272.5	16.2	330.3	17.9	381.9	2.68
275.6	17.7	332.4	15.1	384.0	2.74
278.7	18.0	335.5	13.8	386.0	2.82
280.8	19.3	337.5	13.7	387.1	2.99
282.8	19.0	340.6	12.6	389.1	2.60
285.9	20.4	342.7	10.7	392.2	2.57
289.0	20.7	345.8	9.64	394.3	2.45
291.1	21.4	347.8	8.02	397.4	2.53
294.2	22.0	350.9	7.99	399.4	2.33
296.3	22.8	353.0	7.17		

solution (ii) 0.0228 mol dm^{-3}, $P_m = 0.002620$

T(K)	$10^5 P_m T_{2p}$ (s)	T(K)	$10^5 P_m T_{2p}$ (s)	T(K)	$10^5 P_m T_{2p}$ (s)
246.7	9.69	308.6	14.5	370.5	3.76
257.1	12.7	319.0	13.3	380.9	3.12
267.4	15.7	329.3	11.4	391.2	2.79
277.7	18.2	339.6	9.36	401.5	2.68
288.0	20.4	349.9	7.01		
298.3	16.1	360.2	5.05		

Appendix 1.5

Paramagnetic induced chemical shift on solutions of $[Cu(Me_6tren)def](ClO_4)_2$ in def. The error in chemical shift does not exceed the digital resolution of 0.5Hz. Downfield shifts are positive.

solution (ii) 0.0228 mol dm^{-3}, P_m = 0.002620

T(K)	$\Delta\omega$(Hz)	T(K)	$\Delta\omega$(Hz)	T(K)	$\Delta\omega$(Hz)
246.7	8.61	298.3	5.17	349.9	11.89
257.1	6.55	308.6	5.77	360.2	16.52
267.4	5.32	319.0	6.28	370.5	22.21
277.7	4.57	329.3	7.33	380.9	26.75
288.0	4.09	339.6	8.91	391.2	29.86

Appendix 1.6

^{1}H line broadening measurements on solutions of $[Cu(Me_6tren)dma](ClO_4)_2$ in dma (the experimental error in individual P_mT_{2p} values is ca ±5%).

solution (i) 0.132 mol dm^{-3}, P_m = 0.01303

T(K)	$10^4 P_m T_{2p}$(s)	T(K)	$10^4 P_m T_{2p}$(s)	T(K)	$10^4 P_m T_{2p}$(s)
255.0	1.92	296.3	3.97	337.5	7.37
265.3	3.03	306.6	4.44	347.8	9.13
275.6	3.07	316.9	5.19	353.0	9.93
285.9	3.26	327.2	6.21	368.5	11.1

solution (ii) 0.211 mol dm^{-3}, P_m = 0.01995

T(K)	$10^4 P_m T_{2p}$(s)	T(K)	$10^4 P_m T_{2p}$(s)	T(K)	$10^4 P_m T_{2p}$(s)
255.0	1.57	296.3	3.31	337.5	7.13
265.3	2.13	306.6	3.89	347.8	8.00
275.6	2.54	316.9	4.81	353.0	8.09
285.9	2.80	327.2	4.68	368.5	9.29

Appendix 1.7

Paramagnetic induced chemical shift on solutions of $[Cu(Me_6tren)dma](ClO_4)_2$ in dma. The error in chemical shift does not exceed the digital resolution of 0.5Hz. Downfield shifts are positive.

solution (i) 0.132 mol dm^{-3}, P_m = 0.01303

T(K)	$\Delta\omega$(Hz)	T(K)	$\Delta\omega$(Hz)	T(K)	$\Delta\omega$(Hz)
255.0	1.0	296.3	3.5	337.5	3.9
265.3	0.6	306.6	3.9	347.8	3.9
275.6	1.8	316.9	3.6	358.2	3.6
285.6	2.1	237.2	3.9	368.5	3.5

A.2 Nickel(II) species in solution

Appendix 2.1

Stopped-flow spectrophotometric k_{obs} data for anation of
$[Ni(Me_6tren)dmf]^{2+}$ by X^- in dmf solution (ionic strength adjusted to
0.5 mol dm^{-3} with sodium perchlorate).

$X^- = Br^-$
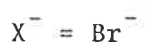
$[Ni(Me_6tren)dmf^{2+}]_o$ ($\times 10^3$ mol dm^{-3})	$[Br^-]_o$ ($\times 10^2$ mol dm^{-3})	$k_{obs}(278.2K)$ (s^{-1})	$k_{obs}(288.2K)$ (s^{-1})	$k_{obs}(298.2K)$ (s^{-1})
2.097(±0.003)	3.291(±0.017)	40.8(±0.5)	72.6(±0.9)	127(±2)
2.032(±0.004)	4.380(±0.021)	42.2(±0.7)	71.5(±0.9)	117(±2)
2.097(±0.003)	5.758(±0.048)	37.0(±0.4)	74.4(±1.1)	109(±2)
2.032(±0.004)	6.482(±0.119)	36.2(±0.4)	73.1(±0.9)	105(±2)
2.097(±0.003)	7.404(±0.091)	40.2(±0.5)	67.3(±0.9)	123(±2)
2.097(±0.003)	8.226(±0.009)	39.4(±0.4)	68.9(±0.8)	119(±2)
2.032(±0.004)	8.760(±0.010)	36.9(±0.4)	67.7(±0.8)	105(±2)

$X^- = N_3^-$
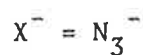
$[Ni(Me_6tren)dmf^{2+}]_o$ $(\times 10^4 mol\ dm^{-3})$	$[N_3^-]_o$ $(\times 10^3 mol\ dm^{-3})$	$k_{obs}(278.2K)$ (s^{-1})	$k_{obs}(288.2K)$ (s^{-1})	$k_{obs}(298.2K)$ (s^{-1})
0.4500 (±0.0094)	0.5003 (±0.0057)	20.0 (±0.5)	48.2 (±1.0)	65.9 (±1.8)
0.8956 (±0.0457)	1.001 (±0.009)	32.7 (±0.6)	56.3 (±1.3)	105 (±2)
1.698 (±0.011)	2.127 (±0.004)	34.6 (±0.6)	69.3 (±1.1)	131 (±2)
1.698 (±0.011)	4.235 (±0.029)	43.0 (±0.6)	84.2 (±1.5)	159 (±3)
7.098 (±0.016)	7.367 (±0.045)	50.8 (±0.7)	91.5 (±1.4)	181 (±3)
1.698 (±0.011)	8.506 (±0.048)	50.3 (±1.0)	95.1 (±1.5)	176 (±3)
11.40 (±0.02)	11.67 (±0.16)	56.2 (±0.8)	110 (±2)	190 (±3)
7.098 (±0.016)	12.28 (±0.06)	55.7 (±0.8)	111 (±2)	203 (±3)
11.40 (±0.02)	15.23 (±0.09)	58.0 (±0.8)	119 (±2)	225 (±3)
7.098 (±0.016)	17.19 (±0.15)	60.7 (±0.9)	127 (±2)	226 (±4)
11.40 (±0.02)	20.30 (±0.16)		136 (±2)	239 (±4)
1.698 (±0.011)	21.27 (±0.04)	65.1 (±1.3)	129 (±2)	237 (±5)
7.098 (±0.016)	24.56 (±0.04)	66.7 (±0.9)	127 (±2)	
11.40 (±0.02)	25.38 (±0.03)	73.0 (±1.1)	148 (±3)	

$X^- = NCS^-$
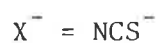
$[Ni(Me_6tren)dmf^{2+}]_o$ $(x10^4 mol\ dm^{-3})$	$[NCS^-]_o$ $(x10^3 mol\ dm^{-3})$	$k_{obs}(278.2K)$ (s^{-1})	$k_{obs}(288.2K)$ (s^{-1})	$k_{obs}(298.2K)$ (s^{-1})
0.4946(±0.0107)	0.5191(±0.0052)	12.6(±0.5)	24.2(±0.8)	30.2(±1.3)
0.8644(±0.0187)	1.194 (±0.012)	19.3(±0.6)	34.0(±1.1)	64.2(±1.3)
0.8644(±0.0187)	1.433 (±0.029)	28.6(±1.4)	50.3(±2.8)	
1.274 (±0.010)	1.574 (±0.012)	30.3(±2.2)	53.4(±5.4)	94.7(±4.4)
1.274 (±0.010)	3.148 (±0.021)	37.9(±3.6)	71.0(±2.7)	119 (±2)
4.981 (±0.023)	5.751 (±0.033)	38.9(±1.1)	76.0(±0.7)	139 (±5)
1.274 (±0.010)	7.870 (±0.020)	40.6(±4.1)	71.9(±2.7)	132 (±3)
7.307 (±0.044)	9.165 (±0.036)	34.3(±0.4)	84.8(±1.2)	158 (±2)
9.548 (±0.018)	9.247 (±0.130)	38.9(±0.5)	84.7(±1.2)	143 (±2)
4.981 (±0.023)	11.50 (±0.24)	42.5(±0.3)	77.7(±0.6)	150 (±1)
9.548 (±0.018)	15.41 (±0.14)	42.0(±0.5)	79.4(±1.2)	150 (±2)
6.683 (±0.025)	17.57 (±0.15)	39.1(±2.1)	75.3(±3.2)	141 (±5)
9.548 (±0.018)	20.55 (±0.16)	43.3(±0.5)	84.5(±1.2)	152 (±2)
6.683 (±0.025)	25.10 (±0.04)	38.2(±1.1)	75.4(±4.3)	138 (±1)
9.548 (±0.018)	25.69 (±0.03)	42.1(±0.5)	85.3(±1.3)	156 (±2)

Appendix 2.2

[1]H line broadening measurements on solutions of $[Ni(Me_6tren)dmf](ClO_4)_2$ in dmf (the experimental error in individual P_mT_{2p} values is ca ±5%).

solution (i) 0.159 mol dm^{-3}, P_m = 0.01291

T(K)	$10^4P_mT_{2p}$(s)	T(K)	$10^4P_mT_{2p}$(s)	T(K)	$10^4P_mT_{2p}$(s)
228.5	6.16	325.0	3.21	360.6	2.47
269.2	13.1	330.2	3.25	370.8	1.25
284.4	11.9	335.3	3.38	375.8	1.04
299.2	7.74	340.4	3.52	381.0	0.845
304.4	6.09	340.4	3.44	386.0	0.701
314.8	3.89	345.5	3.36		
320.0	3.42	350.5	2.83		

solution (ii) 0.415 mol dm^{-3}, P_m = 0.03248

T(K)	$10^4P_mT_{2p}$(s)	T(K)	$10^4P_mT_{2p}$(s)	T(K)	$10^4P_mT_{2p}$(s)
228.5	4.35	320.0	4.28	360.6	2.24
248.8	8.01	330.2	4.39	365.7	1.82
269.2	10.0	335.2	4.60	370.8	1.46
289.3	10.1	345.5	4.04	375.9	1.21
299.2	7.80	350.5	2.99	381.0	0.970
314.8	4.61	355.5	2.53		

Appendix 2.3

Paramagnetic induced chemical shift measurements on solutions of
$[Ni(Me_6tren)dmf](ClO_4)_2$ in dmf. The error in chemical shift does not
exceed the digital resolution of 0.5Hz. Downfield shifts are positive.

solution (i) 0.159 mol dm^{-3}, $P_m = 0.01291$

T(K)	$\Delta\omega$(Hz)	T(K)	$\Delta\omega$(Hz)	T(K)	$\Delta\omega$(Hz)
228.5	8.1	320.0	4.6	360.6	10.9
248.8	5.6	325.0	5.8	370.8	13.7
269.2	3.3	335.3	8.1	375.8	17.6
284.4	2.1	340.4	9.5	381.0	19.9
304.4	1.1	345.5	8.5	386.0	20.9
314.8	3.0	350.5	10.1		

Appendix 2.4

[1]H line broadening measurements on solutions of $[Ni(Me_6tren)def](ClO_4)_2$ in def (the experimental error in individual P_mT_{2p} values is ca ±5%).

solution (i) 0.0635 mol dm^{-3}, $P_m = 0.007615$

T(K)	$10^4P_mT_{2p}$(s)	T(K)	$10^4P_mT_{2p}$(s)	T(K)	$10^4P_mT_{2p}$(s)
215.5	2.11	291.0	10.8	343.3	2.54
220.6	2.96	297.0	10.3	348.3	2.56
225.6	3.59	303.1	8.74	350.3	2.40
230.6	5.30	308.1	6.68	353.4	2.29
235.7	6.08	313.1	6.65	356.4	2.14
240.7	8.20	318.2	5.49	358.4	2.06
245.7	9.19	323.2	4.40	361.4	1.83
255.8	11.0	323.2	4.32	363.4	1.80
260.8	11.9	328.2	3.72	366.4	1.55
265.8	12.0	330.2	3.30	368.4	1.50
270.9	11.9	333.2	3.03	370.5	1.31
275.9	12.7	333.2	3.08	373.5	1.22
280.9	11.9	338.3	3.05	375.5	1.11
286.0	11.9	340.3	2.66	378.5	0.989

solution (ii) 0.0212 mol dm^{-3}, $P_m = 0.003774$

T(K)	$10^4P_mT_{2p}$(s)	T(K)	$10^4P_mT_{2p}$(s)	T(K)	$10^4P_mT_{2p}$(s)
215.5	2.89	275.9	12.0	338.3	3.63
235.8	5.95	286.0	11.7	343.3	2.89
255.8	11.8	308.1	7.70		
265.8	13.8	328.2	3.71		

Appendix 2.5

Paramagnetic induced chemical shift measurements on solutions of
$[Ni(Me_6tren)def](ClO_4)_2$ in def. The error in chemical shift does not
exceed the digital resolution of 0.5Hz. Downfield shifts are positive.

solution (i) 0.0635 mol dm^{-3}, P_m = 0.007615

T(K)	$\Delta\omega$(Hz)	T(K)	$\Delta\omega$(Hz)	T(K)	$\Delta\omega$(Hz)
230.6	4.8	280.9	1.5	343.3	3.7
240.7	3.8	291.0	1.2	353.4	5.0
250.8	3.8	303.1	1.0	363.4	5.4
255.8	2.3	313.1	1.6	373.5	6.1
260.8	1.8	323.2	1.1	378.5	6.4
270.9	1.7	333.2	2.4		

A.3 Cobalt(II) species in solution

Appendix 3.1

Stopped-flow spectrophotometric k_{obs} data for anation of $[Co(Me_6tren)dmf]^{2+}$ by X^- in dmf solution (ionic strength adjusted to 0.5 mol dm^{-3} with sodium perchlorate).

$X^- = Br^-$

$[Co(Me_6tren)dmf^{2+}]_o$ ($\times 10^3$ mol dm^{-3})	$[Br^-]_o$ ($\times 10^2$ mol dm^{-3})	k_{obs}(278.2K) (s^{-1})	k_{obs}(288.2K) (s^{-1})	k_{obs}(298.2K) (s^{-1})
0.9282(±0.0047)	1.512(±0.004)	6.91(±0.08)	12.0(±0.3)	23.3(±0.4)
1.392 (±0.003)	2.714(±0.008)	6.68(±0.07)	13.3(±0.3)	23.3(±0.4)
1.020 (±0.002)	3.964(±0.019)	6.85(±0.13)	12.8(±0.3)	22.3(±0.4)
1.020 (±0.002)	5.550(±0.047)	7.23(±0.14)	14.0(±0.3)	22.4(±0.4)
1.392 (±0.003)	6.786(±0.010)	7.36(±0.16)	14.9(±0.3)	23.2(±0.4)
1.020 (±0.002)	7.928(±0.009)	7.93(±0.18)	15.7(±0.4)	22.1(±0.5)

$X^- = N_3^-$
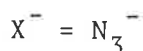
$[Co(Me_6tren)dmf^{2+}]_o$ ($\times 10^4$ mol dm^{-3})	$[N_3^-]_o$ ($\times 10^3$ mol dm^{-3})	k_{obs}(278.2K) (s^{-1})	k_{obs}(288.2K) (s^{-1})	k_{obs}(298.2K) (s^{-1})
0.2207(±0.0054)	0.5018(±0.0057)	26.8(±0.4)	42.5(±0.7)	51.2(±0.9)
0.9442(±0.0368)	1.053 (±0.020)	48.2(±0.6)	85.3(±1.2)	133 (±2)
1.657 (±0.038)	1.907 (±0.028)	86.5(±1.4)	154 (±3)	214 (±5)
1.443 (±0.037)	2.632 (±0.019)	124 (±2)	199 (±4)	266 (±4)
2.512 (±0.039)	3.783 (±0.025)	175 (±3)	258 (±5)	
1.657 (±0.038)	4.023 (±0.036)	186 (±3)	300 (±5)	
2.209 (±0.038)	5.018 (±0.021)	209 (±4)	299 (±5)	
3.456 (±0.040)	6.141 (±0.062)	236 (±5)		

$X^- = NCS^-$
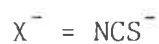
$[Co(Me_6tren)dmf]_o$ $(x10^4 mol\ dm^{-3})$	$[NCS^-]_o$ $(x10^3 mol\ dm^{-3})$	$k_{obs}(278.2K)$ (s^{-1})	$k_{obs}(288.2K)$ (s^{-1})	$k_{obs}(298.2K)$ (s^{-1})
0.4739 (±0.0139)	0.5649 (±0.0059)	7.85 (±0.09)	14.8 (±0.3)	27.8 (±0.4)
1.339 (±0.019)	1.594 (±0.015)		28.4 (±0.4)	49.1 (±0.7)
3.046 (±0.039)	3.390 (±0.037)		53.3 (±0.6)	88.3 (±1.6)
1.399 (±0.019)	3.984 (±0.031)	33.1 (±0.4)	61.3 (±0.8)	
3.153 (±0.037)	4.178 (±0.025)			104 (±2)
3.563 (±0.040)	5.649 (±0.018)	58.0 (±0.7)	97.7 (±1.5)	143 (±3)
4.436 (±0.041)	7.981 (±0.034)	64.6 (±1.0)	134 (±2)	203 (±3)
4.899 (±0.042)	8.357 (±0.051)		120 (±2)	190 (±3)
3.153 (±0.037)	8.856 (±0.050)	79.5 (±1.7)		
4.997 (±0.023)	9.689 (±0.022)			248 (±4)
1.737 (±0.020)	9.742 (±0.053)	82.7 (±1.1)	150 (±3)	259 (±5)
1.390 (±0.037)	12.91 (±0.17)	111 (±2)	204 (±3)	281 (±6)
7.322 (±0.044)	16.12 (±0.04)	139 (±2)	231 (±4)	
1.764 (±0.038)	18.45 (±0.15)	157 (±3)	279 (±6)	
2.530 (±0.039)	23.06 (±0.04)	209 (±4)		
5.808 (±0.043)	24.36 (±0.04)	210 (±4)		
6.752 (±0.044)	26.50 (±0.06)	254 (±5)		
7.090 (±0.044)	27.37 (±0.41)	273 (±5)		
11.44 (±0.05)	30.36 (±0.40)	296 (±5)		

Appendix 3.2

[1]H line broadening measurements on solutions of $[Co(Me_6tren)dmf](ClO_4)_2$ in dmf (the experimental error in individual P_mT_{2p} values is ca $\pm 5\%$).

solution (i) P_m = 0.01909

T(K)	$10^4P_mT_{2p}(s)$	T(K)	$10^4P_mT_{2p}(s)$	T(K)	$10^4P_mT_{2p}(s)$
223.4	6.98	304.4	17.5	360.6	3.64
233.5	7.98	314.8	16.1	365.7	2.89
243.7	9.57	325.0	12.5	370.8	2.32
253.9	11.0	330.2	12.2	375.9	2.03
264.1	12.3	340.4	8.09	379.0	1.70
274.2	14.7	345.5	7.06	381.0	1.56
284.4	14.3	350.5	5.62	384.0	1.32
294.3	17.1	355.5	4.38		

solution (ii) P_m = 0.03059

T(K)	$10^4P_mT_{2p}(s)$	T(K)	$10^4P_mT_{2p}(s)$	T(K)	$10^4P_mT_{2p}(s)$
228.5	6.38	309.6	15.3	364.7	3.28
238.6	7.68	320.0	13.4	368.8	2.47
248.8	8.98	330.2	12.5	372.9	1.97
259.0	10.0	340.4	7.75	375.9	1.83
269.2	12.2	345.5	6.86	379.0	1.50
279.4	12.8	350.5	5.53	381.0	1.42
289.3	14.2	355.5	4.77	384.0	1.23
299.2	15.0	360.6	3.16		

Appendix 3.3

Paramagnetic induced chemical shift measurements on solutions of

$[Co(Me_6tren)dmf](ClO_4)_2$ in dmf. The error in chemical shift does not

exceed the digital resolution of 0.5Hz. Dowfield shifts are positive.

solution (i) P_m = 0.01909

T(K)	$\Delta\omega$(Hz)	T(K)	$\Delta\omega$(Hz)	T(K)	$\Delta\omega$(Hz)
223.4	1.2	314.8	-1.4	365.7	-0.7
233.5	0.5	325.0	-1.5	370.8	0.1
253.9	0.9	330.2	-0.9	375.9	0.8
264.1	0.0	340.4	-1.6	379.0	1.4
274.2	0.1	345.5	-0.8	381.0	0.9
284.4	-0.3	350.5	-1.2	384.0	2.8
294.3	-1.3	355.5	-1.0		
304.4	-0.8	360.6	-0.9		

solution (ii) 0.03059

T(K)	$\Delta\omega$(Hz)	T(K)	$\Delta\omega$(Hz)	T(K)	$\Delta\omega$(Hz)
228.5	1.1	309.6	-0.1	364.7	0.9
238.6	2.3	320.0	0.3	368.8	3.3
248.8	1.5	330.2	-0.8	372.9	5.6
259.0	1.3	340.4	-0.6	375.9	5.7
269.2	0.8	345.5	0.3	379.0	8.7
279.4	0.9	350.5	0.5	381.0	9.5
289.3	0.9	355.5	0.6	384.0	10.3
299.2	0.3	360.6	0.8		

Appendix 3.4

[1]H line broadening measurements on solutions of $[Co(Me_6tren)def](ClO_4)_2$ in def (the experimental error in individual P_mT_{2p} values is ca $\pm5\%$).

solution (i) $P_m = 0.008500$

T(K)	$10^4P_mT_{2p}$(s)	T(K)	$10^4P_mT_{2p}$(s)	T(K)	$10^4P_mT_{2p}$(s)
225.6	7.23	313.1	13.2	361.4	3.95
230.6	9.30	318.1	14.0	363.4	3.46
235.7	9.91	321.2	14.0	366.4	3.17
240.7	12.1	323.2	13.1	368.4	2.84
245.7	11.4	326.2	14.4	370.5	2.68
250.8	12.0	328.2	13.5	373.5	2.22
255.8	14.2	331.2	11.4	376.5	1.97
260.8	12.7	336.3	10.5	378.5	1.88
265.8	12.9	338.3	9.70	380.5	1.67
270.9	13.4	341.3	7.82	383.5	1.47
275.9	12.8	343.3	7.80	386.5	1.29
280.9	12.8	346.3	7.27	388.6	1.19
286.0	11.6	348.3	6.63	391.6	1.03
291.0	12.0	350.3	6.04	393.6	0.966
297.0	13.9	353.4	5.48	396.6	0.877
303.1	13.9	356.4	4.76	398.6	0.812
308.1	13.3	358.4	4.21		

solution (ii) P_m = 0.01250

T(K)	$10^4 P_m T_{2p}$(s)	T(K)	$10^4 P_m T_{2p}$(s)	T(K)	$10^4 P_m T_{2p}$(s)
225.6	7.34	286.0	11.5	351.3	5.85
228.6	7.83	291.0	12.4	353.4	5.49
230.6	8.22	297.0	13.2	356.4	4.90
233.6	8.50	303.1	14.4	358.4	4.75
235.7	8.96	308.1	13.7	361.4	3.97
238.7	9.06	313.1	14.9	366.4	3.05
240.7	9.73	318.2	14.7	368.4	2.88
243.7	10.4	323.2	14.0	371.5	2.56
245.7	10.8	326.2	13.0	376.5	2.10
248.8	11.4	328.2	12.4	378.5	1.86
250.8	11.7	333.3	11.0	381.5	1.63
255.8	11.9	336.3	10.3	386.5	1.29
260.8	11.9	338.3	10.0	388.6	1.17
265.8	11.9	340.3	8.88	391.6	0.976
270.9	11.2	343.3	8.31	396.6	0.781
275.9	11.3	346.3	7.83	398.6	0.795
280.9	11.1	348.3	7.25		

Appendix 3.5

Paramagnetic induced chemical shift measurements on solutions of

$[Co(Me_6tren)def](ClO_4)_2$ in def. The error in chemical shift does not

exceed the digital resolution of 0.5Hz. Downfield shifts are positive.

solution (i) P_m = 0.008500

T(K)	$\Delta\omega$(Hz)	T(K)	$\Delta\omega$(hz)	T(K)	$\Delta\omega$(Hz)
225.6	5.3	313.1	4.2	361.4	9.5
230.6	4.5	318.2	4.1	363.4	10.4
235.7	4.4	321.2	4.1	366.4	11.2
240.7	3.9	323.2	4.3	368.4	12.2
245.7	4.1	326.2	4.1	370.5	12.8
250.8	4.0	328.2	4.3	373.5	14.9
255.8	3.8	331.2	4.7	376.5	16.5
260.8	3.9	336.3	4.9	378.5	17.2
265.8	3.8	338.3	5.1	380.5	19.1
270.9	3.9	341.3	5.8	383.5	22.2
275.9	4.0	343.3	5.9	386.5	23.9
280.9	4.0	346.3	6.2	388.6	25.6
286.0	4.3	348.3	6.5	391.6	29.2
291.0	4.2	350.3	7.0	393.6	31.0
297.0	3.9	353.4	7.5	396.6	33.9
303.1	4.0	356.4	8.2	398.6	36.4
308.1	4.1	358.4	9.0		

solution (ii) $P_m = 0.01250$

T(K)	$\Delta\omega$(Hz)	T(K)	$\Delta\omega$(Hz)	T(K)	$\Delta\omega$(Hz)
297.0	5.0	338.3	6.3	378.5	24.2
308.1	5.0	348.3	7.9	388.6	37.1
318.2	4.9	358.4	11.0	398.6	53.1
328.2	5.5	368.4	16.5		

Published papers from this work

Some of the material in this thesis has been published and appears in the chemical literature under the following titles:

1. "Solvent Exchange and Anation on Five-Coordinate (N,N-Dimethylformamide) (2,2'2"-tris(dimethylamino)triethylamine) copper(II)."

    S.F. Lincoln, J.H. Coates, B.G. Doddridge, A.M. Hounslow and D.L. Pisaniello, Inorg.Chem., 1983, 22, 2869.

2. "Proton Nuclear Magnetic Resonance Study of N,N-Dimethylformamide Exchange on (N,N-Dimethylformamide) 2,2',2"-Tri(N,N-Dimethylamino) Triethylamine Manganese(II) and its Cobalt(II) and Copper(II) Analogs".

    S.F. Lincoln, A.M. Hounslow, D.L. Pisaniello, B.G. Doddridge, J.H. Coates, A.E. Merbach and D. Zbinden, Inorg.Chem., 1984, 23, 1090.

3. "Anation and Solvent Exchange on (N,N-Dimethylformamide) 2,2',2"-Tri(N,N-Diethylamino)Triethylamine nickel(II) and Solvent Exchange on Bis(N,N-Dimethylformamide)2,2',2"-Triaminotriethylamine nickel(II).

    S.F. Lincoln, J.H. Coates, B.G. Doddridge and D.L. Pisaniello, Aust. J.Chem., 1984, 37, 947.

4. "Ligand Substitution on (N,N-Dimethylformamide)(2,2',2"-tri (N,N-dimethylamino)triethylamine) cobalt(II)".

    S.F. Lincoln, B.G. Doddridge and J.H. Coates, J.Chem.Soc., Dalton Trans., 1985, 413.

5. "Proton Nuclear Magnetic Resonance Study of N,N-Diethylformamide Exchange on (N,N-Diethylformamide)(2,2',2"-tris(dimethylamino) triethylamine)cobalt(II) and its Copper(II) Analogue".

    S.F. Lincoln, A.M. Hounslow, B.G. Doddridge, J.H. Coates, A.E. Merbach and D. Zbinden, Inorg.Chim.Acta, 1985, 100, 207.

6. "Solvent Exchange on (N,N-Diethylformamide)[2,2',2"-tri (N,N-dimethylamino)triethylamine]nickel(II)."

    S.F. Lincoln, J.H. Coates, B.G. Doddridge and A.M. Hounslow, Aust.J. Chem., 1986, 39, 367.